The Distribution of Aluminum in Beaufort Sea and the Development of a Sequential Injection Method for the Determination of Aluminum in Natural Waters

by

Timothy Giesbrecht
B.Sc., University of Victoria, 2007

A Thesis Submitted in Partial Fulfillment
of the Requirements for the Degree of

MASTER OF SCIENCE

in the Department of Chemistry

Supervisory Committee

The Distribution of Aluminum in Beaufort Sea and the Development of a Sequential Injection Method for the Determination of Aluminum in Natural Waters

by

Timothy Giesbrecht
B.Sc., University of Victoria, 2007

Supervisory Committee

Dr. Jay T. Cullen, (School of Earth and Ocean Science)
Co-Supervisor

Dr. Dave Berg, (Department of Chemistry)
Co-Supervisor

Dr. Roberta Hamme, (School of Earth and Ocean Science)
Departmental Member

Dr. Peter Wan, (Department of Chemistry)
Outside Member

Abstract

Supervisory Committee
Dr. Jay T. Cullen, (School of Earth and Ocean Science)
Supervisor
Dr. Dave Berg, (Department of Chemistry)
Co-Supervisor and Departmental Member
Dr. Roberta Hamme, (School of Earth and Ocean Science)
Departmental Member
Dr. Peter Wan, (Department of Chemistry)
Outside Member

Here we report vertical profiles of dissolved (0.2 μm filtered) Aluminum (Al) for eight stations in the Beaufort Sea in the Canadian Arctic, six of which are along a transect extending from the coastal shelf northeast of the Mackenzie River delta out to the Beaufort Sea. Sampling was performed aboard the CCGS Sir Wilfrid Laurier in September 2007 and all analyses were performed in a Class 100 clean space at the University of Victoria. Vertical profiles of dissolved Al in the water column displayed surface maxima, subsurface minima and a general increase in concentration with depth as is characteristic of a "scavenged" trace element in seawater. Concentrations of dissolved Al for the upper 1000 m were generally low ranging from the < 1 nmol kg^{-1} observed in the sub-surface minimum corresponding to the Pacific inflow layer and increasing to ~6-10 nmol

kg^{-1} with depth. The surface maxima at stations for Al was associated with relatively fresh surface water (26-30 PSS) that is believed to be the result of seasonal sea-ice melt. This correlation suggests that the melting of sea-ice with entrained sediments may be an important mechanism for the delivery of Al and associated trace metals to the water column of the Beaufort Sea. We also report measurements of "total Al" (unfiltered and acidified to pH 1.7 for two year prior to analysis) for the Arctic Ocean which indicate that a significant proportion of Al in the water column is present in the > 0.2 μm fraction. These measurements and the hydrographic data along the transect indicate the transport of a cold, saline, metal enriched water mass off of the continental shelf into the Canada Basin. This water mass appears to reflect the return of cold, high salinity slope water originally emplaced on the shelf by upwelling favourable winds. Alternatively, this water mass may be the product of brine exclusion from sea-ice formation during the previous winter that was unable to vacate the shelf due to the persistent upwelling observed throughout 2007. This finding suggests that the convection of cold, dense shelf water may be a mechanism for supplying the deep waters of the Arctic with an injection of water containing a significant Al content.

In addition, a low volume sequential injection analysis (SIA) method is proposed for determination of elevated concentrations of Al, like those typically observed in coastal and river waters. A thorough optimization of the chemistry and instrumental parameters was performed along with an extensive investigation into potential interferents. The method was found to be largely free of interferents at environmentally relevant concentrations and was determined to

have a detection limit of 24 nM. The precision of the method was reported to be 2% at 75 nmol kg^{-1} and analysis of the SLRS-4 certified reference material validated the accuracy of the method. Analysis of several samples that were previously analyzed via flow injection analysis (FIA) and standardized with consensus values of an open ocean reference material indicated the method returned comparable values for the Al concentration in the samples. Development and optimization of the SIA has resulted in an accurate and precise low-cost method of analysis that is both sensitive and relatively free from interference for the detection of nano-molar levels of Al in coastal and natural waters.

Table of Contents

List of Tables

List of Figures

Acknowledgments

I would like to thank my supervisor and friend, Dr. Jay Cullen for allowing me to further my education and providing a work environment that permitted creativity and ingenuity. I felt I could work independently yet knew that you would always be there to provide insight when I was in need. Thank you to Dr. Dave Berg for your co-supervision so that I could continue my studies in the Department of Chemistry. I would also like to give thanks to Nes Sutherland and Kristina Brown for their assistance in the labourious task of sample collection from the trace metal rosette. Also, I would like to thank Humfrey Melling for leading a successful scientific expedition and for educating me on the characteristics of brine-exclusion waters. I would like to acknowledge the Captain and Crew of the CCGS Sir Wilfrid Laurier; without their assistance this work would not have been possible. Lastly, I would like to thank my parents, Jerry and Gem, for supporting me in my education and often putting my education before their own needs.

Dedication

I would like to dedicate this manuscript to my wife, Mary Anne, and my son Archer. You both mean the world to me and I am very thankful to have you both in my life. Thank you for being patient and supportive during the completion of my studies and I look forward to what the future has in store for us all.

1. Introduction to Aluminum Geochemistry

Despite Aluminum (Al) being the third most abundant element in the earth's crust, with a crustal abundance of 8.4% by weight (Hans Wedepohl, 1995; Taylor, 1964), Al is found only at the nano-molar (10^{-9} M) level in the world's oceans given its propensity to adsorb to sinking particulate material. Aluminum displays considerable inter-basin spatial variability in the world ocean with higher concentrations at the sea surface and elevated concentrations in the interior of the north Atlantic compared to deep Pacific waters (Figure 1). This inter-ocean fractionation has been explained by Orians and Bruland (1986), by invoking progressive scavenging of dissolved Al from the water column as waters age and transit along the path of the global thermohaline circulation. The scavenging of Al is thought to occur either by a passive or active process. The passive removal of Al is suggested to occur via adsorption of Al on to surfaces of particulate matter (such as detrital rain) as they descend to the ocean floor (Hydes, 1983; Orians and Bruland, 1985). However, support for the active removal of Al is evident in the nutrient-like profiles of dissolved Al observed for some ocean regions (Hydes et al., 1988; Kramer et al., 2004; Stoffyn, 1979), and in controlled mesocosm experiments (Moran and Moore, 1988) suggesting a biological uptake of Al. Furthermore, Al has been shown to be incorporated into the siliceous frustules of living diatoms (Gehlen et al., 2002), thereby indicating an active uptake process. Regardless of the mechanism used to scavenge the

dissolved Al, these particles degrade and dissolve as they descend the water column and in doing so, supply the deep waters of the ocean with a source of dissolved Al.

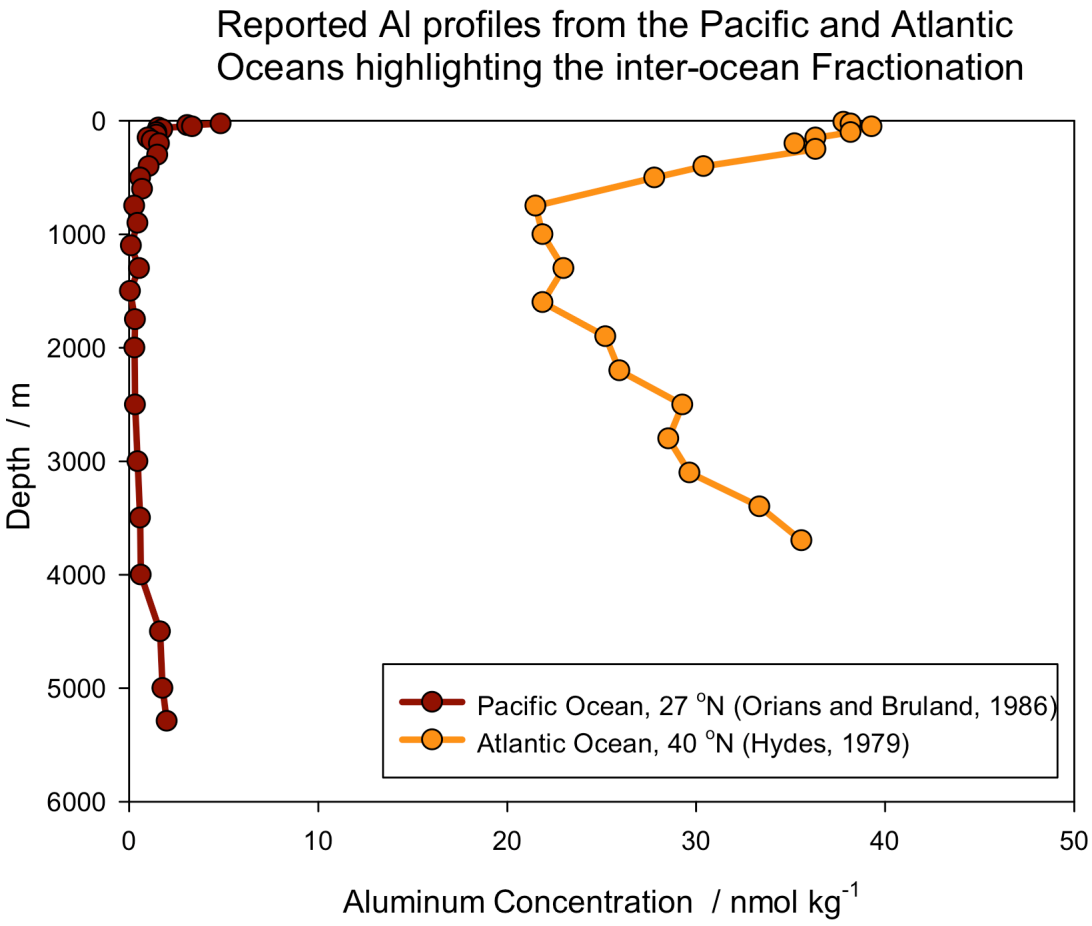

Figure 1 - Profiles of Al from the Pacific (Orians and Bruland, 1986) and Atlantic (Hydes, 1979) Oceans showing the marked differences observed for the two basins. The low Al concentrations in the Pacific are due to the short residence time of Al in the water column, which has been estimated to be 50-200 years and attenuated aeolian flux experienced in the terrestrially remote Pacific (Orians and Bruland, 1985).

Initial investigations into the distribution of Al proposed that riverine input may be a major source of Al to the oceans (Stoffyn and Mackenzie, 1982).

However, fluvial input of Al has been shown to be strongly attenuated by estuarine removal process such that little of this Al ever reaches the open ocean (Hydes and Liss, 1977; Mackin and Aller, 1984). The main source of Al to the open ocean is deposition and partial dissolution of aeolian dust to the surface waters. A typical Al distribution is characterized by a surface maximum resulting from this atmospheric input, a sub-surface minimum, and a gradual increase with depth due to the scavenging and remineralization processes discussed above.

The Al concentration in seawater is an important property to quantify as it represents a potent geochemical tracer of the input of lithogenic material to the world's oceans. For example, the flux of Al to the ocean surface correlates well with the input of the bioactive element, iron (Fe), as shown in Figure 2 below. However, in the ocean interior, vertical profiles of these two elements diverge as biological remineralisation and scavenging processes affect the distribution of these elements differently. The depositional flux of Fe and surface concentrations of Fe can control the composition and productivity of the marine microbial community, most notably in the spatially expansive high nutrient low-chlorophyll (HNLC) regions of the ocean (Martin and Fitzwater, 1988). Indeed, estimates suggest that primary productivity in 30 to 40 percent of the world ocean is limited by the availability of Fe (Armbrust, 2009; Moore et al., 2001). However, given the low open ocean concentrations observed for Fe (pico-molar to low nano-molar) and the difficulties associated in cleanly sampling and analyzing for Fe, an indirect method for determining its surface distribution and aeolian flux

component is desirable. Therefore the correlation between Al and Fe surface distributions (Figure 2), at least on short temporal and spatial scales allows Al to provide information about the input and distribution of Fe in surface waters. Indeed, Al may represent a useful aeolian tracer any telluric element, natural or anthropogenic, that is predominantly delivered to the ocean surface as an aerosol or dust.

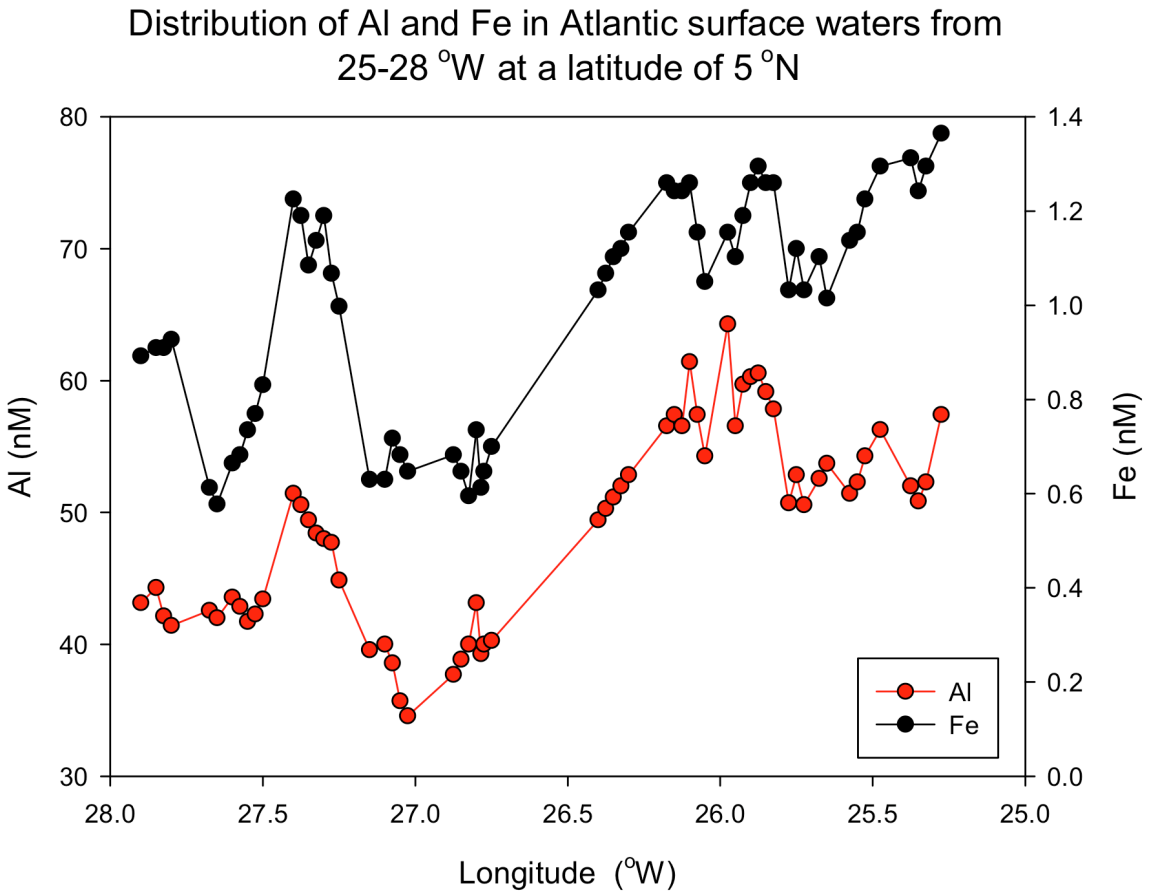

Figure 2 - The distribution of Al and Fe in Atlantic surface waters between 25°W and 28°W along a latitude of 5°N showing the concomitant variations over short spatial scales. Data taken from Measures and Vink (2001).

Until recently, measurements of Al for the Arctic in the literature were sparse, with only a few reported studies (Measures, 1999; Moore, 1981). However there has been renewed interest in the area, particularly with regard to trace metal distributions. This is largely due to the recently celebrated international polar year (IPY) and the launch of the GEOTRACES program. As part of these programs, Middag et al. (2009), recently published the first vertical distributions of dissolved Al for the Arctic for an impressive 44 stations that extended over much of the Eurasian and Makarov Basins (See Figure 3). Middag et al. (2009) reported very low (~1 nM) concentrations in dissolved Al for the surface waters of the Arctic and a nutrient like increase with depth, reaching concentrations as high as 28 nM. The low surface concentrations and the absence of a surface maximum led Middag et al. (2009) to conclude that the surface waters experienced little or no influence from aeolian dust input. Moore (1981) also noted the lack of a surface maximum, relative to more dramatic Atlantic profiles in the literature at the time (Hydes, 1979), in his vertical profile of reactive Al (unfiltered and unacidified sample analyzed at natural pH) that was collected while transiting over the Lomonosov Ridge aboard a floating ice-raft (Figure 3; Figure 14). In retrospect a modest (~0.5 nM), but detectable, surface maximum exists. By contrast, Measures (1999) reported concentrations for reactive Al ranging from 2-20 nM for the surface waters of the Arctic and noted a general trend of higher concentrations in the Canadian Basin and lower values in the Eurasian Basin. The apparent correlation between high reactive Al values and the observation of “dirty sea-ice” at these sampling locations led Measures

(1999) to postulate that the melting of sea-ice containing sediment may be an important mechanism for the transport of trace metals to the surface waters of the Arctic Basins.

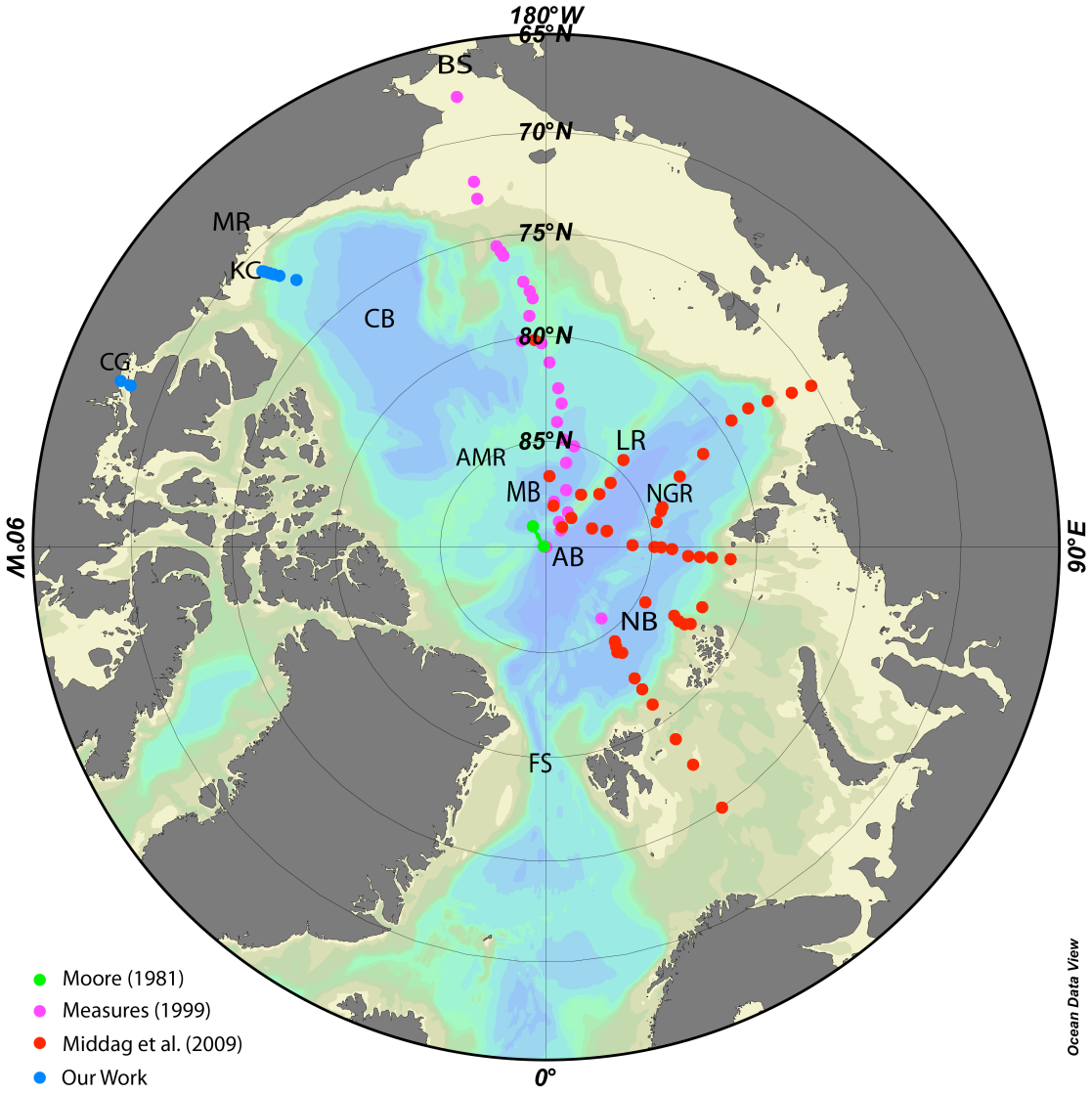

Figure 3 - Map displaying the locations of sampling for other investigators who have reported Al distributions for the Arctic Ocean. The locations of the Kugmallit Canyon transect and Coronation Gulf stations that are the focus of this work are shown in blue. KC: Kugmallit Canyon Transect, CG: Coronation Gulf Stations, MR: Mackenzie River, BS: Bering Strait, CB: Canada Basin, MB: Makarov Basin, AB: Amundsen Basin, NB: Nansen Basin, FS: Fram Strait, AMR: alpha-Mendeleev Ridge, LR: Lomonosov Ridge, NGR: Nansen Gakkel Ridge.

Here we report the vertical distribution of dissolved Al for six stations along a transect of the Canada Basin, north-east of the Mackenzie river outflow as well as for two inshore stations in the Coronation Gulf. These measurements constitute the first reporting of dissolved Al for the Canada Basin. In addition, we report the vertical distribution of “total Al” (unfiltered, acidified to pH = 1.7 for two years) for the six stations along the transect. To our knowledge, this is the first reporting of total Al for the Arctic Ocean.

2. Sampling and Experimental

2.1 Location and Sampling

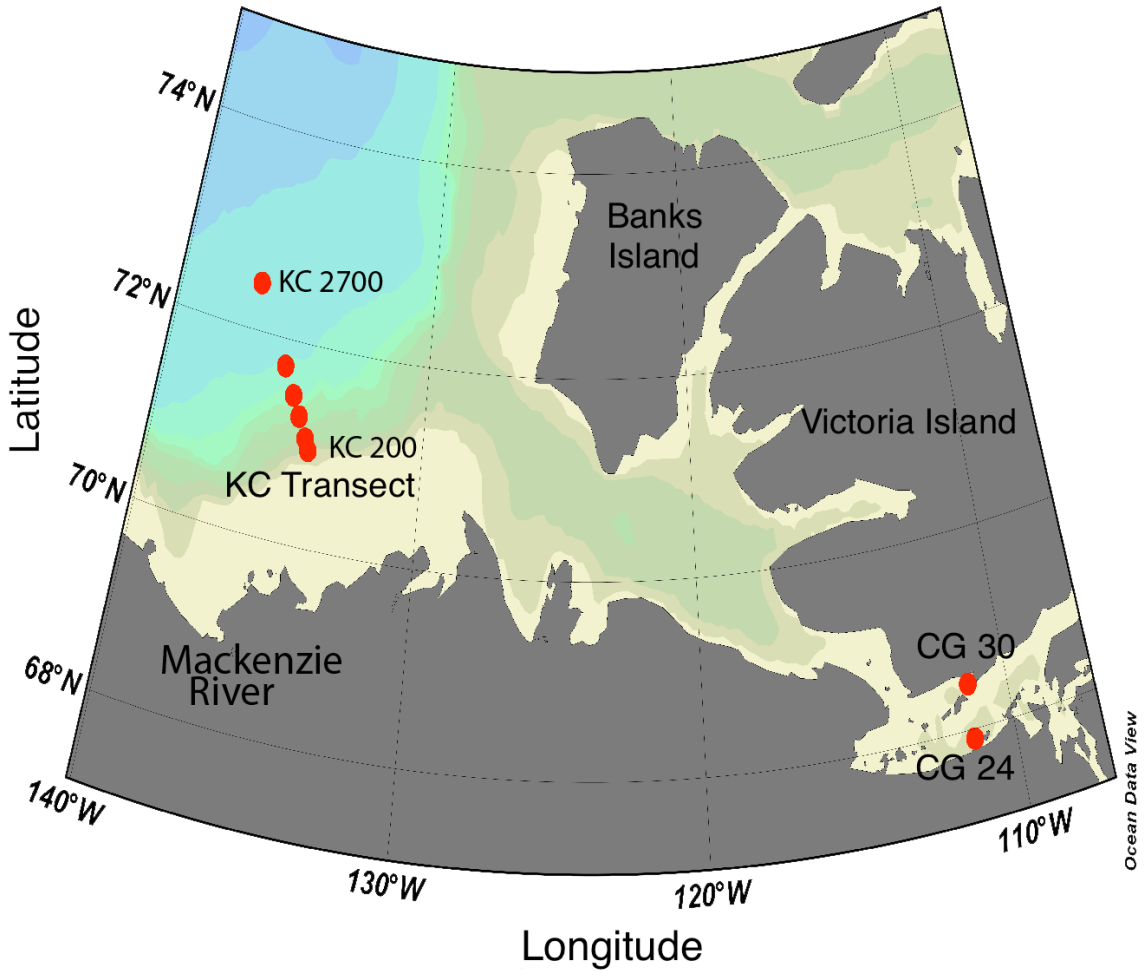

Figure 4 – Locations of Sampling shown as red circles. The six points along the Kugmallit Canyon transect are numbered according to their bottom depth with the most northern station having a depth of 2700 meters and the most coastal station in the transect having a bottom depth of 200 meters.

Sampling was performed in 2007 aboard the CCGS Sir Wilfrid Laurier from September 14 to October 1 using a new trace metal rosette equipped with twelve 12 L GO-Flo bottles (General Oceanics, Miami FL, USA). The locations of sampling are shown in Figure 4. Filtering of the dissolved samples was performed immediately after collection using a 0.22 μm capsule Opticap® filter (Millipore). All samples destined for Al analysis were acidified to pH 1.7 using trace metal grade HCl (Seastar Baseline) and stored in either low-density poly ethylene (LDPE) or polymethylpentene (PMP) bottles that had been previously cleaned according to a three step protocol described below.

2.2 Analytical Cleaning Protocol

As a first step of the cleaning process, the bottles were placed in a detergent bath (Sparkleen) and allowed to soak for one week to remove any organics that remained from the manufacturing process. The bottles were then rinsed with reverse osmosis (RO) water until all visible residues were removed and then were subsequently rinsed three times with deionized water with a resistance of at least 18.9 MΩ cm^{-1} from a Millipore Element deionized water station (Millipore). This water will from now on be referred to as Milli-Q. For the second stage of cleaning the bottles were filled with 6 M reagent grade HCl that had been diluted with Milli-Q and stored for 1 month. The bottles were then rinsed a minimum of four times in Milli-Q and filled with 1 M environmental grade HCl that had been diluted with Milli-Q and remained in the bottles until their use

onboard the ship (approximately 2 months). To minimize contamination during handling, transportation, and storage, the bottles were placed inside two LDPE plastic bags.

All reagents and standards were stored in either Teflon (FEP) or LDPE bottles and were initially cleaned using the above-mentioned protocol. Subsequent cleaning of the reagents or standard bottles involved soaking the bottles in a 1 M trace metal grade acid bath set to 60 degrees Celsius for a minimum of 12 hours followed by rinsing with copious amounts of Milli-Q. All cleaning was performed in a clean space so as to minimize contamination.

2.3 FIA Manifold for Aluminum Determination

Al concentrations were determined using a flow injection analysis (FIA) method adapted from Brown and Bruland (2008) and Resing and Measures (1994) involving the chelation of the metal with lumogallion (2,2',4'-trihydroxy-5-chloroazobenzene-3-sulfonic acid) and subsequent detection of the fluorescence of the Al-lumogallion complex when irradiated. The proposed structure of the Al-lumogallion complex is shown in Figure 5.

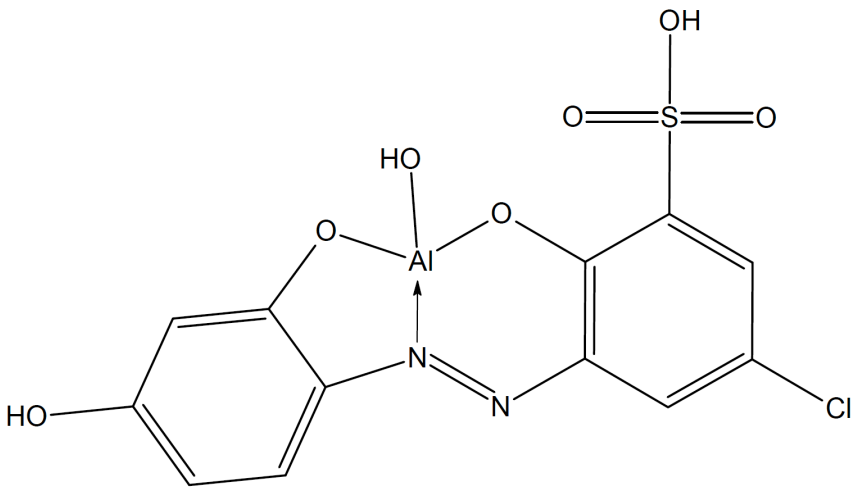

Figure 5 - Chemical structure of Al-lumogallion complex

Fluorometric detection of the Al-lumogallion complex was performed using a Shimadzu RF-535 fluorometer with excitation and emission wavelengths set at 485 nm and 552 nm respectively. The lumogallion method of detection requires that the Al to be measured be either in a free ionic state or loosely bound such that it may readily complex with lumogallion prior to detection. Thus, all of the measurements of Al in this manuscript are for Al of this variety and do not account for the Al that is tightly bound in mineral lattices at the time of analysis. A schematic of the FIA manifold used for the Al measurements is shown in Figure 6.

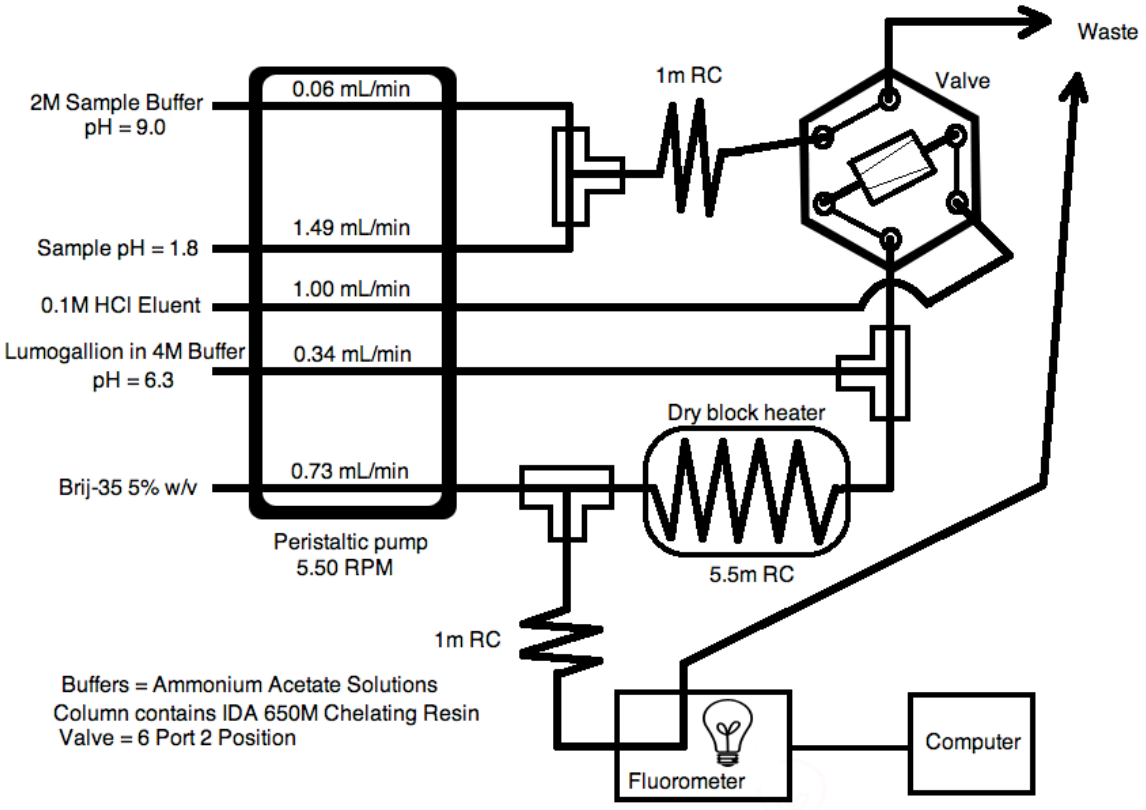

Figure 6 – FIA Manifold used for the Al analyses performed. Variations from the manifold used by Brown and Bruland (2008) include the absence of a pre-conditioning step, which eliminates the need for a second valve, a reduced pump speed, and a shorter amount of reaction coil placed in the dry block heater.

Key differences between the method used here and that of Brown and Bruland (2008) are the lack of a column conditioning step and a slower pump speed and concomitant reduction of reagent flow rates. We opted not to include the column conditioning step as it required the use of a second injection valve, and felt based on the arguments and results posed by Brown and Bruland (2008) that the benefit of the column conditioning step (~6% increase in sensitivity) was outweighed by our ability to reduce both instrument complexity and analysis time for our relatively (compared to open Pacific Ocean samples) high Al samples

collected in the Arctic. According to Brown and Bruland (2008), the incorporation of a column conditioning step increased the Al retention of the column, which was seen as a 6% increase in the method's sensitivity for a 60 s load time. The increased sensitivity was attributed to the iminodiacetate (IDA) sites of the pre-concentration resin not being protonated at the time of sample introduction, thereby making the column less susceptible to sample "breakthrough" (Brown and Bruland, 2008). By contrast, it was argued that "if the buffered sample were to be loaded onto a protonated form of the resin [i.e. an unconditioned column], the dissolved Al first entering the column would not be complexed by the IDA functional groups during the time necessary for the ion exchange sites to be deprotonated" (Brown and Bruland, 2008). In light of these arguments we felt that the minimal (6%) increase in sensitivity did not merit the increased complexity of the FIA manifold and additional time required to analyze each sample. Furthermore, the use of lower flow rates should largely eliminate the requirement to precondition the column since the lower flow rates will increase the time the sample will be in contact with the IDA resin, thereby increasing the possibility that Al will be retained on the column. Another deviation from the method of Brown and Bruland (2008) is the use of a 2 cm commercially available pre-concentration column equipped with non-metal frits (Global FIA), which has since been adopted by Brown (Pers. Comm.). Other minor modifications include the inadvertent increase in the volume of Brij-35 supplied to the reagent stream, the use of commercially available reaction coils (Global FIA), and the use of an ASX-260 autosampler (CETAC).

Data acquisition, valve actuation and autosampler operations were accomplished using the Flo-ZF software (Global FIA, Fox Island WA, USA) and a serial data acquisition card (Omega Controllers). The operating parameters of the dry block heater, fluorometer, and data acquisition card are provided in the table below.

Table 1 - Operating Parameters for Shimadzu RF-535 Fluorometer and Omega Data Acquisition Card

Parameter	Value
Shimadzu RF-535 Fluorometer	
Chart Recorder Output	10 mV
Range Setting	1
High Sensitivity	On
Response Setting	Slow
Excitation Wavelength	485 nm
Emission Wavelength	552 nm
Omega RS-232 Data Acquisition Card	
Input Voltage Range	0 - 0.1 V
Input 1	00.00
Read 1	00.00
Input 2	05.00
Read 2	08.00

2.3.1 Reagent Preparation

The reagents used for the FIA method were prepared as reported by Brown and Bruland (2008) with the ammonium acetate (NH_4CH_3COO) buffers prepared in 2 L bulk solutions to minimize day to day variability. Nevertheless, a summary of the reagent preparation is provided below:

Ultra-pure NH_4CH_3COO: Trace metal grade NH_4CH_3COO crystals were synthesized in the class 100 laboratory space by bubbling high purity anhydrous ammonia gas at 34.5 kPa (5 psi) into acetic acid that was twice distilled in a Teflon sub-boiling distillation apparatus. The solution was cooled throughout the process by placing the bottle containing the acetic acid in a room temperature water bath to facilitate the formation of the NH_4CH_3COO crystals. Furthermore, the process was typically halted before all the acetic acid was able to react and the supernatant was poured off to minimize the incorporation of contaminating metals into the crystal lattice. Milli-Q was then added to the NH_4CH_3COO crystals to yield a saturated solution that has a reported concentration of 19.2 M (Brown and Bruland, 2008). This saturated solution was then used to prepare the two buffers described below.

Sample Buffer: The 2 M NH_4CH_3COO buffer was prepared by adding 232 g of the saturated NH_4CH_3COO solution to a 2 L Teflon bottle, which was then filled with Milli-Q and adjusted to a pH of 9.0 ± 0.1 with trace metal grade ammonium hydroxide.

Reaction Buffer: The 4 M NH_4CH_3COO buffer was prepared in the same manner as above but twice the mass of the saturated NH_4CH_3COO solution was used and the pH was adjusted to 6.3 ± 0.1 with trace metal grade ammonium hydroxide.

Lumogallion: The 4.8 mM stock solution was prepared by adding 50 mg of lumogallion to 30 mL of Milli-Q in a Teflon bottle. For the lumogallion-buffer solution, 1 mL of this stock was added per 100 mL of the reaction buffer.

Brij-35 solution: A 5% w/w solution was prepared by dissolving 50 g of solid Brij-35 (available from Sigma-Aldrich) into a 1 L Teflon bottle filled with Milli-Q. To facilitate complete dissolution of the surfactant, the solution was placed on a shaker table for several hours prior to use.

Eluent: A 0.1 M HCl eluent was prepared for the elution of the column by adding 20 mL of concentrated trace metal grade HCl to 2 L of Milli-Q water.

2.3.2 Precision, Blank Determination and Limit of Detection

To minimize the potential for contamination, all sample analyses were performed in a Class 100 laboratory (i.e a laboratory with a certified air quality of less than 100 particles ≥0.5μm/ft^3 or less than 3520 particles ≥0.5μm/m^3). Furthermore, All samples were analyzed a minimum of three times to achieve an adequate standard deviation by pre-concentrating on the Toyopearl IDA column for 70 or 120 seconds depending on the concentration range of the external calibration. For samples in excess of 50 nmol kg^{-1}, the pre-concentration column was replaced with a sample loop as pre-concentration was not required at elevated concentrations. With the column in place, the precision (%RSD) of the method was determined to be 1.8% based on replicate analyses (n=4) of a 5.4 nmol kg^{-1} Al sample. The limit of detection (3σ) was determined on several occasions to be 0.1 nmol kg^{-1}, typical for the method (Brown and Bruland, 2008). A loading blank, corresponding to the blank from the NH_4CH_3COO sample buffer and sample acidification process was determined by loading Milli-Q (that had been acidified in the same manner as the samples) onto the pre-concentration

column in intervals from 10 to 240 seconds. The slope of the linear response that was obtained by plotting the average peak height as a function of load time was then multiplied by the load time used for the analyses of the samples (typically 70 or 120 seconds) to yield the peak height due to the sample buffer and the acidification process of the samples. A separate 3 point standard addition of Al to acidified Milli-Q was then performed to determine the sensitivity of the method for this matrix. The loading blank was then determined by dividing the above calculated peak height for the acidified Milli-Q by the slope of the standard addition curve. In all instances this blank was less than 0.5 nmol kg^{-1} and were typically around 0.2 nmol kg^{-1}. In addition, the above process could be used to also determine the reagent stream blank by extrapolating the curve for the variable load time of the acidified Milli-Q to zero. The resulting peak height corresponded to a zero load time and when this peak height was subjected to the standard addition curve, the resulting concentration was always below the detection limit reported for the method.

2.3.3 Accuracy and analysis of SAFe Inter-laboratory Standard

To ensure accuracy and reliability of the data presented, analysis of samples from the SAFe inter-calibration program (Johnson et al., 2007) was performed in addition to the daily external calibration curve and blank determination. The results from the analysis of the SAFe samples are presented in Table 2 and for the most part show good conformance with the values reported by Brown and Bruland (2008) and Middag et al. (2009). It appears that Al concentration in the

deep sample, D2 563 was slightly elevated from that reported by the others (Brown and Bruland, 2008). However, our determination of the Al content in the D2 sample falls within the range of acceptable values for the D2 SAFe sample (1.06 ± 0.09 nmol kg^{-1}) when the results from all the participating investigators are averaged (Brown et al., 2010). The slightly elevated concentrations observed for the sample could be the result of minor contamination of the sample through repeated use or may be due to variability in the cleanliness of the bottles used to store the SAFe sample.

Table 2 - Analysis of SAFe inter-calibration samples and comparison to values reported by Brown and Bruland (2008)

Sample	Concentration Al (nmol kg^{-1})	Standard Deviation (nmol kg^{-1})	n
	This Work:		
SAFe S #103	1.60	0.06	4
SAFe S #103	1.57	0.08	4
SAFe S #103	1.65	0.11	3
SAFe S #103	1.66	0.17	4
SAFe S #104	1.53	0.11	4
SAFe S #544	1.67	0.07	8
SAFe S #544	1.62	0.03	6
SAFe D2 #563	1.14	0.03	4
SAFe D2 #563	1.13	0.05	6
	Brown and Bruland (2008):		
SAFe S #57	1.64	0.08	5
SAFe S #214	1.68	0.06	5
SAFe S #574	1.68	0.07	5
SAFe D2 #543	1.00	0.11	4
SAFe D2 #545	1.00	0.12	4
SAFe D2 #549	0.97	0.11	4
SAFe D1 #12	0.67	0.09	5
SAFe D1 #251	0.59	0.12	3
SAFe D1 #563	0.59	0.07	4
Average Al Content in SAFe Samples from incorporation of results from all Participants			
SAFe S	1.71	0.10	5
SAFe D2	1.06	0.09	5

3. Dissolved and Total Aluminum for the Canadian Arctic

3.1 Hydrography of Kugmallit Canyon Transect

The physical and geochemical properties of the Canadian Basin (see Figure 4) have been studied extensively in the last 30 years with the various water masses in the region being identified and characterized by McLaughlin et al. (1996). The waters along the transect display features characteristic of the Western Arctic (WA) where the upper 1000 meters consists of a relatively fresh (26-30 PSS) surface layer, a high nutrient water layer of Pacific origin centered at ~150 m and an Atlantic water mass centered about 400 m depth that is warmer and more saline than its Pacific counterpart. Figures 7 and 8 show the cross-sectional distributions of temperature, salinity, and dissolved oxygen observed along the transect with temperature and dissolved oxygen in colour (Figures 7 and 8 respectively) and salinity in contours. From Figure 7 it is evident that the cold ($T_{min} \approx -1.5°C$), relatively fresh water from the Pacific is centered around a salinity of 33, which is in agreement with findings from other investigators (Aagaard et al., 1981; McLaughlin et al., 1996; Moore et al., 1992). This nutrient enriched water (see Figure 9 for nutrient profiles) originates from the Bering sea and enters the Arctic Ocean via the Bering Strait and is further modified as it transits across the productive shelf of the Chuckchi Sea and enters the Canada Basin. Due to the shallow nature of the Bering Strait, the waters entering the

Arctic are relatively shallow Pacific waters. McLaughlin et al. (1996) have shown that this Bering Sea water is confined to the Canada Basin with its front lying over the alpha-Mendeleev Ridge (Figure 3) and serves as a distinguishing feature between Western Arctic (WA) and Eastern Arctic (EA) water mass assemblies. However, this front does not appear to be permanently stationed over the ridge as Middag et al. (2009), reported the presence of Pacific origin waters for stations in the Makarov Basin. In descending the from the Pacific to Atlantic waters, one encounters an oxygen minimum (Figure 8) at salinity of ~34.2 that is identified as the lower halocline water (McLaughlin et al., 1996). Below this, water of Atlantic origin dominates and is characterized as warmer (-0.16 to 0.6°C) and more saline (S > 34) than the Pacific waters above. This water mass also displays a local temperature maximum, which appears in Figure 7 at about 400 m depth.

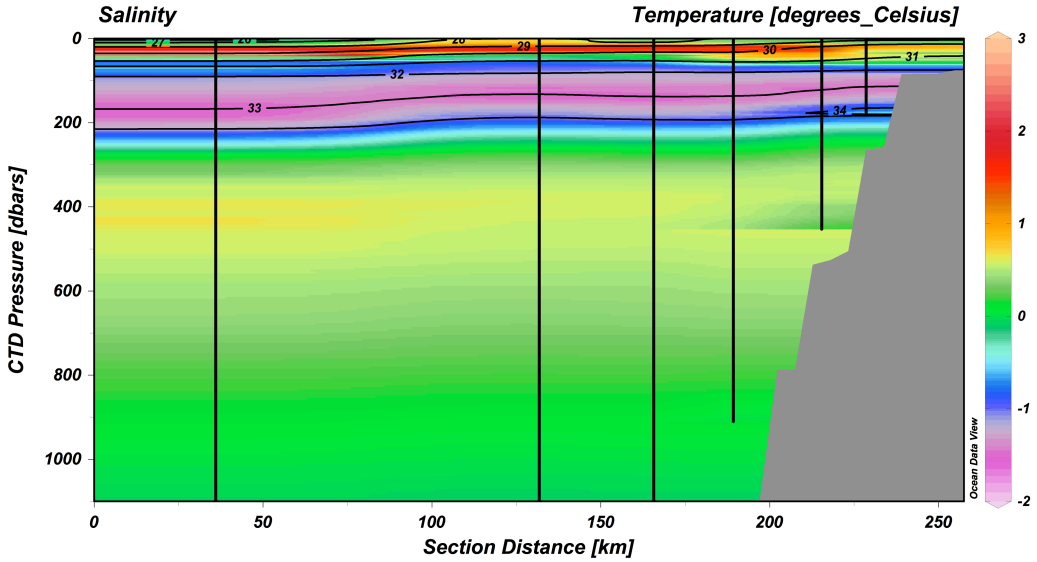

Figure 7 - Temperature and salinity distribution along the KC transect. Temperature is in colour and salinity is in contours. The presence of the Pacific origin waters is evident in the cold layer shown in purple at ~150 meters depth with a salinity of ~33 PSS. Waters of Atlantic origin are centered around the local temperature maximum at 400m depth.

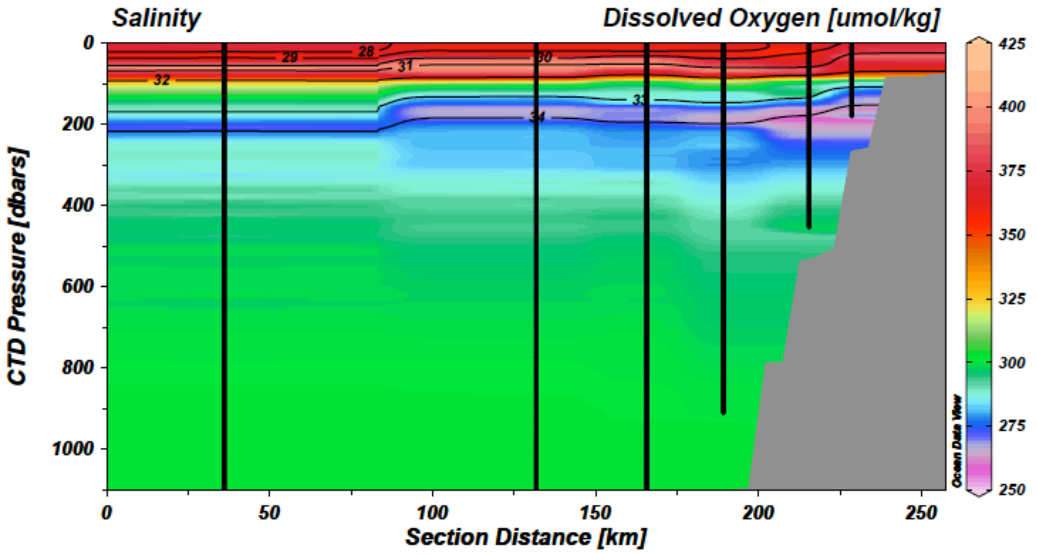

Figure 8 - Dissolved oxygen distribution along the KC transect. Dissolved oxygen is shown in colour and salinity is in contours. The lower halocline water corresponds to the dissolved oxygen minimum shown in purple with a salinity ~34 PSS.

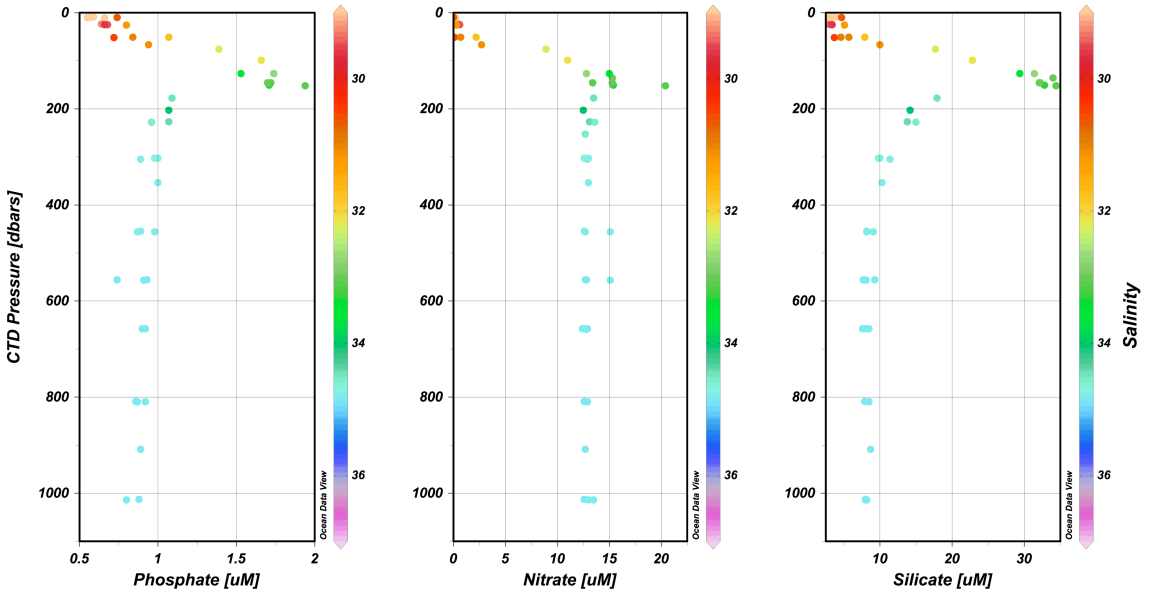

Figure 9 - Nutrients profiles with salinity shown in colour for the six stations along the transect. Note that the nutrient maxima are all centered at a salinity of ~33 PSS corresponding to the nutrient enriched waters of the Pacific inflow from the Bering Sea.

3.2 Distribution of Dissolved Aluminum

3.2.1 Kugmallit Canyon Transect

The vertical distribution of dissolved Al for the six stations along the transect are shown in Figure 10 with a cross-sectional view of the dissolved Al for the transect presented in colour in Figure 11. The red data points in Figure 10 are suspected or known to have been contaminated during the sampling or analysis process and are not included in the colour plot of Figure 11. In order to be labelled as potentially contaminated, a sample would have to display a markedly different salinity than that reported by the CTD for the sample depth

indicating incomplete closure of the GO-Flo bottle at depth and loss of sample integrity. Samples that also were determined to have a lower total Al (Section 3.3) concentrations than dissolved Al concentrations were also labelled as contaminated since the dissolved fraction should be entirely contained in the total Al sample. As can be seen from Figure 10, the dissolved Al displays a similar vertical profile to those observed for other major ocean basins, namely a surface maximum (1-4 nmol kg^{-1}), a sub-surface minimum (< 1 nmol kg^{-1}), and a gradual increase with depth.

The sub-surface minima in the dissolved Al profiles in Figure 10 correspond to the nutrient rich waters of Pacific origin that pass through the Bering Strait and are centered on ~150 m isobath throughout the Canada Basin. The low dissolved Al observed in this water mass is consistent with the known interbasin fractionation (Figure 1) of the element first reported by Orians and Bruland (1985), which indicated that the dissolved Al content in the Pacific Ocean to be 8-40 times lower than that observed by Hydes (1979) for the western Atlantic. This inter-ocean variability is attributed to the short oceanic residence time for Al, estimated by Orians and Bruland (1985) to be on the order of 100-200 years. Below this water mass we encounter the warmer, more saline waters of Atlantic origin and a gradual increase in dissolved Al concentration with depth. The increased Al content in the Atlantic origin waters is in agreement with profiles reported by Orians and Bruland (1985; 1986) and Hydes (1979) for the Pacific and Atlantic Ocean basins respectively.

Figure 10 indicates that the highest dissolved Al observed throughout the water column for all stations along the transect corresponded to the deepest sample collected for a given station. For the three open ocean stations (KC2700 – KC1500) the dissolved Al reached a maximum of 5 - 7 nmol kg^{-1} at a depth of ~1000 m. Approaching the continental slope with stations KC1000 and KC500 we observe increasing dissolved Al concentrations at depth, which is likely due to the samples being collected in close proximity of the water-sediment interface. From the vertical profile in Figure 10 for KC200, it is apparent from the surface maximum and the generally low concentrations of dissolved Al that only the strongly stratified surface and Pacific layers were sampled at the station. Nevertheless, the maximum dissolved Al concentration of just over 3 nmol kg^{-1} was measured near the bottom at 178 meters depth.

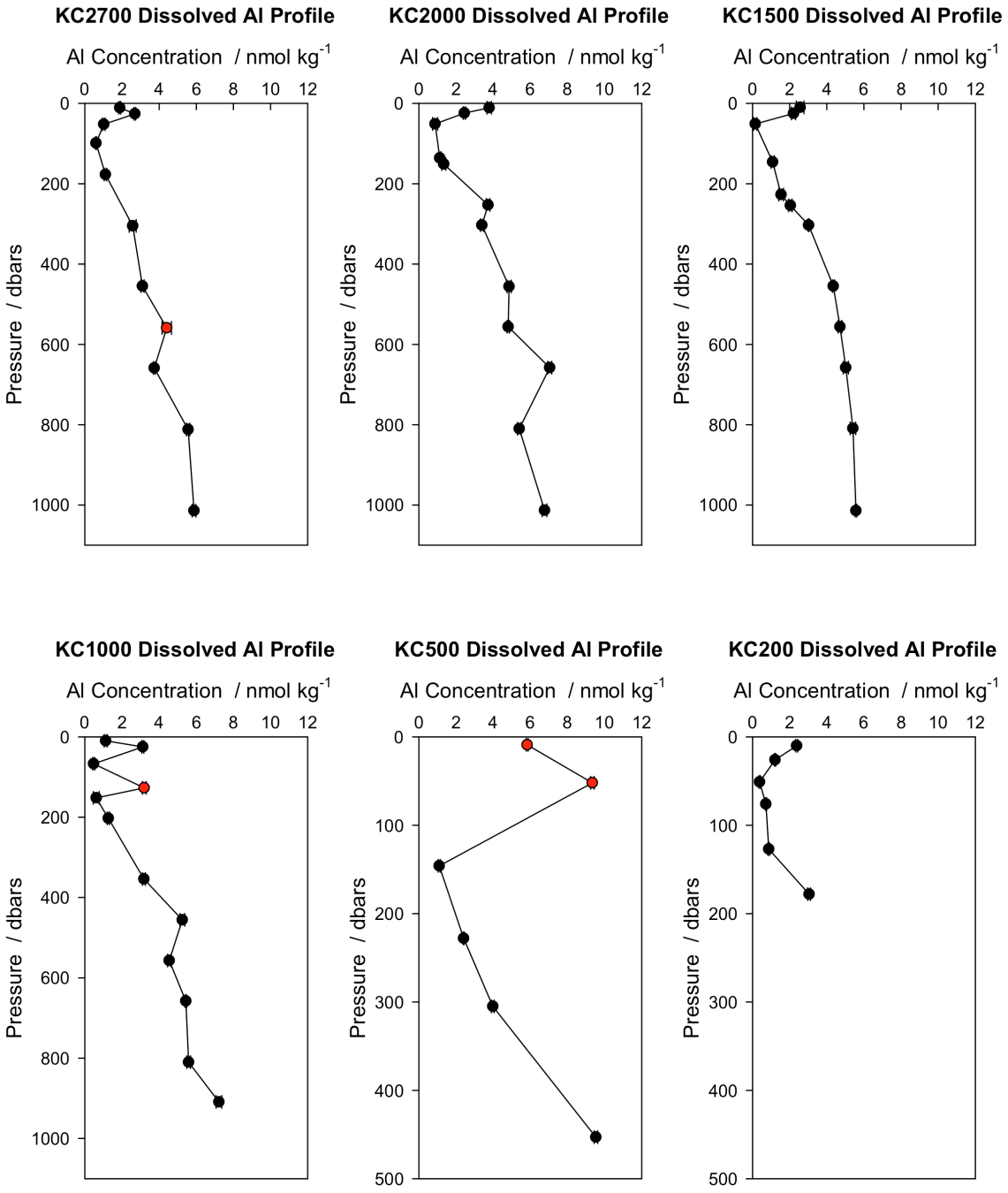

Figure 10 - Vertical profiles of dissolved Al for the 6 stations along the KC transect. Points in red are suspected or are known to have been contaminated.

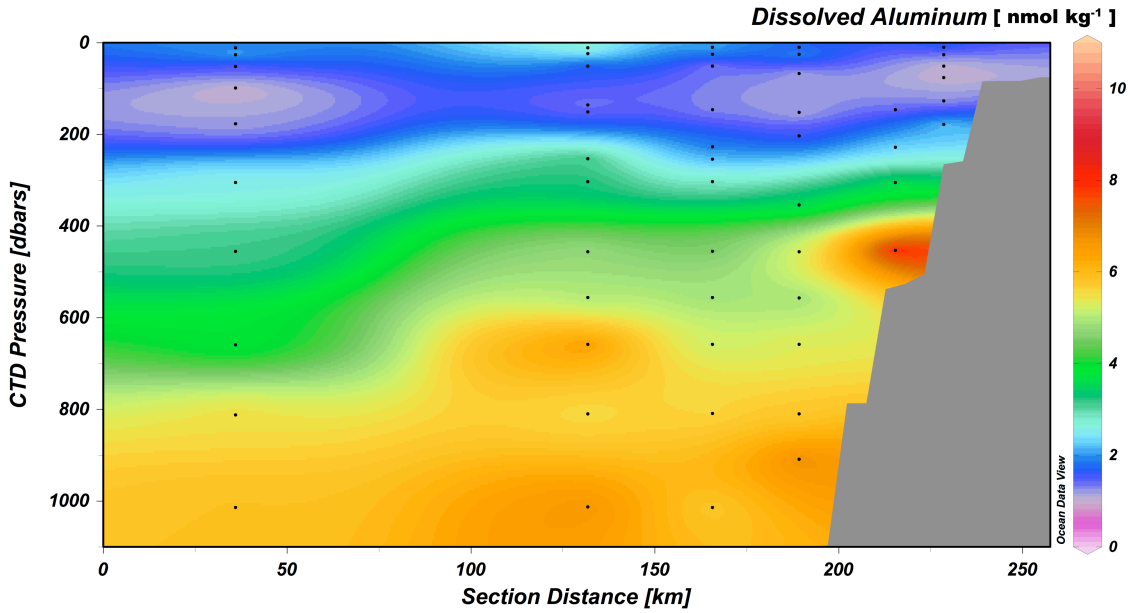

Figure 11 - Colour plot of Dissolved Al along the KC transect. The colour scale on the right is in units of nmol kg^{-1}.

The presence of a surface maximum has not been observed by other investigators that have reported vertical Al profiles for the Arctic Ocean (Middag et al., 2009; Moore, 1981), particularly the Eurasian and Makarov basins. However, Measures (1999) reported concentrations of 2-20 nM for the surface waters of the Arctic Ocean with higher values observed in the Canadian Basin and lower values in the Eurasian Basin. A likely reason for the lack of a surface maximum in Moore (1981) and Middag et al. (2009) is the location of their sampling. Their samples were collected in the ice-pack and were thus unlikely encountering waters that had experienced the impact of recent significant sea-ice melt. Indeed, Moore (1981) collected his samples aboard an ice-raft that transited from the Makarov Basin, over the Lomonosov Ridge, and into the Amundsen Basin while maintaining a minimum latitude of 88ºN. Surface

salinities observed by Moore (1981) and Middag et al. (2009) were ≥ 30 PSS. By contrast, Figure 7 indicates that salinities in the upper 40 meters of the transect sampled here were as low as 26 PSS suggesting considerable sea-ice melt in the region. Furthermore, preliminary barium (Ba) data for the surface waters along the transect "shows that the concentration of Ba decreases as salinity decreases, with a slope indicative of dilution with fresh water with very low Ba concentrations" (Orians, 2010). Given that the nearest alternative source of fresh water, the Mackenzie river (see Figure 4), has a Ba concentration of ~520 nmol kg^{-1}, it is evident that this is not the source of the fresh water (Orians, 2010). The lack of a fresh water influence from the Mackenzie river at our stations is likely a consequence of the intense upwelling favourable winds in the region for much of 2007 (Melling, 2009). Indeed, easterly winds like those observed have been reported to "…draw deeper waters to the shelf surface and drive plume waters [i.e. the Mackenzie river plume] west and offshore (Carmack and MacDonald, 2002). By contrast, the absence of winds or the presence of downwelling favourable winds tend to drive the plume waters eastward and against the coast (Carmack and MacDonald, 2002). The influence of the Mackenzie river on our study site would be expected to more pronounced at such times.

The presence of moderately fresh water and surface maxima in dissolved Al support Measures (1999) proposal that the melting of "dirty sea-ice" represents an important mechanism for the delivery of trace metals to the surface waters of the Arctic Ocean via partial dissolution of the entrained sediments. The

details of how sediment becomes entrained in sea-ice is not well understood, however it is thought to form in the narrow zone between land fast ice and waters that are two deep (typically below 30m) to facilitate entrainment of sediment (Carmack and MacDonald, 2002; Eicken et al., 2005). The work of Eicken et al. (2005) indicates that the re-suspension of sediment during periods of frazil ice formation is required for sediment to become entrained in sea ice. This is further supported by the work of Kempema et al. (1989) who also reported an interaction between frazil ice and re-suspended sediment. Recently the total amount of sediment transported by sea ice over the Chukchi and Beaufort shelves was estimated to be 5 – 8 tonnes (Eicken et al., 2005). The observation of the surface dissolved Al distribution along the transect showed spatial variability with no clear trend towards the shelf suggests that the melting of sea ice containing sediment may be the source of the enhance dissolved Al concentrations reported for the surface waters.

The presence of a surface maximum in the Al concentrations of surface waters of the Arctic may also represent the partial dissolution of terrigenous aerosols that were directly deposited onto the surface waters. Indeed, in 2007 the Arctic experienced the lowest sea-ice coverage ever recorded, leaving the location of sampling in the Canada Basin largely devoid of sea ice (NSIDC, 2007). Furthermore, sampling occurred just a couple of weeks after the sea-ice extent minimum; thus the surface waters were likely exposed to atmospheric inputs for much of the late summer and early fall. Results of a calculation

performed by Middag et al. (2009), suggest that aeolian dust input to the Arctic Ocean would produce a steady state concentration of dissolved Al of 1-3.5 nmol kg^{-1} for the surface waters. To perform the above calculation, Middag et al. (2009) used the highest estimate of aeolian dust input (0.14 g $m^{-2}y^{-1}$) reported by Darby et al. (1989) in combination with the Al input model of Measures and Brown (1996) with solubility of aeolian dust assumed to range between 1.5 and 5%. The range of dissolved Al concentrations predicted by the above calculation are comparable to those observed for the surface waters of the transect. This finding suggests that the inclusion of a second source of Al to the surface waters (i.e. partial dissolution of entrained sediments in sea-ice) is not necessarily required. Given the limited suite of data collected during the cruise by us and fellow collaborators and the supporting circumstantial evidence for both pathways, it is currently not possible to determine their relative contributions or to even distinguish between the two potential sources. It could very well be that both of these processes act on the surface waters in combination to produce the observed surface maxima.

3.2.2 Coronation Gulf Stations

In addition to the six stations of the Kugmallit Canyon transect presented above, two vertical profiles for stations in the Coronation Gulf were analyzed for dissolved Al (Figure 4, Figure 12). Station 24 was located at (67° 54.189' N, 111° 19.601' W) and had a bottom depth of 406 m whereas station 30 was located due north of station 24 (68° 27.440' N, 111° 15.975' W) and was situated in 230

meters of water. The local hydrography is summarized in Figure 13. Stations in the Coronation Gulf were characterized by a lens of warm, relatively fresh (~25 PSS) water at the surface, underlain by a colder, more saline layer at depth. The lower salinities here suggest an absence of Pacific inflow water.

Coronation Gulf stations had low dissolved Al concentrations, with values ranging from 1-3 nmol kg^{-1} and displayed surface maxima and subsurface minima typical for profiles of dissolved Al. The surface maxima observed for these stations are comparable to those observed for the KC transect with concentrations of approximately 2 nmol kg^{-1}. The sample at 100 meters depth is suspected to have been contaminated during the sampling process since the Al and Fe determined from different sample bottles at this depth appear to have significantly and abnormally elevated concentrations. This result suggests that the contamination was likely the result of the GO-Flo sampling device used for the water collection at this depth.

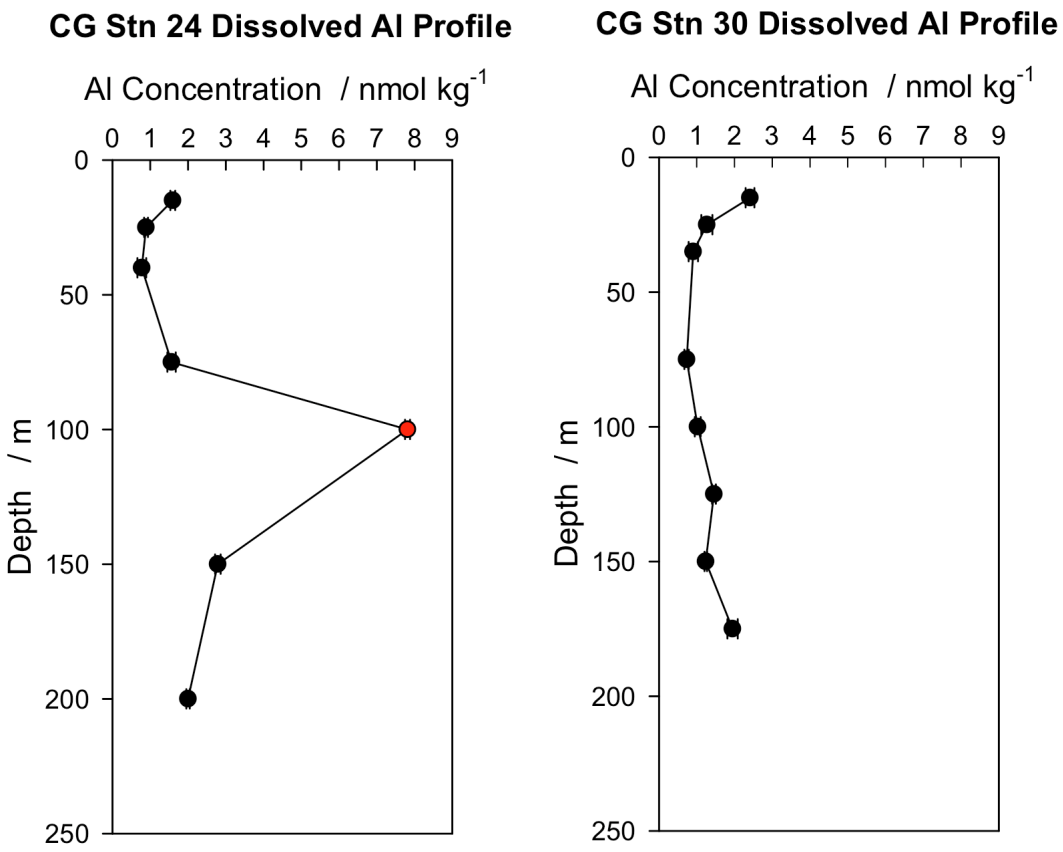

Figure 12 - Vertical profiles of dissolved Al for the Coronation Gulf stations. The point in red is suspected to have been contaminated during sampling. Note that the vertical axis for these stations is depth in meters rather than pressure (dbars).

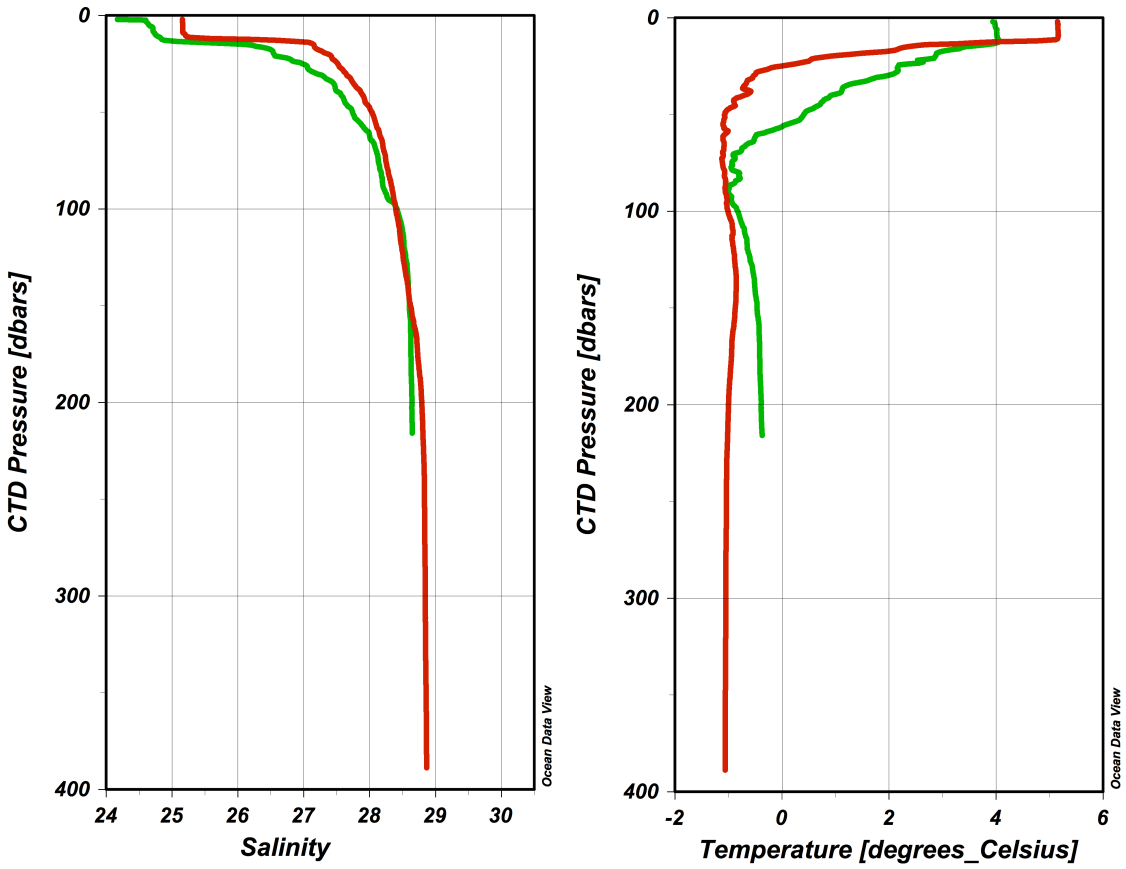

Figure 13 - Temperature and Salinity plots as a function of Pressure for Stations 24 (red) and 30 (green) obtained from the CTD.

With the exception of the presence of a surface maximum, the vertical profiles for dissolved Al reported here agree well with those by Middag et al. (2009) and Moore (1981). Figure 14 is a plot containing the dissolved Al vertical profiles for station KC2700 as well as stations 319-1 and 342-1 reported by Middag et al. (2009). In addition, the vertical profile of reactive Al (unfiltered and unacidified sample) reported for the Makarov Basin by Moore is also plotted in Figure 14 for comparison. Of the 44 stations reported by Middag et al. (2009), stations 319-1 and 342-1 were selected to be included in Figure 14 as they were closest in proximity to those presented by Moore (1981) and this work respectively. From

Figure 14 it is evident that the dissolved Al profile for KC2700 is in good agreement with the neighbouring stations from Middag et al. (2009), showing a general increase with depth and arriving at a concentration of ~6 nmol kg^{-1} at 1000 meters.

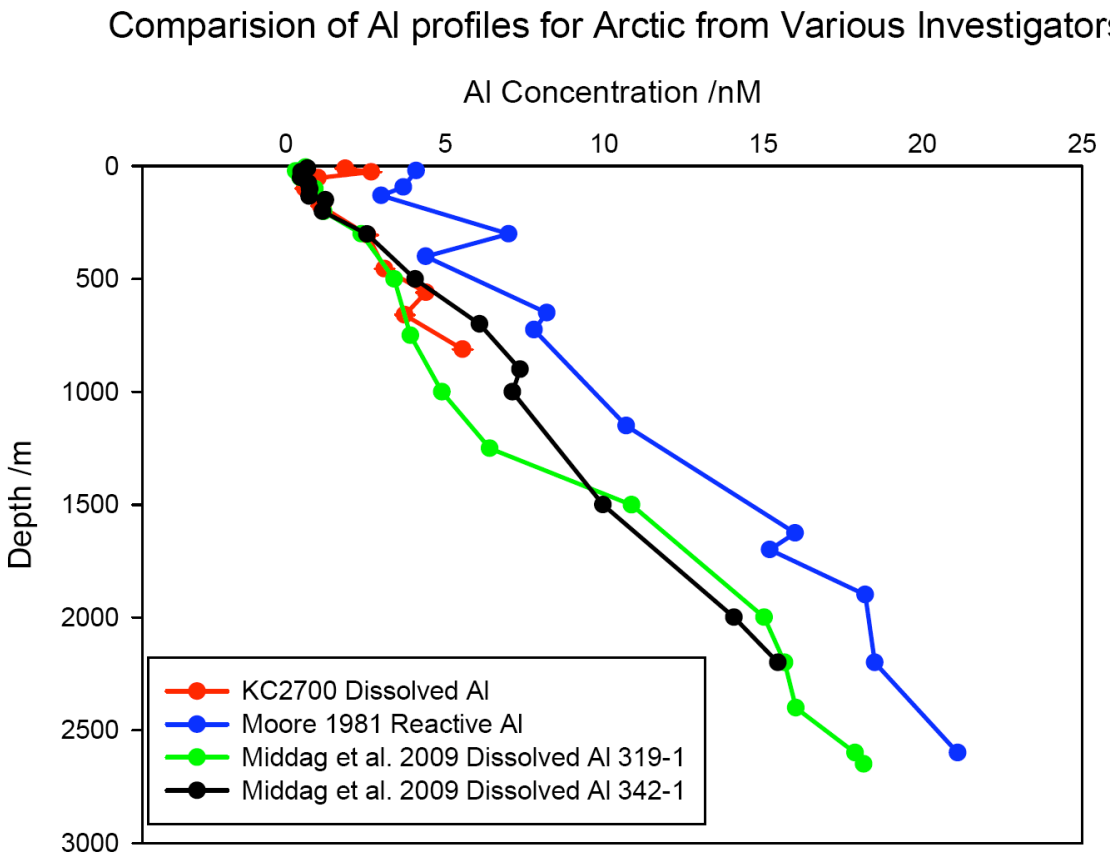

Figure 14 - Comparison of the dissolved Al at KC2700 from the Beaufort Sea to that of Middag et al. (2009) dissolved and Moore's (1981) reactive Al.

3.3 Distribution of Total Aluminum

Samples collected along the KC transect were also analyzed for "total Al". These samples were collected unfiltered, acidified to pH 1.7 (in the same manner as the dissolved Al samples), and stored for two years in acid cleaned LDPE

bottles prior to analysis. It is worthwhile noting that the defining difference between total Al and reactive Al collected by other investigators (Measures, 1999; Moore, 1981) is that the former is acidified for prolonged storage. As such, it is expected that the concentration of Al measured in a total Al sample will exceed that of a corresponding dissolved or reactive Al sample since the acidification process will presumably leach a considerable portion of Al from the alumino-silicates that remain in the unfiltered sample. This is supported by dilute acid leaching experiments performed by Moore and Millward (1984) that suggested up to 20% of the total Al present in atmospheric particulates was not strongly bound in mineral lattices and readily entered solution after the dust laden filter had been shaken in 0.1N HCl for only 2 hours. To our knowledge these samples represent the first reporting of total Al for the Arctic Ocean.

3.3.1 Kugmallit Canyon Transect

Figure 15 shows the vertical profiles of total Al for the six stations of the Kugmallit Canyon transect. The cross-sectional distribution of the total Al along the transect is shown in Figure 16 with the total Al concentrations shown in colour and contours. It is evident from Figure 15 that the total Al profiles experience more variability in their vertical distributions than their dissolved Al counterparts but for the most part retain the general characteristics typical of Al profiles from the World's ocean basins (Hydes, 1979; Moran et al., 1992; Obata et al., 2004; Orians and Bruland, 1985). In particular, the more offshore stations all display a surface maximum with concentrations ranging from 5-20 nmol kg^{-1}, a

sub-surface minimum of ~2-3 nmol kg^{-1} corresponding to the Pacific inflow, and a gradual increase with depth. However, the shallow stations KC500 and KC200 exhibit irregular profiles and much elevated concentrations that reached as high as 268 nmol kg^{-1} at the 200 meter station. From Figure 16 it can be seen that approaching the continental slope the total Al concentrations rapidly increase, particularly at depth for the coastal stations.

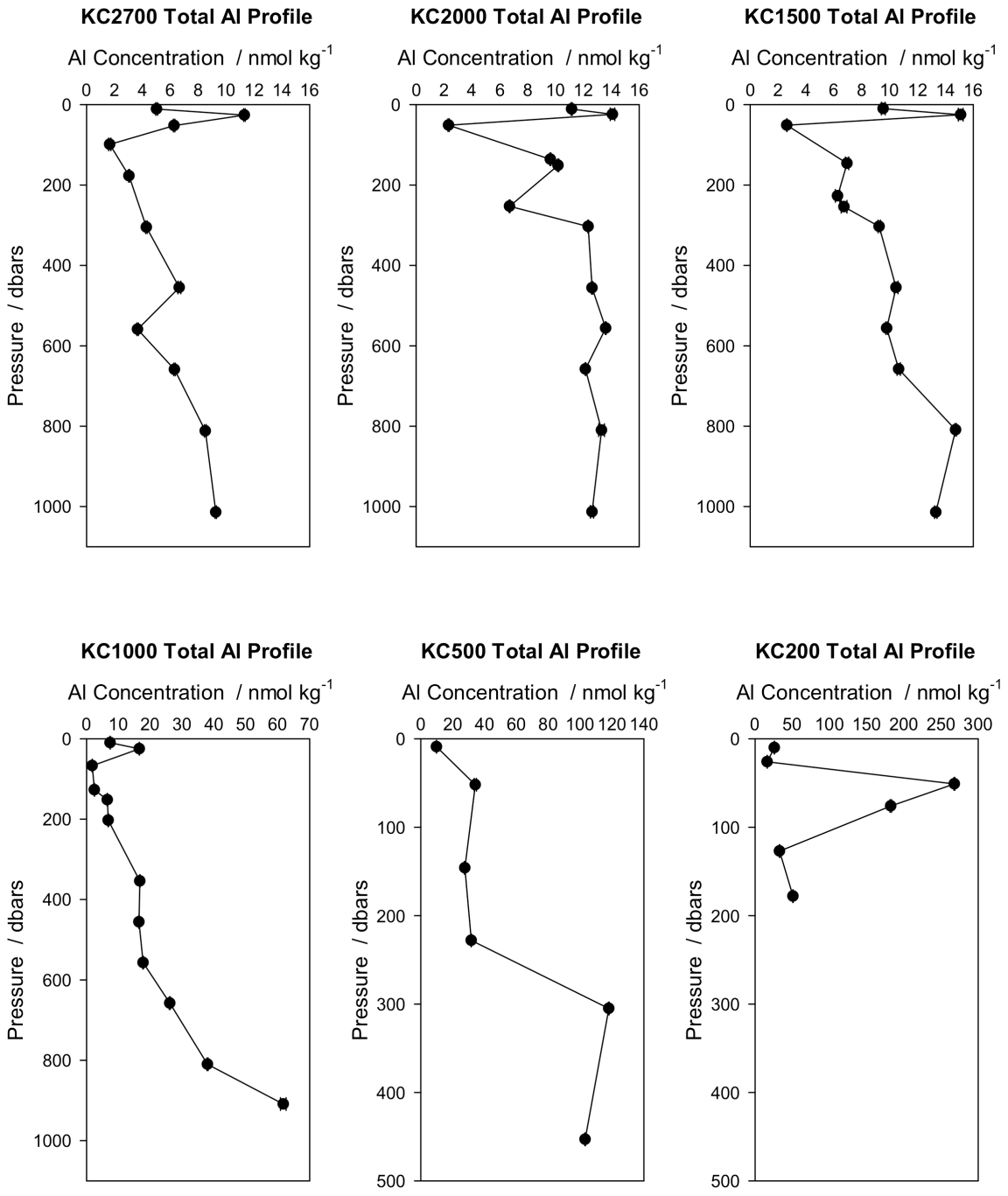

Figure 15 - Vertical profiles of total Al for the 6 stations along the KC transect. Note the 500 and 200 meter stations deviation from the scavenged-like profile typically observed for Al.

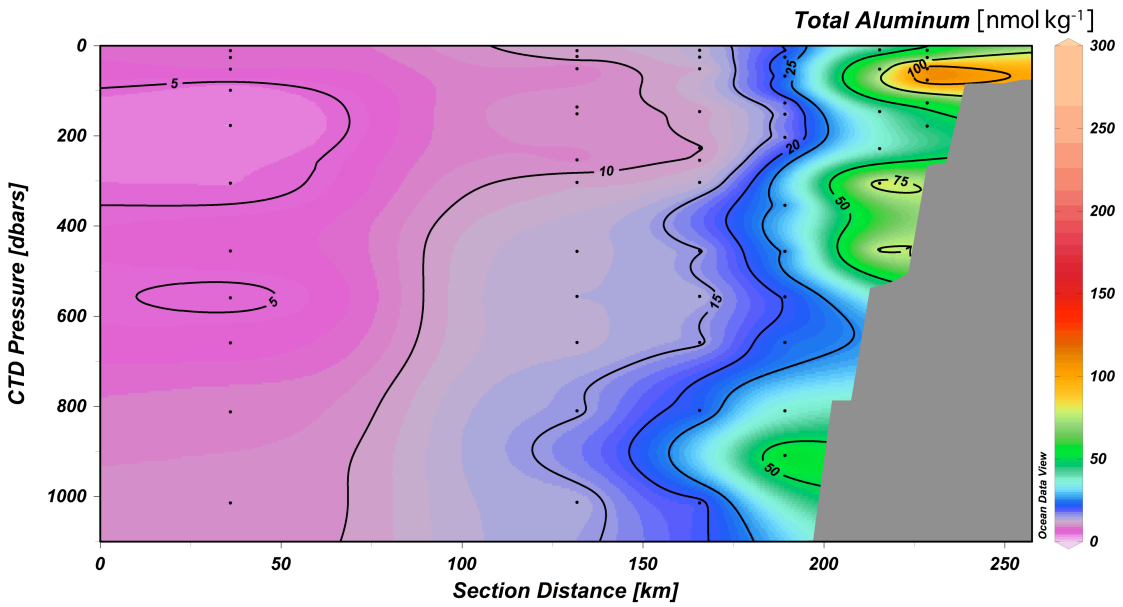

Figure 16 - Colour and contour plot of "total Al" along the KC transect. Note the considerably elevated concentrations of Al neighbouring the continental shelf. The colour scale on the right is in nmol kg^{-1}. The absence of a 250 nmol kg^{-1} contour for the 200 m station is an artifact of the gridded averaging performed by the Ocean Data View software in generating the figure and the relatively low resolution of the trace metal sampling. Caution should, therefore, be exercised when interpreting the contour plots.

Figure 17 shows the percentage of the total Al observed along the transect that corresponds to the dissolved Al fraction. In general, as one approaches the continental shelf, the dissolved component of the total Al measured becomes increasingly attenuated, suggesting that a significant particulate contribution to the total Al is present near the shelf. Indeed, with the exception of the surface samples, the dissolved Al faction for the most coastal station was typically less than 10% of the total Al observed. By contrast, for KC2700 the dissolved Al constitutes approximately half of the total Al observed

for the station. From Figure 17 it is evident that a considerable fraction of the Al in the water column resides in the particulate (>0.2 μm) phase.

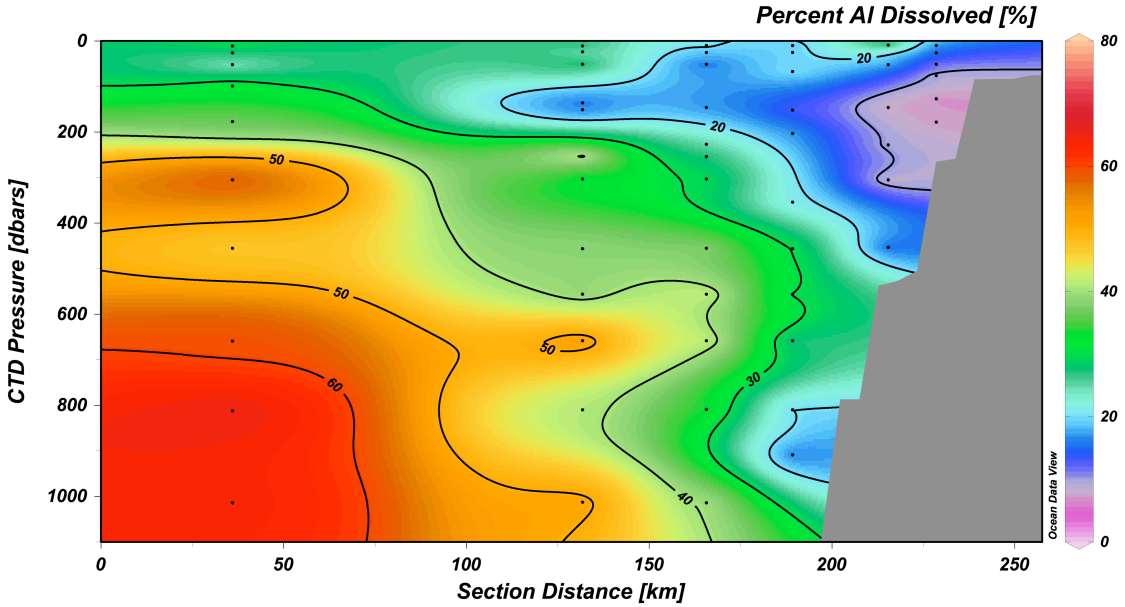

Figure 17 - Percent of total Al that is in the dissolved phase indicating a significant particulate load in the waters as one approaches the continental shelf. The percent of total Al in the dissolved phase is calculated by dividing the concentration of Al determined for the dissolved Al sample by that determined for the total Al sample and multiplying by 100 to represent the data as a percentage of total Al.

Interestingly, it is postulated that for the open ocean the dissolved Al fraction comprises of over 90% of all the Al in the water column (Broeker and Peng, 1982; Measures, 1999). The discrepancy between this proposed partitioning and that reported for the most off shore stations of Figure 15 is largely due to the KC stations being moderately close to shore and the fact that the Arctic Ocean, with its extensive shelves and considerable riverine discharge, is much more terrestrially influenced than most other ocean basins (Aagaard et al., 1981).

3.3.2 Upwelling of Canadian Basin waters onto Mackenzie shelf

The high total Al and particulate load neighbouring the continental shelf as evident from Figures 16 and 17 suggest that a considerable amount of sediment material has been re-suspended into the deep waters of the coastal stations. Although the cause of this re-suspended sediment is not known for certain, it is believed that this is the result of Canada basin waters being upwelled onto the Mackenzie shelf, thereby disturbing the sediment along the shelf. Indeed, the persistence and strength of the prevailing winds from the East-South-East (Melling, 2009) in 2007 likely displaced the sea-ice and low salinity surface waters westward and offshore, resulting in the region of the Mackenzie shelf to experience considerable upwelling. Thus cool halocline waters of the adjacent Canada Basin were upwelled onto the shelf and driven inshore, possibly reaching the surface at some locations (Melling, 2009). Upwelling of this magnitude would likely result in considerable re-suspension of sediment, thereby accounting for the elevated total Al concentrations and particulate load observed for the coastal stations. Further evidence of upwelling is found in an expansion of a temperature-salinity plot for the bottom waters for the six stations along the transect (Figure 18). From Figure 18 it can be seen that the curves for all the stations along the transect essentially overlap one another supporting a common source for subsurface waters. This finding is in agreement with what would be expected for waters from the Canada Basin being upwelled onto the shelf.

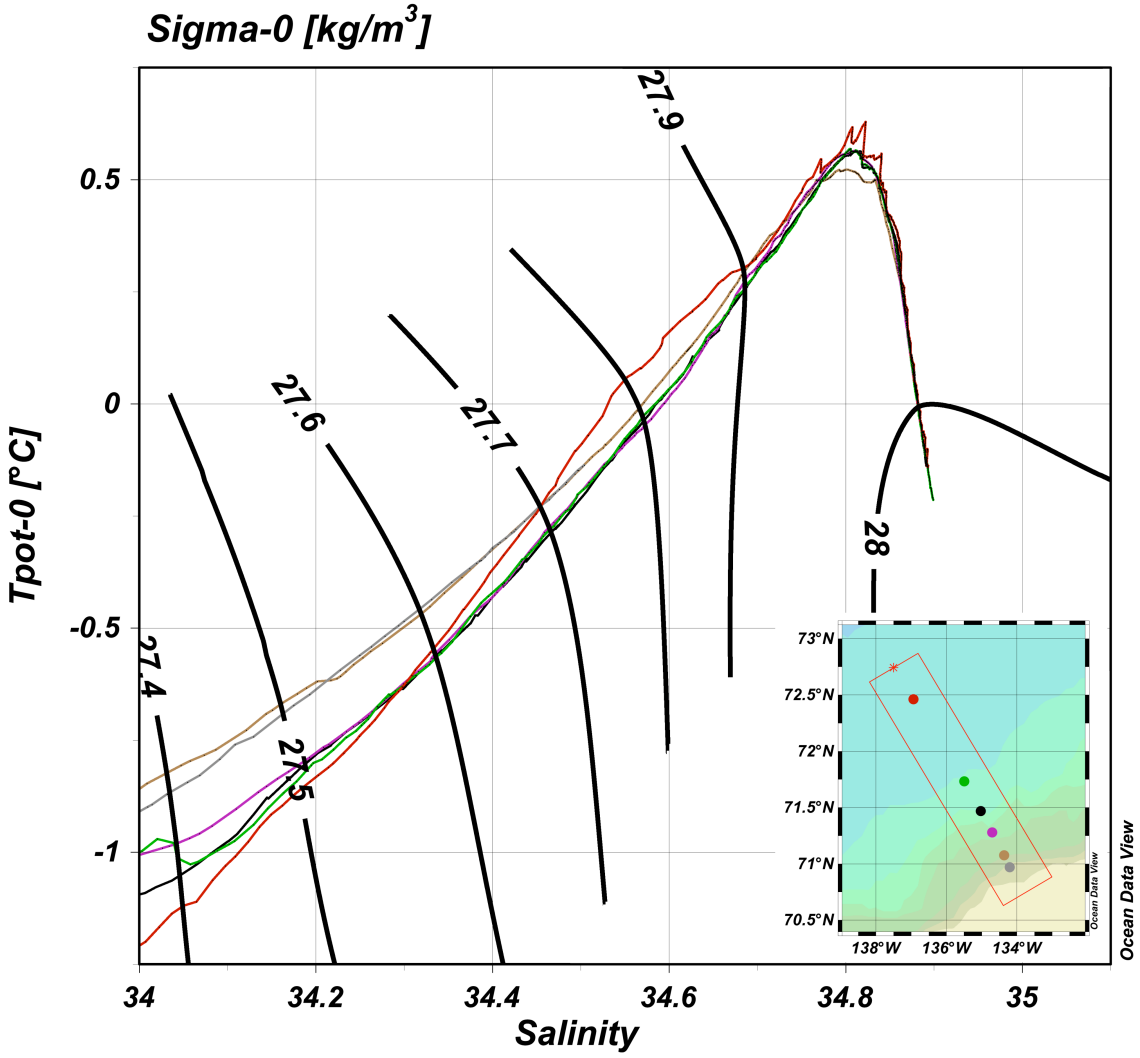

Figure 18 – Temperature-salinity plot for the bottom waters for all six stations along the transect. The observation that each of the curves are very close to one another on the plot indicates that the deep waters along all the stations of the transect likely share the same source. Furthermore, this plot which suggests that Canada Basin waters were upwelled onto the shelf during the time of sampling. KC2700: Red, KC2000: Green, KC1500: Black, KC1000: Purple, KC500: Brown, KC200: Grey.

3.3.3 Brine Enriched Shelf Waters

The high total Al waters neighbouring the continental slope may also result from shelf water that has experienced significant brine exclusion during sea-ice formation. This cold, saline brine-enriched shelf water inevitably descends the continental slope, eventually spreading out over the Canada Basin. The existence of dense, shelf brine waters has been discussed extensively in the literature (Aagaard et al., 1981; Melling, 1993; Melling and Lewis, 1982; Williams et al., 2008). The formation of brine waters over the extensive continental shelves of the Arctic Ocean may result in a significant amount of trace metals being supplied to the Arctic Basins as they cascade down the continental slope and spread out along their respective isopycnals (Measures and Edmond, 1992; Middag et al., 2009). This process is likely to resuspend sediment (Moran and Moore, 1991) the partial dissolution of which could serve as an additional source of Al to the deep waters (Middag et al., 2009). This dissolution may increase with depth given the enhanced solubility of aluminosilicates with increasing pressure (Moore and Millward, 1984). This is supported by the findings of Rusakov et al. (2004), which reported that the dense, shelf-derived waters from the Barents Sea delivers terrigenous particulate matter, rich in Al into the Nansen Basin. However, the lack of pronounced T and S anomalies in Figure 18 indicate that the impact of brine exclusion on the observed total Al distribution indicates brine exclusion to have only a relatively minor effect on the bottom waters along the transect during our study period.

3.4 Concluding Remarks

The dissolved Al profiles reported here for a transect extending beyond the Kugmallit canyon into the Canada Basin of the Beaufort Sea display a surface maximum and a scavenged-like profile, similar to those reported for other ocean basins. Contrary to previous profiles of dissolved Al for the Arctic Ocean, the surface waters along the transect were characterized by a surface maximum in dissolved Al concentrations. This apparent discrepancy is thought to be due to the locations of sampling and the degree in which other investigators were observing sea-ice melt. For the dissolved Al reported here, the surface maxima occur in a lens of relatively fresh water, with salinities as low as 26 PSS, which is approximately four salinity units lower than that observed by other investigators who have reported Al profiles for the Arctic (Middag et al., 2009; Moore, 1981). Analysis of preliminary Ba data for the surface waters along the transect indicate the source of the fresh water input to be due to sea-ice melt as opposed to the Mackenzie river plume (Orians, 2010). This is in agreement with the region experiencing consistent easterly winds that forced the ice and Mackenzie river plume offshore and away from the Kugmallit Canyon transect.

Our findings support the model put forth by Measures (1999) that the melting of sea-ice containing entrained sediments may be an important source of trace metals such as Al to the surface waters of the Arctic. Surface maxima may also have been driven in part as the result of increased aeolian deposition of terrestrially derived Al given the drastically reduced sea-ice coverage in the

Canada basin observed during our study in 2007. Currently, we are incapable of distinguishing between the two potential sources, thus their relative importance in contributing to the surface dissolved Al concentration remains unresolved.

Collection and analysis of total Al samples along the transect indicate that within the water column there exists a significant portion of Al that resides in the particulate (>0.2 μm) phase. This is particularly evident near the continental shelf where concentrations of total Al exceeded 260 nmol kg^{-1} at the 200-meter station. This finding suggests that previous assumptions regarding the partitioning of Al within the water column may require refinement.

The presence of relatively cold, dense waters at the bottom depths of the coastal stations is thought to be due to the upwelling of Canada Basin halocline waters onto the continental shelf. Evidence of upwelling is found in an expansion of a temperature-salinity plot for the bottom waters for the six stations along the transect (Figure 18) whereby the curves for all stations along the transect converge, thereby indicating a common source for the subsurface waters. The presence of Canada Basin waters on the continental shelf is likely due to the upwelling favourable winds that were observed for much of the year prior to our time of sampling (Melling, 2009). Upwelling of this nature is likely to result in considerable re-suspension of sediments, which may account for the elevated concentrations of total Al observed at depth for the three most coastal stations. These bottom waters contain significantly elevated concentrations of Al that

result from re-suspension and partial dissolution of terrigenous and sediment particulates. Al concentrations at depth could further intensify due to the pressure-dependent solubility of solid phase Al (Moore and Millward, 1984).

4. Development of a Low Volume method for the Determination of Al in Coastal and Natural Waters

Although many techniques have been developed for the determination of Al in natural waters (MacCarthy et al., 1993), few have the sensitivity required for use in coastal waters and even fewer for are capable of measurements of Al at oceanic concentrations (Brown and Bruland, 2008; Measures and Edmond, 1989; Orians and Bruland, 1986; Resing and Measures, 1994). Furthermore, many of the methods developed involve chelating the analyte with a ligand, with subsequent detection by spectrophotometric, or sometimes by the more sensitive, fluorometric means (MacCarthy et al., 1993). Often many of these methods are plagued with interferences from other metals due to the ligand's poor selectivity for the analyte. The ligand's shortcomings are typically then accounted for by the addition of a second ligand to the sample to mask (complex) the interfering element, thus requiring further intervention on the part of the analyst. Historically, this was not an issue as these methods were primarily developed as batch methods that required the analyst to perform a considerable amount of sample manipulation. Nevertheless, many of the more sensitive and user-friendly chemistries have been adapted for use in flow-based methods, thus making the method amenable to automation (Bohrer et al., 1998; Resing and Measures, 1994).

Despite the above noted downsides to the derivitization and detection approach, a few methods using this analytical scheme have been developed that are relatively free from interference yet sensitive enough for the determination of Al at the nano-molar (nM) levels found in seawater. In particular, Orians and Bruland (1986) have described a method whereby the Al in a 250 g sample is extracted with 8-hydroxyquinoline and subsequently detected using atomic absorption spectroscopy. This method however is not compatible with shipboard determination, is labour intensive, and requires a considerable amount of sample. Measures and Edmond (1989) have successfully performed Al determinations at seawater concentrations by chelating the Al in a 15 mL sample with 1,1,1-trifluoro-2,4-pentadione and extracting the sample into an organic solvent for detection by electron capture detection gas chromatography. This method, while capable of shipboard use, suffers from a lack of non-contaminating instrumentation capable to automate the solvent extraction, thereby limiting the sample throughput for the method (Measures and Edmond, 1989).

One methodology that has seen considerable use in the determination of Al in seawater involves the chelation of the analyte with lumogallion (2,2',4'-trihydroxy-5-chloroazobenzene-3-sulfonic acid) followed by fluorometric detection of the complex at ~570 nm when excited with light of ~485 nm wavelength. The method was first described by Shigematsu et al. (1967) as a sensitive method for the fluorometric detection of Al or Gallium depending on the reaction pH used, but noted an interference from iron. Hydes and Liss (1976) later adapted the

chemistry for use in a batch method for the determination of Al in natural waters and reported a detection limit of 1.9 nM. Furthermore, they reported that the interference due to iron was less significant than previously reported by Shigematsu et al. (1967), but noted that fluoride attenuated the analytical signal. To account for the affects of fluoride, Hydes and Liss (1976) employed an incremental calibration procedure. This method was improved upon by Howard et al (1986) by incorporation of a surfactant, Triton X-100, to yield a micellar-enhanced fluorescence signal. The addition of the surfactant resulted in an improved detection limit of 0.4 nM and a precision of 3% for a 10 nM sample. In search of an efficient method for the shipboard determination of Al that permitted automation and minimized sample preparation, Resing and Measures (1994) adapted the lumogallion chemistry for use with flow injection analysis (FIA). Their system involved pre-concentration of the sample onto a 8-hydroxyquinoline (8-HQ) column and also incorporated the use of a surfactant. However, these investigators opted to employ Brij-35 as their surfactant as they observed that the previously used Triton X-100 produced a significant amount of background fluorescence at the same wavelength the Al-lumogallion complex was found to fluoresce. Resing and Measures (1994) reported a detection limit of 0.15 nM and a precision of less than 2% at 2 nM for their flow-based method. Despite the methods wide acceptance, Tria et al. (2007) noted the method could benefit from the incorporation of a commercially available resin. The synthesis of the 8-HQ resin is reported to be very time consuming, requiring 7 to 15 hours to synthesize depending on the procedure followed (Dierssen et al., 2001; Landing et al.,

1986). Also, variable inter-batch quality has resulted in Tria et al (2007) reporting variable elution patterns resulting in non-ideal peaks when using 8-HQ. Recently, Brown and Bruland (2008) improved on the flow based method with the use of a commercially available IDA pre-concentration resin, online buffering of the acidified seawater sample and the inclusion of a column conditioning step to minimize sample break through. These improvements appear to have resulted in a slight reduction in the detection limit for the method, which was reported to be 0.1 nM (Brown and Bruland, 2008).

The goal of this work is to develop a low volume sequential injection method for the accurate and precise determination of Al in aqueous media at nano-molar concentrations. The use of a SIA manifold will permit an on-demand approach to providing the various reagents to the reagent stream rather than a continuous flow of reagents as is used in FIA methods. It is believed that this approach will greatly reduce the consumption of reagents and sample as well as reduce the volume of waste produced. Furthermore, the use of a high precision rotary style pump that is capable of accurately delivery fluids on the micro-litre scale should allow for an unparalleled level of optimization of the reaction chemistry, potentially increasing the sensitivity of the method. Lastly, the high level of automation associated with SIA should permit the development of a method that is capable of high sample throughput while minimizing the amount of sample handling from the analyst.

4.1 SIA Instrumental Setup

Typically, manifolds for sequential injection analysis (SIA) are comparatively more complex than those used in flow injection analysis (FIA). However, the SIA manifold reported here for the low volume determination of elevated concentrations of Al in coastal and natural waters is relatively simple with valve actuation, data acquisition, as well as operation of the low volume rotary piston pump (MilliGAT, GlobalFIA Fox Island, WA USA) and the ASX-260 auto-sampler all being controlled via a computer using the FloZF software (Global FIA).

As can be seen from Figure 19, the manifold consists primarily of a selection valve (with a minimum of 4 ports) connected to 5 meters of mixing coil that is then connected to a MilliGAT rotary style pump via the central port of the valve. This particular pump is capable of aspirating and dispensing volumes on a microlitre (μL) scale with high precision. These components of the SIA manifold were supplied as a part of a Mini-Flo Pro Zone Fluidics system that is commercially available from Global FIA and are used for the interlacing and delivery of all the reagents with the exception of the Brij-35 surfactant. The delivery of the surfactant to the reagent stream is performed using a combination of a peristaltic pump and a second selection valve that is situated down-stream of the peristaltic pump. The Brij-35 solution is constantly being pumped through 2-stop Tygon tubing and into the selection valve where it is typically being recycled into the bulk 5% Brij-35 solution.

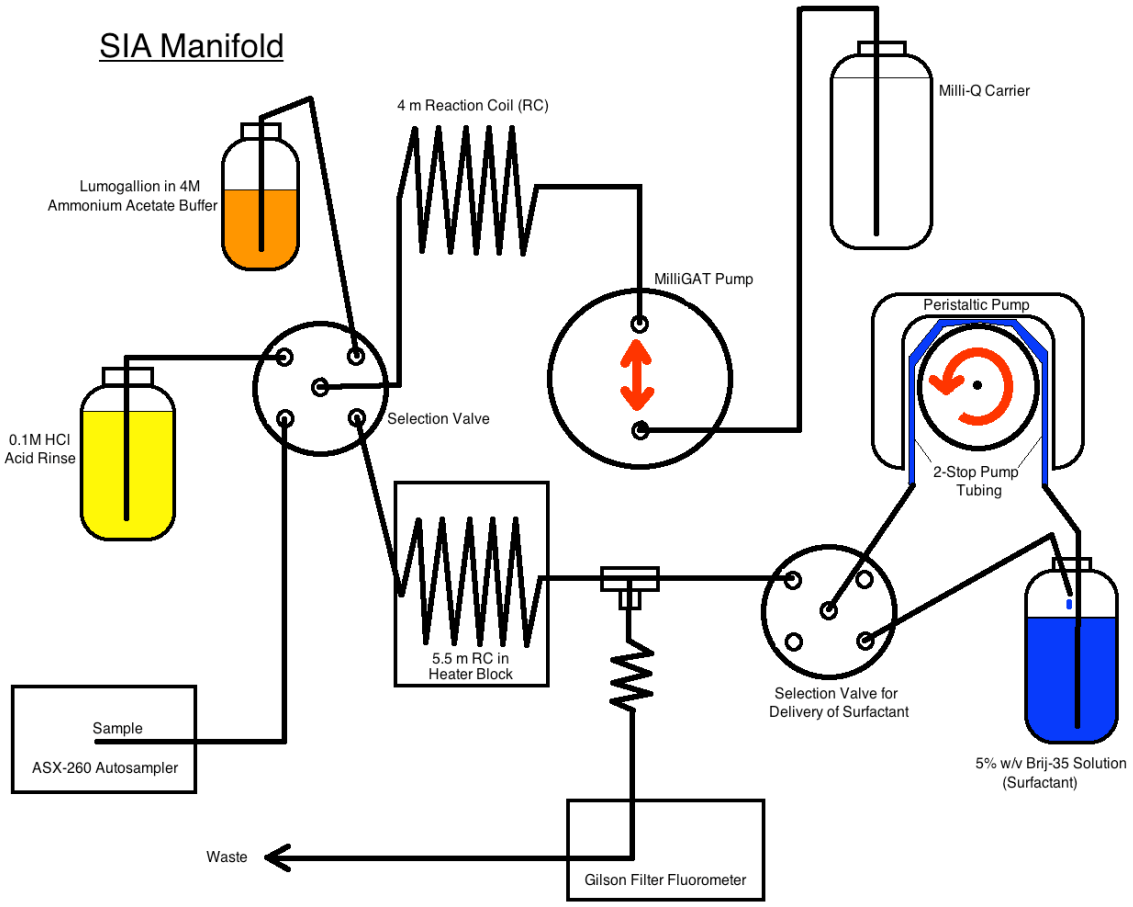

Figure 19 - Schematic of SIA manifold. MilliGAT Pump is a rotary style push-pull pump capable of micro-litre precision

However, when the selection valve is actuated, the surfactant is sent to a T-connection where it meets the reagent stream containing the lumogallion – sample mixture that has passed through the heater (see below) and is en route to the detector. It should be noted that the setup used for the delivery of the surfactant to the reagent stream essentially mimics a second MilliGAT pump that could also be used to deliver the surfactant provided one was available. Immediately after the T-connection described above, the reagent stream (now containing the surfactant) is passed through a 1-meter reaction coil to ensure

adequate incorporation of the Al-lumogallion complex into the micellar system prior to reaching the flow cell of the detector. As mentioned earlier, it is believed that the incorporation of the Al-lumogallion complex within a micelle results in an enhancement of the fluorescent signal due to the increased rigidity of the complex.

The kinetics for the formation of the Al-lumogallion complex have been reported to be rather sluggish, with batch methods performed at room temperature requiring samples to sit overnight to allow the complex to fully develop. Thus, in order to determine the Al content of a sample in a timely manner using this method of detection it is often necessary to heat the sample in the presence of the chelating ligand for a short period to assist the formation of the Al-lumogallion complex. The heating of the reagent stream for the method presented above is performed by placing 3 reaction coils totalling 5.5 meters inside an aluminum block that is cut to fit in a commercially available dry block heater. The dry block heater is capable of maintaining a temperature to within +/- 0.1°C and was set to a constant temperature of 55.5°C, same as that used for the FIA analyses performed previously. However, investigation into the effects of different reaction temperatures on the analytical signal were performed, the results of which will be discussed later on in the chemical optimization section.

The detection of the Al-lumogallion complex was performed by flowing the reagent stream through a 9 μL quartz flow cell of a Gilson Model 121 filter

fluorometer. A diagram depicting the arrangement of the filters around the flow cell along with the operating parameters used for the fluorometer is shown in Figure 20. The excitation wavelength that is incident on the flow cell is regulated by positioning a blue filter immediately in front of the cell so as to allow only light of this colour to irradiate the contents of the flow cell. Similarly, two filters (light blue and orange) were placed in series and fastened to the emission side of the flow cell block, resulting in an effective slit width of approximately 100 nm. The approximate size of the emission slit was determined by the absorption spectrum shown in Figure 21, which resulted from placing the two emission filters in series. The fluorometer's slit width is represented in Figure 21 as the region of the spectrum that does not experience absorption (500 – 600 nm), indicating that light of this wavelength is capable of passing through the series of emission filters. An example of a sequence used for a single determination of the Al content in a sample is shown in Appendix 1.

Schematic and Operating Parameters of the Filter Fluorometer used in the SIA Optimization and Analysis

Operating Parameters of Gilson Model 121 Fluorometer	
Parameter	**Setting**
Effective Slit Width	~100 nm
Range	0.005 R.F.U
Output Port	Auxiliary
Auxiliary Output	1V Full Scale
Time Constant	2.0 seconds

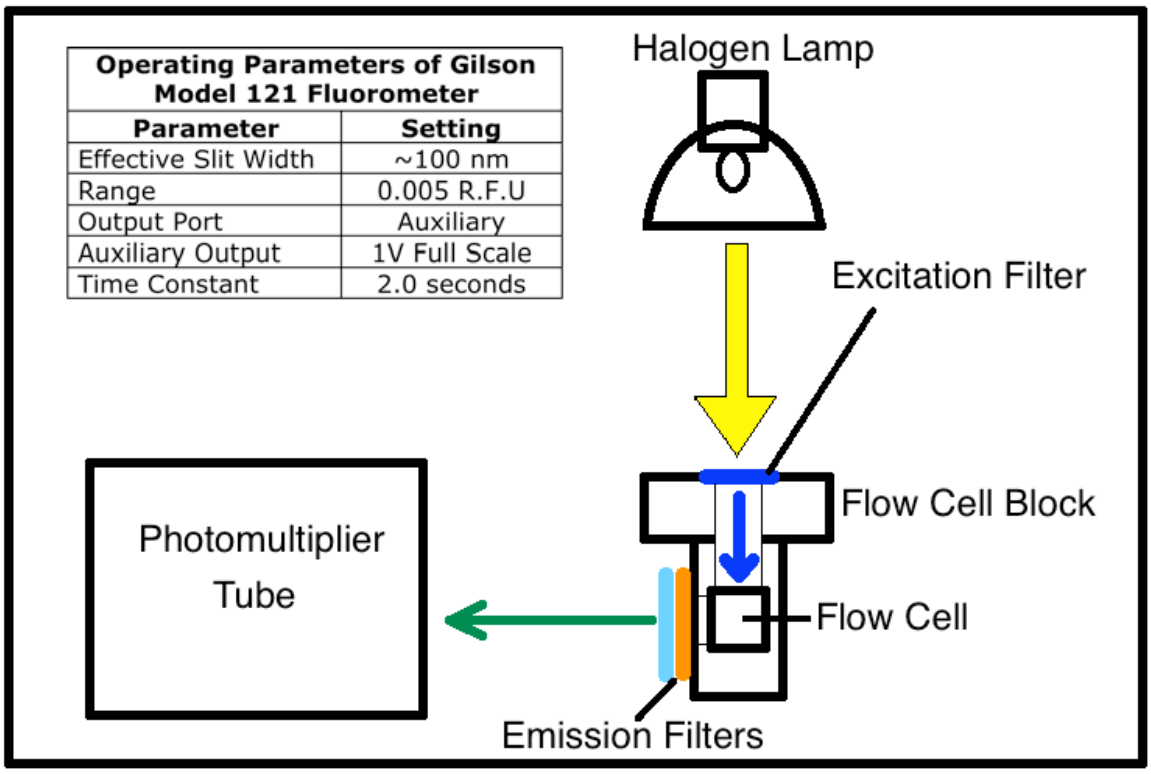

Figure 20 - Schematic and operating parameters of Gilson Model 121 filter fluorometer used for the SIA optimization analysis. Location of excitation and emission filters around flow cell are shown as thick lines coloured in the filters approximate colour.

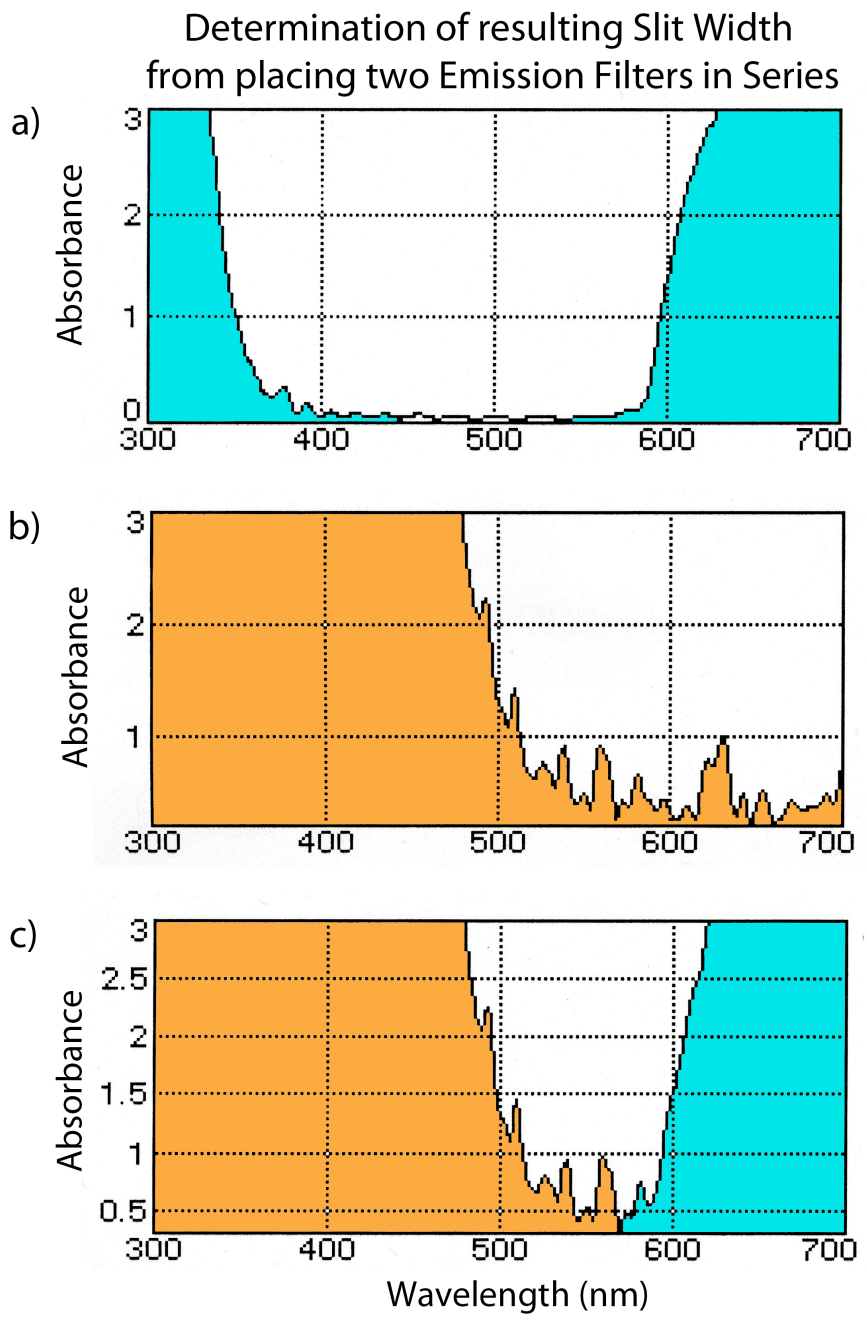

Figure 21 - Determination of effective slit width of Gilson Model 121 filter fluorometer from placing two emission filters in series. Coloured areas correspond to the region of the spectrum where the orange or light blue filter absorbed light. a) Absorbance spectrum of light blue emission filter alone. b) Absorbance spectrum of orange emission filter. c) Absorbance spectrum resulting from placing the two filters in series. The effective slit width is indicated as the ~100 nm non-coloured region shown in Figure c).

4.2 Optimization of Chemistry and Operating Conditions

Although all the reagents used in the SIA method were prepared in the same manner as those used for the FIA, ratioing the flow rates from the FIA analysis for use on the SIA manifold has the potential of resulting in non-ideal chemistry for the formation of the Al-lumogallion complex. Thus in order to determine the ideal ratios between the various chemical reagents, as well as to establish the effects that flow rate and temperature of the reagent stream have on the precision and intensity of the analytical signal, a systematic approach to the optimization of all these parameters was implemented. The optimization of the above mentioned variables were performed by repeatedly analyzing a sample with an Al concentration of 75 nmol kg^{-1} while altering only one parameter at a time. The matrix of the Al sample was Milli-Q de-ionized water that had been acidified to pH ~1.8 by the addition of 1 mL of two times distilled reagent grade HCl. This acidification process is identical to that use for sample preservation. After each adjustment of the variable of interest, the sample was analyzed several (8-10) times to confidently determine the effects the alteration had on the analytical signal. In particular, the resulting peak height was monitored for its intensity and consistency, as they are to be indicative of the methods potential sensitivity and precision respectively. The optimizations discussed below are presented in the order in which they were performed.

4.2.1 Initial Values of Parameters to be Optimized

In order to have a starting point to the optimization process it was necessary to assign some initial values for the parameters that were to be optimized. For the sample zone volume and the flow rate of the MilliGAT pump, the initial values were arbitrarily set to 200 μL and 30 μL s^{-1} respectively. As for the heater temperature and the pump speed of the peristaltic pump (used for the delivery of the Brij-35 surfactant), the values used in the FIA method presented in Chapter 2 were selected as the initial values for the SIA optimization. A summary of the initial conditions used to begin the systematic optimization process is shown Table 3.

Table 3 - Initial Values used to Commence the Optimization Process

Parameter to be Optimized	Initial Value
MilliGAT Pump	
Volume of Lumogallion Buffer Zone	20 μL
Volume of Sample Zone	200 μL
Total Volume of Sample used	200 μL
Number of Sample Zones	1
Flow Rate of MilliGAT Pump (Reagent Stream)	30 μL s^{-1}
VWR Digital Heatblock	
Heater Temperature	55.5°C +/- 0.1°C
Rainin Dynamax RP-1 Peristaltic Pump	
Pump Speed	5.50 RPM
Surfactant Flow Rate	13 μL s^{-1}

4.2.2 Review of Chemical Ratios utilized in other Methods

The first optimization performed involved determining the ideal ratio for the sample and lumogallion buffer as it has been reported that the formation and fluorescence of the Al-lumogallion complex is sensitive to pH, with an ideal reaction pH of 5.0-5.6 (Brown and Bruland, 2008; Resing and Measures, 1994). Furthermore, it was necessary to determine the volume of sample required to give an adequate analytical signal. With the expectation of making a calibration curve that would extend to ~200 nmol kg^{-1}, it was essential that the peak height observed for a 74 nmol kg^{-1} Al sample would have to correspond to at least 30% of full-scale. Thus, with a range of 0-10 Volts (as set from the data acquisition card), a 74 nmol kg^{-1} sample would have to yield a peak height of at least 3 Volts to meet the previously set expectations.

To commence the optimization, it was arbitrarily decided that the sample would be introduced in 200 μL zones with varying volumes of lumogallion buffer on either side of these sample zones. The validity of this assumed sample zone volume is examined in a subsequent step of the optimization process. In order to get an idea as to the appropriate range of volumes of lumogallion per 200 μL of sample to consider, we turned to existing methods in the literature that utilized this particular method of detection. Table 4 displays the flow rates or volumes of all the reagents used by other investigators. In addition, the reagent ratios have

been determined and are presented in Table 4 in a format that allows for easy comparison to those used for the SIA chemistry optimization.

Table 4 - Comparison of chemistry and mixing ratios used by existing batch and flow based methods. Values have been converted into SIA relevant ratios to facilitate comparison.

Data	FIA or Batch Method			
	Hydes and Liss (1976)	**Resing and Measures (1994)**	**Brown and Bruland (2008)**	**Our FIA Setup**
Type of Method	Batch Method	FIA with pre-concentration	FIA with pre-concentration	FIA with pre-concentration
Flow Rates (mL/min)				
Eluent*	N/A	0.6	0.60	1.01
Lumogallion Buffer	L ~ 0.55 - 1.1 mL B = 0.5 mL	0.16	0.16	0.39
Brij-35	N/A	0.1	0.10	0.78
Sample	50 mL	2.5	2.50	1.36
Sample Buffer*	N/A	1 mL per 125 mL offline	0.10	0.08
Column Conditioning Buffer*	N/A	N/A	0.60	N/A
Relevant Reagent Ratios:				
Lumogallion Buffer : (200 μL) Eluent (Sample in Batch Method)	L ~ 2.2 - 4.4 : 200 B = 2 : 200	53 : 200	53 : 200	77 : 200
Approximate Concentration of Lumogallion at detector	2.9 - 5.8 μM	442 μM	442 μM	642 μM
Brij-35 : (1000 uL) Lumogallion + Eluent**	N/A	132 : 1000	132 : 1000	642 : 1000

L = Lumogallion B = Buffer
* These reagents not used in SIA analysis
** Assuming a 1000 μL Reagent Zone

From Table 4 it can be seen that the flow-based methods utilized by Resing and Measures (1994) as well as by Brown and Bruland (2008) suggest that 53 μL of the lumogallion buffer is required per 200 μL of eluent. Similarly, the FIA method used for the analyses reported in this manuscript suggest a lumogallion – sample ratio of 77 : 200 μL. However, it should be noted that the eluent used in these methods are considerably more acidic than our samples, which are typically stored at pH 1.8-2.0. Since the lumogallion buffer for the SIA method described needs only to account for the pH of the sample (as an eluent is not used), it is likely that less lumogallion buffer per 200 μL of sample will be required than suggested from the above methods in order to achieve ideal chemistry conditions. Furthermore, given the high concentration of lumogallion present in these reagent streams (442-642 μM), a slight reduction in the volume of lumogallion buffer supplied to the reagent stream will likely have a negligible effect on the aluminum's ability to quantitatively complex with the ligand. Thus, the above suggested lumogallion buffer volumes likely serve as upper estimates for the chemical optimization.

In contrast to the flow-based methods discussed above, the batch method developed by Hydes and Liss (1976) involves the separate addition of the lumogallion and acetate buffer to a seawater or fresh water sample at its natural pH. At the concentrations the lumogallion-buffer solution is prepared for the proposed SIA method, only 2 μL of acetate buffer and 2.2 – 4.4 μL of lumogallion would be added per 200 μL of unacidified sample. However, since this method is

designed for samples at natural pH, we can expect that the volume of buffer required for the SIA method to be higher than suggested by the batch method. Also, given that we intend to analyze acidified samples, there will be an additional acid-labile fraction of Al present that would be absent in a sample stored at natural pH. This fraction is capable of complexing with lumogallion and can thus be detected in addition to the "reactive Al" present in the sample. As such, it may be advisable to increase the concentration of lumogallion present in the reagent stream for the SIA analysis compared to the relatively low (5.8 μM) concentration used for the batch method. Furthermore, Hydes and Liss (1976) have reported that for low concentrations of Al and an excess of lumogallion, the formation of the Al-lumogallion complex approximates first order kinetics. Thus it is believed that increasing the concentration of lumogallion in the reagent stream will facilitate the rapid and quantitative complexation of the Al in the sample, which is desirable for the development of a reliable, and efficient flow based method of analysis. For this reason as well as to allow for a more direct comparison between the SIA method and the currently available FIA methods, we have opted to prepare our lumogallion-buffer reagent in the same manner as the FIA methods noted above (Brown and Bruland, 2008; Resing and Measures, 1994).

4.2.3 Optimization of Lumogallion Buffer : Sample Ratio

In order to determine the optimal chemistry for the formation of the Al-lumogallion complex, the volume of the lumogallion zone that was positioned on

either side of the 200 μL sample zone was varied from 20 to 120 μL in 10 μL increments. Furthermore, to ascertain the volume of sample required to give an adequate analytical signal, additional 200 μL sample zones were added to the reagent stream (to a maximum of 4 zones, totalling 800μL of sample) and the above process of increasing the volume of lumogallion present in the reagent stream was repeated. The results from this optimization process are shown below in Figure 22.

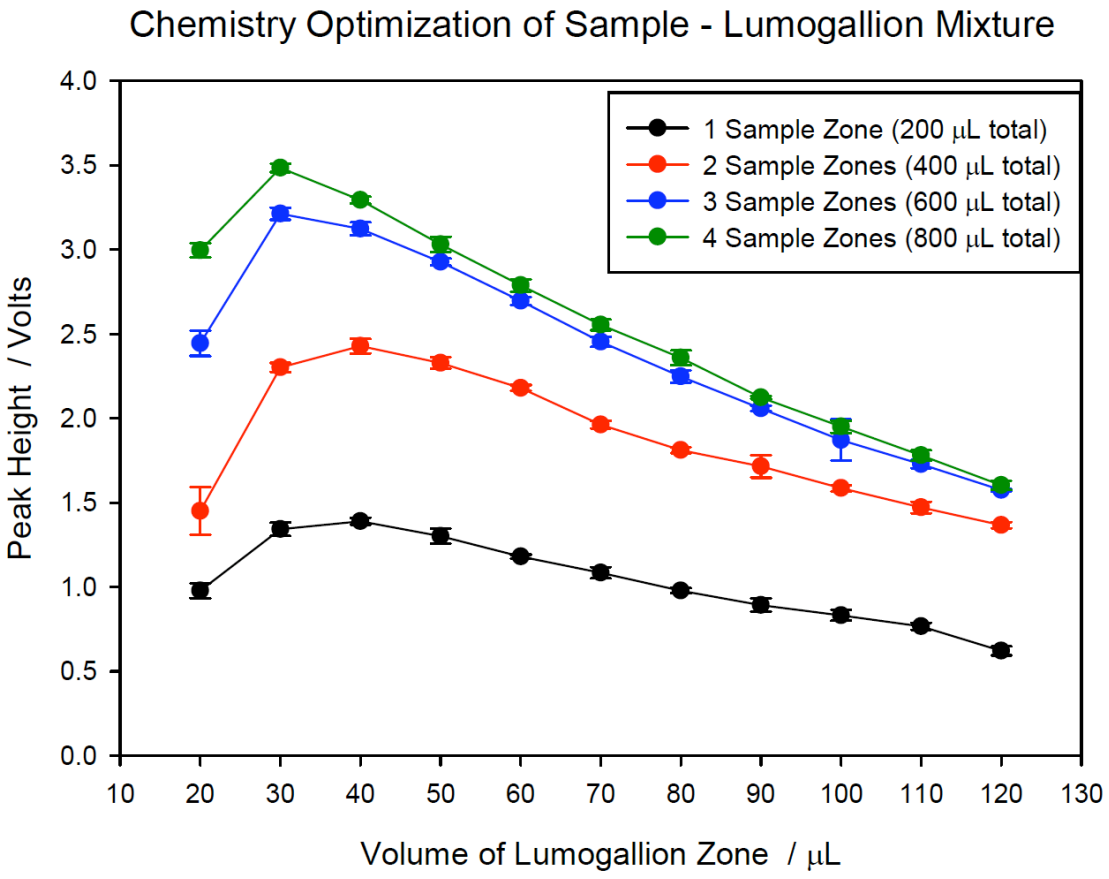

Figure 22 - Optimization of sample : lumogallion ratio. Volume of lumogallion buffer was increased in 10 μL increments to determine the ideal chemical ratio to maximize the intensity of the analytical signal. The process was repeated for increasing number of 200 μL sample zones. Ideal zone volume of lumogallion buffer appears to be 30 – 40 μL.

From Figure 22 it is evident that a 30 - 40 μL lumogallion buffer zone yields the most optimal conditions for the formation of the Al-lumogallion complex. Indeed, for the reagent streams that contained only one or two sample zones, the maximum peak height occurred when a 40 μL of lumogallion buffer zone was used. However when three or four sample zones were present in the reagent stream, the use of a 30 μL lumogallion buffer zone provided the best environment for the formation of the Al-lumogallion complex. It is also apparent when viewing Figure 22 that a minimum of 600 μL of sample is necessary to obtain the desired peak height for the 75 nmol kg^{-1} Al sample (recall that a peak height of at least 3 Volts is required to achieve the desired sensitivity). Furthermore, the presence of an additional 200 μL of sample in the reagent stream appears to sufficiently increase the peak height in the region of optimal chemistry, thus warranting the use of the extra 200 μL of sample. However, the close proximity of the 600 μL and 800 μL curves suggest a situation of diminishing returns such that the use of more than 800 μL of sample will likely not result in a significant enhancement of the peak height. Rather, it is likely that the analytical signal will broaden and eventually plateau as the amount of sample used is increased. As a result, it was concluded that we would adopt the usage of 800 μL of sample per analysis. That is to say that a single peak would be generated from the use of 800 μL of sample and that 10 replicate analyses would require 8 mL of sample. By comparison, the FIA method that was presented in Chapter 2 typically required ~25 mL of sample to perform four replicate analyses; thus the SIA method proposed will likely consume considerably less sample, thus

permitting the analyst to perform more replicate analyses. This ability is sure to provide high precision in the measurements obtained from the SIA method.

In order to arrive at a conclusion for the ideal volume of lumogallion buffer to be used, a second step-wise variation of the lumogallion buffer volume was performed on the Al sample, this time in 5 μL increments and using 800 μL of sample. The results from this optimization are shown in the inset plot of Figure 23.

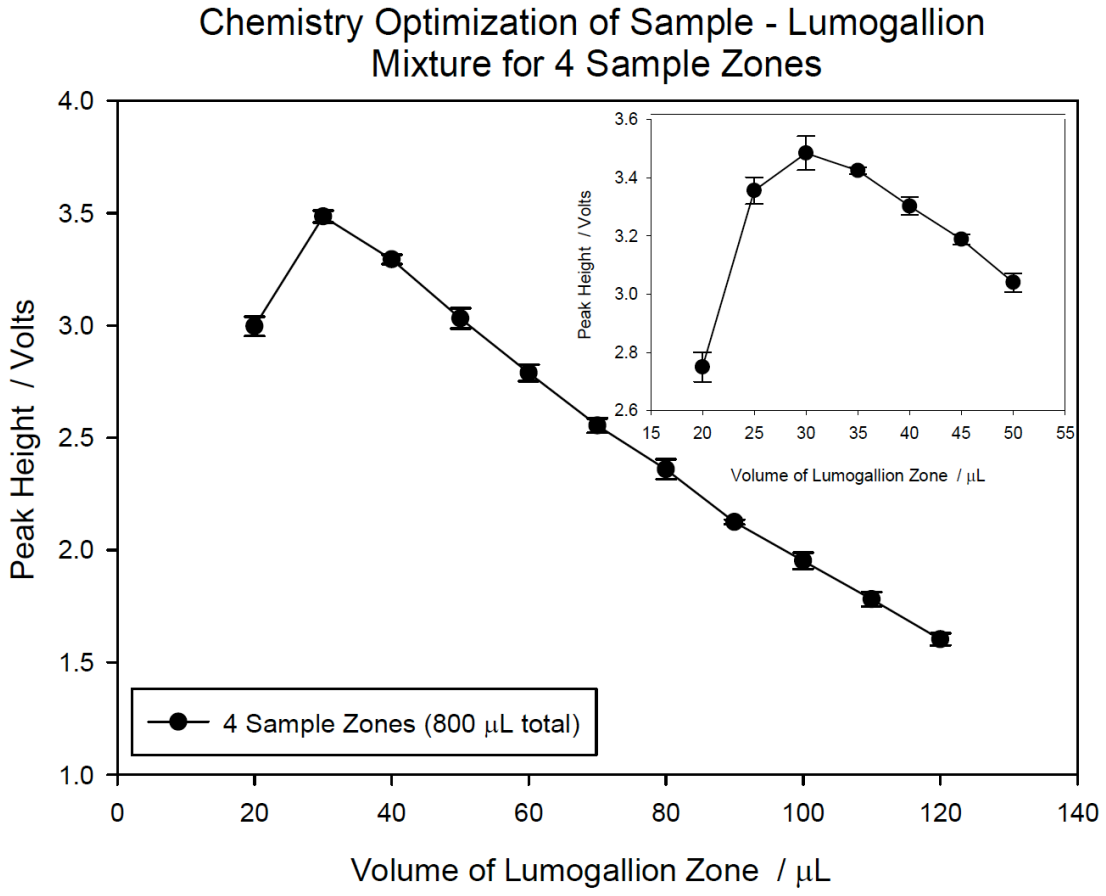

Figure 23 - Sample : Lumogallion ratio optimization for a 4 sample zone reagent stream. Inset figure shows results from increasing the volume of the lumogallion zone in 5 μL increments.

From Figure 23 it is evident that the largest analytical signal occurs when 30 μL zones of lumogallion - buffer are used. However, the large uncertainty in the peak height observed for this volume of lumogallion, as evident by the pronounced error bars shown in the inset plot of Figure 23, suggests that this chemical ratio may result in poor precision for the method. By contrast, the use of 35 μL zones of lumogallion – buffer yields an acceptable peak height for the 75 nmol kg^{-1} sample while maintaining a high level of precision. It was concluded that a zone volume of 35 μL for the lumogallion – buffer provided optimal conditions for the consistent formation of the Al – lumogallion complex and that this volume would be incorporated into the SIA sequence. As a result, a 35 μL lumogallion – buffer zone volume was used for the remainder of the optimization process.

4.2.4 Validation of the 200 μL Sample Zone

The volume of the sample zone was arbitrarily set to 200 μL without any investigation as to whether this volume was ideal. From the previous optimization it was determined that a total sample volume of 800 μL, when interlaced with an optimal volume of lumogallion buffer (35 μL), provided a consistent analytical signal of the desired intensity. Given that the sample was divided into four 200 μL zones that were separated by a total of 5 lumogallion buffer zones (see Figure 24d), there was a total of 175 μL (5 x 35 μL) of lumogallion buffer per 800 μL of sample. Therefore in the optimization that follows, the total volumes of sample and lumogallion buffer were held constant at 800 μL and 175 μL respectively;

with only the degree of interlacing of the reagents being varied. Thus the following is an inquiry into what the ideal number of zones the 800 μL of sample should be divided into when drawn into the reagent stream.

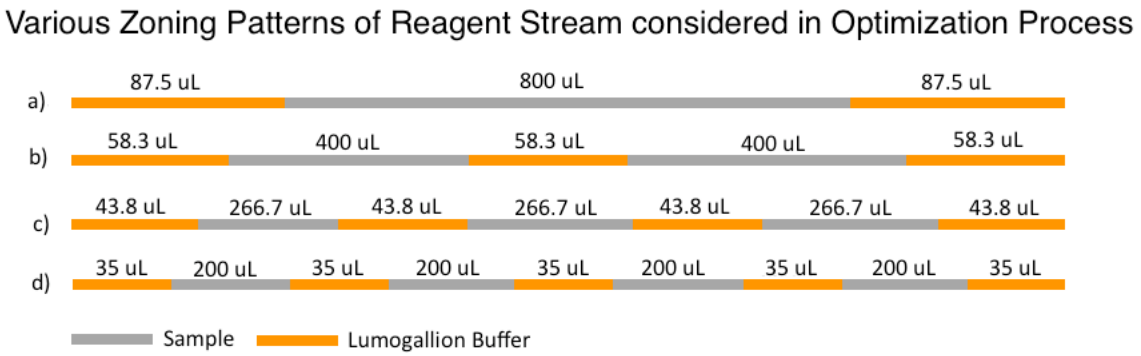

Figure 24 - Zoning patterns used in the division of the 800 μL sample within the reagent stream. The total volume of lumogallion buffer and sample are held constant at 175 μL and 800 μL respectively as this chemical ratio was previously determined to be optimal. Sample zone is depicted in grey and lumogallion buffer in orange, The zoning pattern in d) was used in the prior chemistry optimizations.

From Figure 25 it can be seen that mixing schemes (see Figure 24) containing two or more sample zones yield an analytical signal of adequate intensity and that further dividing of the reagent stream does not result in a detectable increase in the samples peak height. As a result, it may be unnecessary to include the additional valve actuations in the SIA sequence to further interweave the sample and lumogallion-buffer; thus decreasing the time of analysis. However, the precision of the peak height appears to be greatest when the sample is divided up into four equal zones of 200 μL as is shown by the vertical error bars in Figure 25. Since our goal is to develop a method that is both highly sensitive and precise, we opted to include the additional valve actuations

in the SIA sequence and divide the sample into four 200 μL zones (Figure 24d) to maximize the precision for the method. It should be noted that the inclusion of the additional valve actuations to incorporate the elevated degree of mixing resulted in the addition of only 34 seconds to the analysis time relative to the two-sample zone sequence.

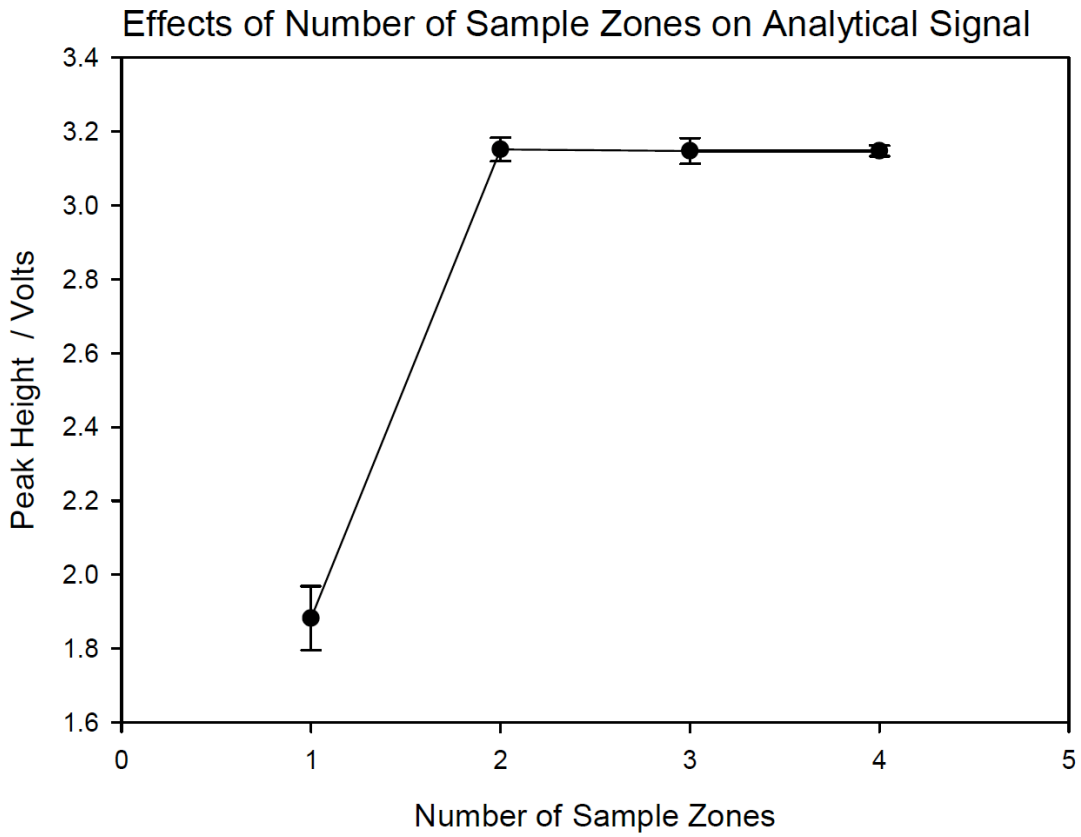

Figure 25 - Effects of dividing the 800 μL of sample into smaller zones on the observed peak height. The division of the sample zones correspond to the depictions in Figure 24; namely 1 sample zone corresponds to 24a), 2 sample zones 24b) and so forth.

4.2.5 Optimization of Reagent Stream Flow Rate

The purpose of this optimization was to determine the effects of the flow rate of the MilliGAT pump, which essentially regulates the time the reagent stream is present in the heater before combining with the surfactant on its way to the detector. Up to this point, the flow rate of the MilliGAT pump was arbitrarily set to 30 μL s^{-1} to perform the optimizations presented above; However, we wish to develop a method that is not only highly accurate and precise, but one that is capable performing the analysis in a timely manner. Thus the goal of this optimization is to observe the effects of increasing the flow rate of the MilliGAT pump has on the intensity and stability of the analytical signal. The results from such an investigation may permit a reduction in the current analysis time by indicating that an increase in the reagent stream's flow rate has a negligible effect on the sample's peak height. Indeed, it is conceivable that increasing the reagents flow rate may result in a more desirable analytical signal, as is often found in gas and liquid chromatographic methods by sharpening the peak's profile and increasing the intensity of the resulting peak or peaks. As mentioned above, this process has the additional benefit of reducing the time of these often time consuming methods of analysis.

For this optimization, the sample and lumogallion-buffer zone volumes were kept at their previously determined optimal values; namely four 200 μL sample zones interlaced between five 35 μL lumogallion-buffer zones. With these

parameters held constant, the flow rate of the MilliGAT pump was varied from 20 - 55 μL s^{-1} and the results from this process are displayed in Figure 26.

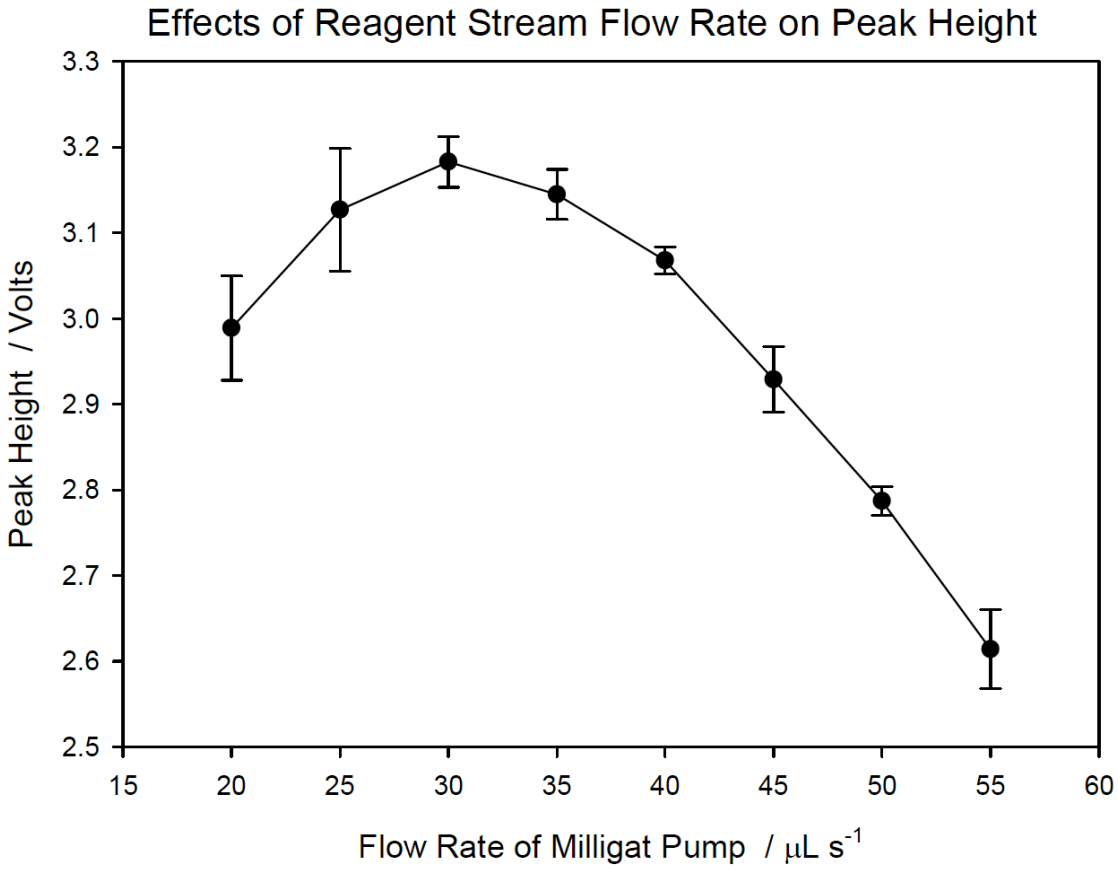

Figure 26 - Effects of the MilliGAT or reagent stream flow rate on the intensity of the analytical signal. Flow rates were increased in 5 μL increments.

From Figure 26 it can be seen that the highest peak was obtained for the sample when a MilliGAT flow rate of 30 μL s^{-1} was used, suggesting that our initial MilliGAT flow rate setting to be the optimal operating condition. It should be noted that when a 40 μL s^{-1} flow rate was used, an increase in the precision of the samples peak height was observed; however, the overall intensity of the analytical signal was noticeably attenuated at this flow rate. Furthermore, it was observed that the use of higher reagent stream flow rates resulted in an apparent

increase in the number of air bubbles present in the reagent stream, making the use of higher flow rates undesirable. As a result we adopted a MilliGAT flow rate of 30 μL s^{-1} for the remainder of the SIA optimizations and analysis.

It is worth noting that this flow rate is comparable to that used in the FIA method presented in Chapter 2; which has an eluent – lumogallion buffer flow rate equivalent to approximately 22.5 μL s^{-1}. By contrast, the FIA methods reported by Resing and Measures (1994) as well as Brown and Bruland (2008) have an effective eluent – lumogallion buffer flow rate of only 12.7 μL s^{-1}. Thus it appears that the use of a 30 μL s^{-1} flow rate for the SIA method is an improvement in terms of efficiency over the existing flow-based methods. It is interesting to note that increasing the flow rate of the reagent stream failed to produce an increase in the intensity of the analytical signal as one with experience in operating gas or liquid chromatographs might have thought. In fact, increasing the flow rate beyond 30μL s^{-1} resulted in a decrease in the sample's peak height. However, the use of a higher flow rate did result in a slight narrowing of the peak's width as predicted from the chromatography analogy mentioned earlier. Also as suspected, increasing the flow rate of the reagent stream resulted in the peak to occur earlier in the data acquisition window as shown in Figure 27.

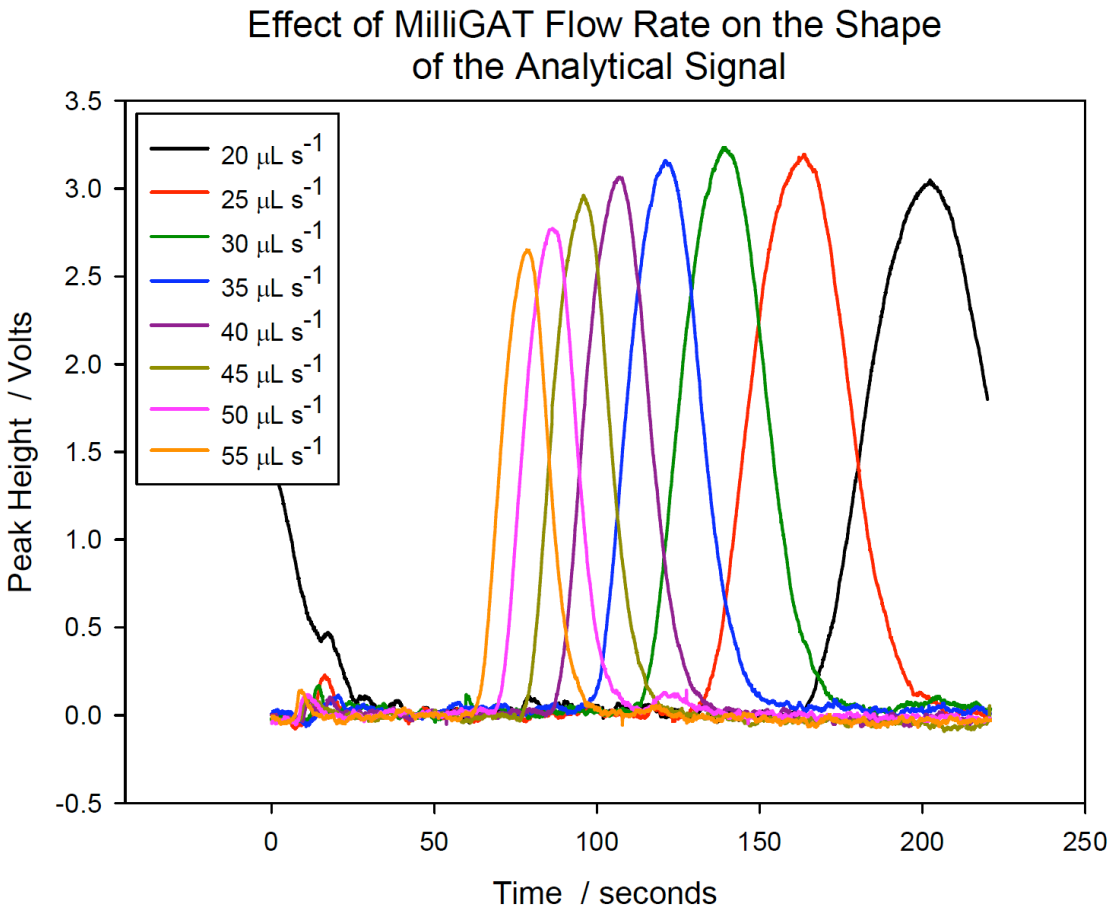

Figure 27 – Location and intensity of analytical signal within the data acquisition window resulting from increasing the reagent stream flow rate. Note the gradual decrease in the peak height at higher flow rates despite a narrowing of the peaks width. This observation indicates that higher flow rates resulted in inadequate developing time for the reagent stream while in the heating block. By contrast, a 20 μL s^{-1} flow rate resulted in a broadening of the reagent stream that was unable to completely pass through the flow cell within the allotted acquisition time.

4.2.6 Effects of Heater Temperature on Intensity of Analytical Signal

The heater temperature was initially set to 55.5°C, which corresponds the temperature setting used for the FIA manifold described in Chapter 2. Nevertheless, an investigation into what effects the changing of the temperature setting of the dry block heater had on the resulting analytical signal was performed. The results from this investigation are shown below in Figure 28.

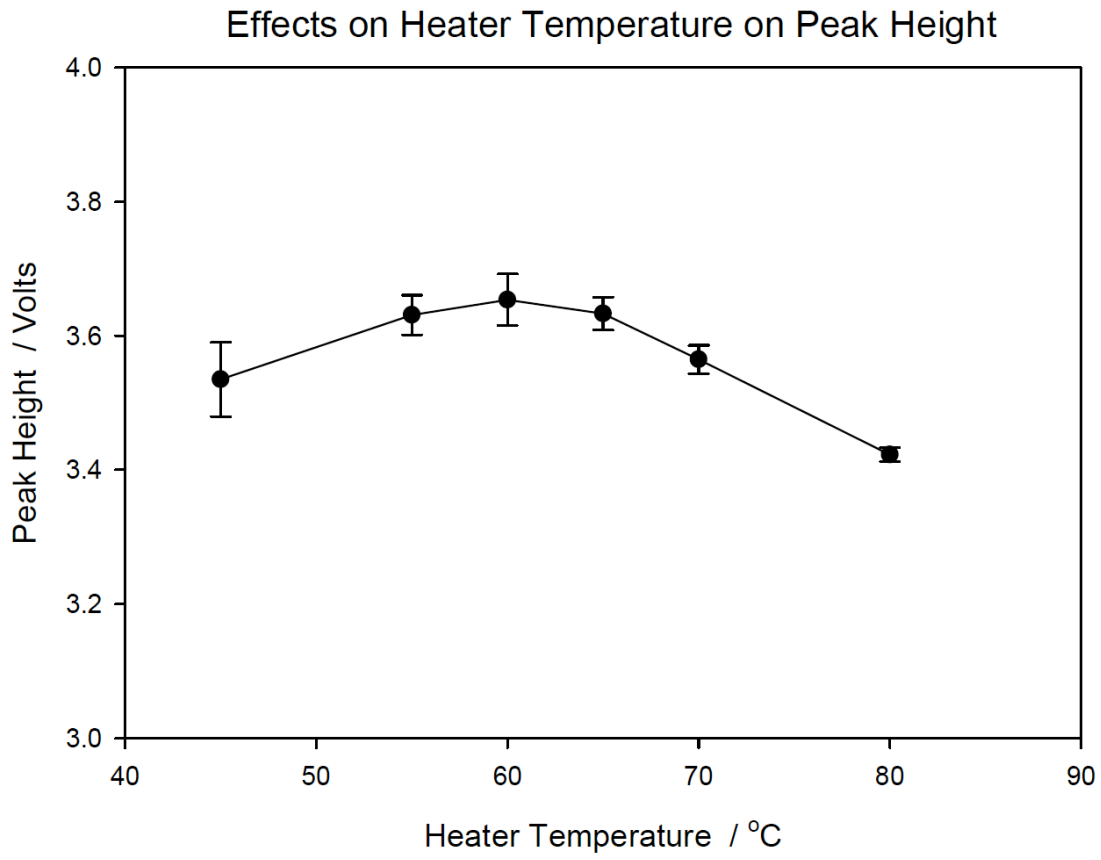

Figure 28 - The effects of increasing the heater temperature on the observed peak height.

It is evident from Figure 28 that, unless at very high heater temperatures, the increasing of the temperature did not result in a significant change in the intensity of the analytical signal. Indeed, in changing the temperature from 55°C - 65°C, there is no discernable increase in the sample's peak height within the error of the measurement. Only at either end of the temperature spectrum does one begin to see a reduction in the signal's intensity. In terms of precision, again there is no real benefit to using one temperature as opposed to another and unless considering those on the fringe of the temperature spectrum shown in Figure 25. It should be noted that this temperature range is in agreement with Resing and Measures (1994) investigation in to the effects of temperature in the development of their FIA method. Resing and Measures (1994) reported that "…increasing the temperature from 22 to 53°C increased the response by a factor of 4. At temperatures above 53°C, the increase in the response diminishes rapidly." As a result, they chose to adopt a temperature of 50°C to take advantage of most of the temperature-based reaction rate improvement while minimizing the potential for $CaSO_4$ precipitation from seawater within the small bore Teflon tubing. Furthermore, based on this investigation performed by Resing and Measures (1994), Brown and Bruland (2008) also opted to use a 50°C heater temperature without reporting an investigation into the effects of the reaction temperature on the analytical response. Based on the above results from our own investigation as well as that performed by Resing and Measures (1994), it was concluded that we would continue to use a heater temperature of

55.5°C for the SIA method. Maintaining this temperature will also permit a more direct comparison of the SIA method to the FIA method presented in Chapter 2.

4.2.7 Optimization of Surfactant Flow Rate

The last optimization in the development of the SIA method was to determine the ideal flow rate for the delivery of the Brij-35 surfactant so as to maximize the signal response as well as utilize as little of the reagent as possible. Up to this point in the optimization process, the peristaltic pump delivering the surfactant to the reagent stream has remained at its initial setting of 5.50 RPM, which corresponds to a flow rate of approximately 13 $\mu L\ s^{-1}$ for the surfactant. By changing the peristaltic pump's revolutions per minute, the amount of surfactant delivered to the reagent stream was varied. The results from this optimization procedure are shown in Figure 29 with the pump speed on the lower x-axis and the corresponding flow rate in micro-litre per second ($\mu L\ s^{-1}$) on the upper x-axis.

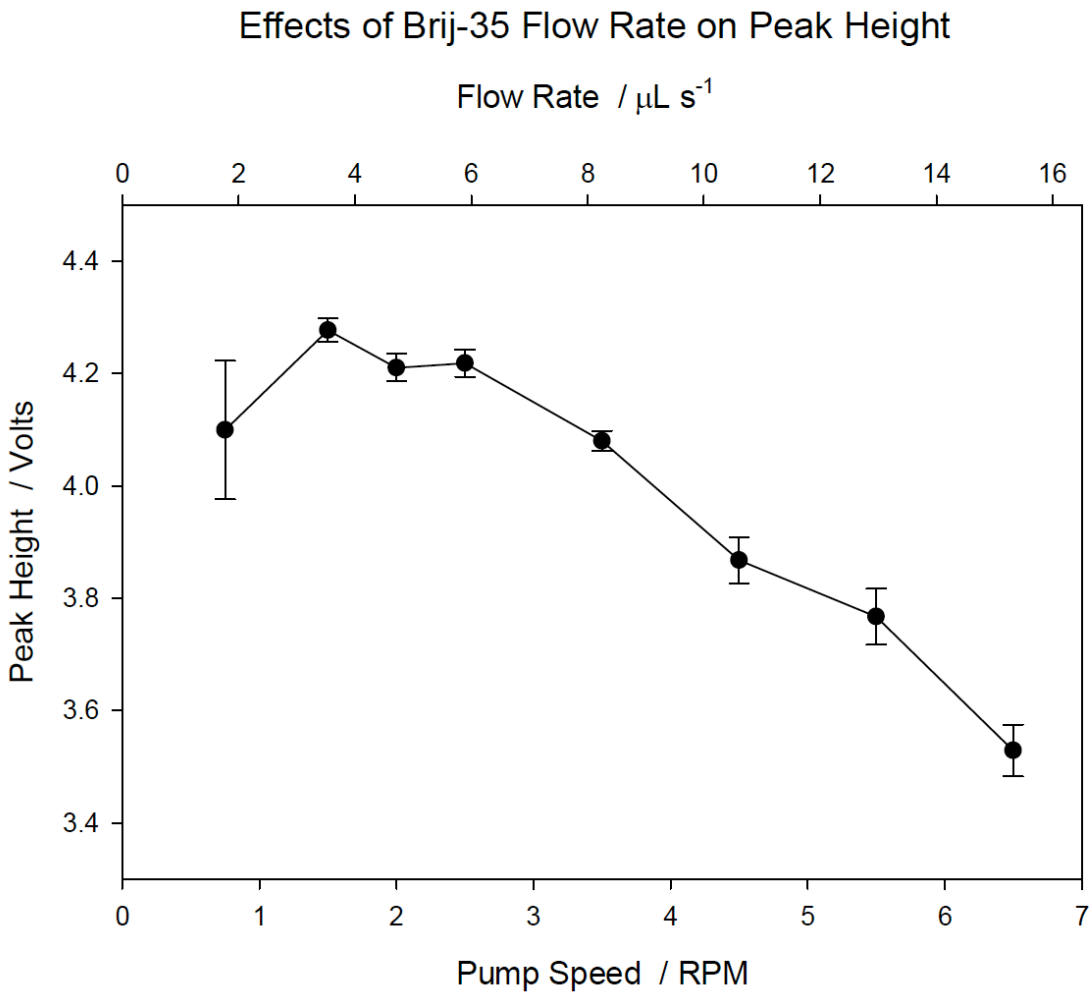

Figure 29 - The effects of Brij-35 concentration within the reagent stream on the intensity of the analytical signal. Note the lower x-axis corresponds to the peristaltic flow rate used to deliver the surfactant while the upper x-axis is the flow rate of the surfactant in μL s^{-1}.

From Figure 29 it appears that a peristaltic pump speed of 1.5 RPM appears to deliver the optimal amount of surfactant to the reagent stream to maximize the intensity of the analytical signal. However, what Figure 29 fails to show is the lack of stability in the resulting baseline when such a small volume of surfactant is used. Indeed, it can be seen from the plots in Figure 30 that delivering the surfactant at a pump speed of less than 2 RPM resulted in

unstable baseline. In particular, periodic spiking of the analytical signal from the detector was observed and is thought to be due to the presence or absence of the surfactant in reagent stream as it passed through the 9 μL flow cell. This was particularly evident when a 0.75 RPM pump speed was used.

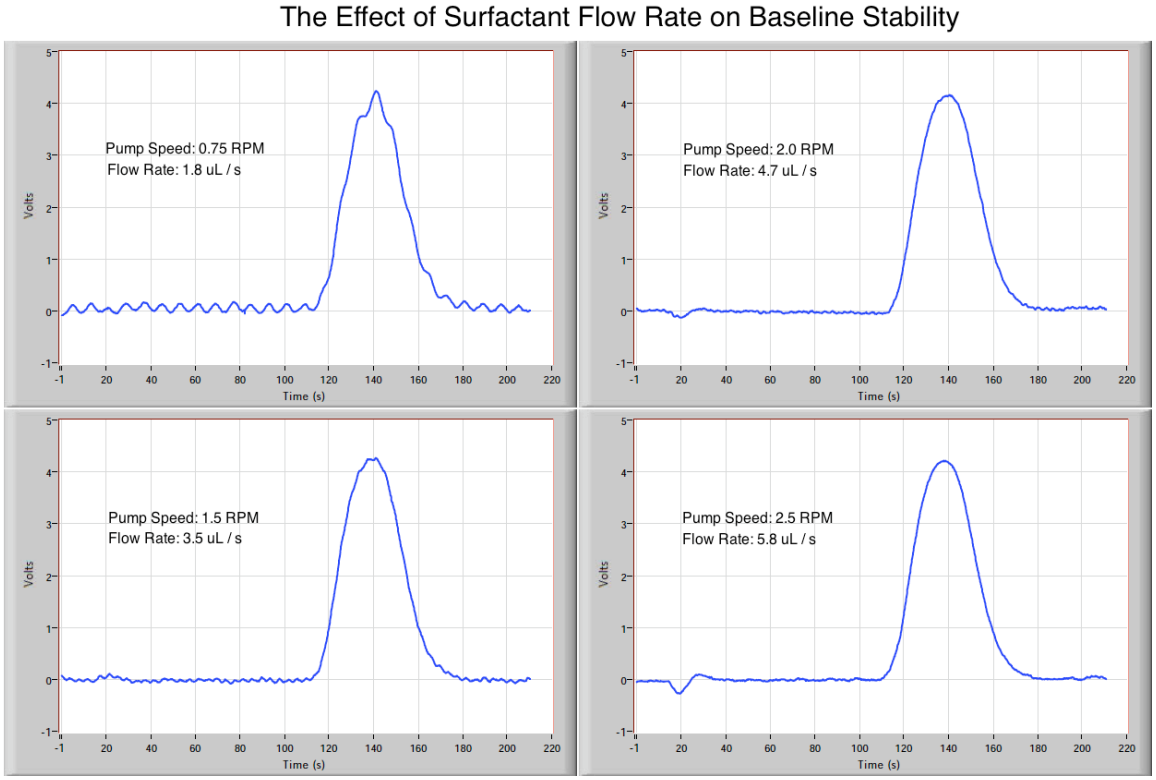

Figure 30 - Screenshots of FloZF data acquisition windows indicating the effects of using a very low flow rate for the delivery of the Brij-35 surfactant. Note the sinusoidal like oscillation of the baseline when pump speeds of less than 2.0 RPM are used.

In light of these findings, it was concluded to use a peristaltic pump speed of 2.25 RPM, which corresponds to a flow rate of approximately 5.3 μL s^{-1}. The selection of a pump speed of 2.25 was based on the fact that over prolonged use, the efficiency of transfer for a peristaltic pump using 2-stop Tygon tubing

tends to decline and results in less of the surfactant reaching the reagent stream. Given this gradual degradation in the pump's efficiency, the peak height plateau observed in Figure 29 at pump speeds of 2 – 2.5 RPM suggests that a pump speed in this region would provide a strong and consistent analytical signal for the entire duration of a lengthy analysis period. Therefore, it was decided to use a pump speed that lay in the middle of this plateau, which corresponded to a pump speed of 2.25 RPM.

In order to compare these findings to the Brij-35 : reagent zone ratios presented in Table 4 for the various FIA methods in the literature; the Brij-35 : Reagent zone ratio for the optimized SIA method was determined to be 176.7 μL : 1000 μL (see Appendix 2 for calculation of this ratio). From Table 4 is can be seen that this ratio is slightly higher than that utilized by Brown and Bruland (2008) as well as Resing and Measures (1994). According to their reported flow rates, these investigators used 132 μL of surfactant per 1000 μL of reagent stream. By contrast, the FIA method reported in Chapter 2 had a considerably higher consumption of the surfactant; using 642 μL of the Brij-35 solution per 1000 μL of reagent stream. However, it should be pointed out that this considerably higher usage of surfactant was the result of an error in a flow rate calculation that went unnoticed until after the analyses reported in Chapter 3 had been performed and it came time to develop the SIA method. As a result of this calculation error, pump tubing with a larger inner diameter than was ideal was used for the delivery of the surfactant to the reagent stream. Had this error been

identified earlier, the FIA method in Chapter 2 would have employed a surfactant : reagent zone ratio that was comparable to those reported for the other FIA methods.

It is worth pointing out that reducing the pump speed from it is initial speed of 5.50 RPM to 2.25 RPM yielded a 60% reduction in the amount of surfactant being delivered to the reagent stream. Furthermore, this reduction in the volume of surfactant reaching the detector resulted in a sizeable increase in the intensity of the analytical signal. It is believed that the use of more surfactant than was required served to actually lower the concentration of the fluorescing Al-lumogallion complex within the reagent stream. This in turn resulted in attenuation of the analytical signal (Figure 29).

4.3 Interference by other Elements

The fluorometric detection of Al by chelation of the metal with lumogallion has been reported to be highly sensitive and relatively free of interference by other elements (Howard et al., 1986). However, in the initial exploration into the use of lumogallion as a fluorescing agent for the detection of Al, Shigematsu et al. (1967) performed an extensive investigation into the potential for interference by other metals. Shigematsu et al. (1967) observed strong negative interference from the addition of Cr^{3+}, Fe^{3+}, Sn^{4+}, Ti^{4+}, V^{5+} as well as minor negative interference from Co^{2+}, Ni^{2+}, and Sc^{3+} although at concentrations (4 ppm) far

exceeding those typically found in oceanic or riverine environments (see Table 5). The negative interference observed from the addition of these metals is thought to be due to a competitive complexation of the lumogallion with the interfering ion that diminishes the amount lumogallion that is available to complex with Al. This in turn results in a reduced fluorescence signal for the sample of interest. Shigematsu et al. (1967) also noted a slight positive interference when a 40 ppb solution of Al was spiked with 200 ppb of Ga^{3+}. This interference is due to Ga^{3+} also forming a complex with lumogallion that has similar fluorescing properties as the Al-lumogallion complex. Thus lumogallion can also be used for the fluorometric detection of Ga^{3+}, although this method would suffer from interference from gallium's more abundant elemental relative, Al.

In the development of a batch method for the detection of Al with lumogallion, Hydes and Liss (1976) reported that the interference from Fe^{3+} to be less than previously reported and determined that Fe^{3+} did not have a significant effect at concentrations of less than 100 ppb. However, Hydes and Liss (1976) did note that the presence of fluoride resulted in an attenuation of the fluorescence signal and suggested that this could "be dealt with by using an incremental calibration procedure." Similarly, Howard et al. (1986) reported a decrease in the fluorescence signal in the presence of Fe^{3+} and F^- for their micelle-enhanced batch method that involved the addition of a surfactant (Triton X-100) to the sample before analysis. To eliminate the potential interference from Fe, Howard et al. (1986) opted to add 1,10-phenanthroline to the sample prior to

the addition of lumogallion to mask the Fe present in the sample. As for fluoride, Howard et al. (1986) observed a 50% suppression in the signal of a 100 ppb Al sample when 1 ppm of fluoride was present, but pointed out that the free fluoride concentration in many natural waters is well below this level due to fluoride's participation in metal complexation and ion pairing. Furthermore, Howard et al. (1986) suggested that this same process is believed to occur in seawater but recommended the use of a standard addition calibration when working in this matrix.

In their integration of the chemistry from the previous batch methods into a FIA manifold, Resing and Measures (1994) revisited the potential for interference by some of the most notable interferents that were reported by Shigematsu et al. (1967), namely Cu^{2+}, V^{5+}, Ti^{4+}, Fe^{3+}, and Ga^{3+}. For their investigation, Resing and Measures (1994) spiked a 12 nmol kg^{-1} Al sample with the elements at 4-1000 times their oceanic concentrations and found no significant attenuation or enhancement of the analytical signal. Resing and Measures (1994) utilized a pre-concentration column and an elevated concentration of lumogallion in the reagent stream to which they attributed the reduced interference exhibited. Indeed, in addition to the obvious benefit of concentrating the analyte, the use of a pre-concentration column also typically separates the analyte from the complex seawater matrix and any interfering ions provided that they are not also retained on the column. Furthermore, the use of a higher lumogallion concentration

coupled with shorter reaction times and a higher reaction pH may serve to reduce the effect of competitive complexation of the ligand by interfering ions.

4.3.1 Initial Evaluation of Potential Interference by other Elements

To determine the effects of potentially interfering ions, a total of 13 elements were selected based on findings of previous studies to determine whether their presence in a sample at an elevated concentration had an adverse effect on the analytical signal. To carry out the initial investigation, a 75 nmol kg^{-1} Al sample prepared in acidified Milli-Q was distributed into several autosampler vials and spiked with 10 μM additions of the potential interfering ion with the exception of elements Mg^{2+}, Ca^{2+}, and F^{-}, which were added at concentrations of 100 mmol kg^{-1}, 40 mmol kg^{-1}, and 2 mmol kg^{-1} respectively. Also, in order to account for any instrument drift or evaporative losses, reference analyses of the 75 nmol kg^{-1} Al sample were performed periodically throughout the analysis. In fact, the order in which the samples are arranged along the x-axis of Figure 31 corresponds to the order in which the samples were analyzed (from left to right).

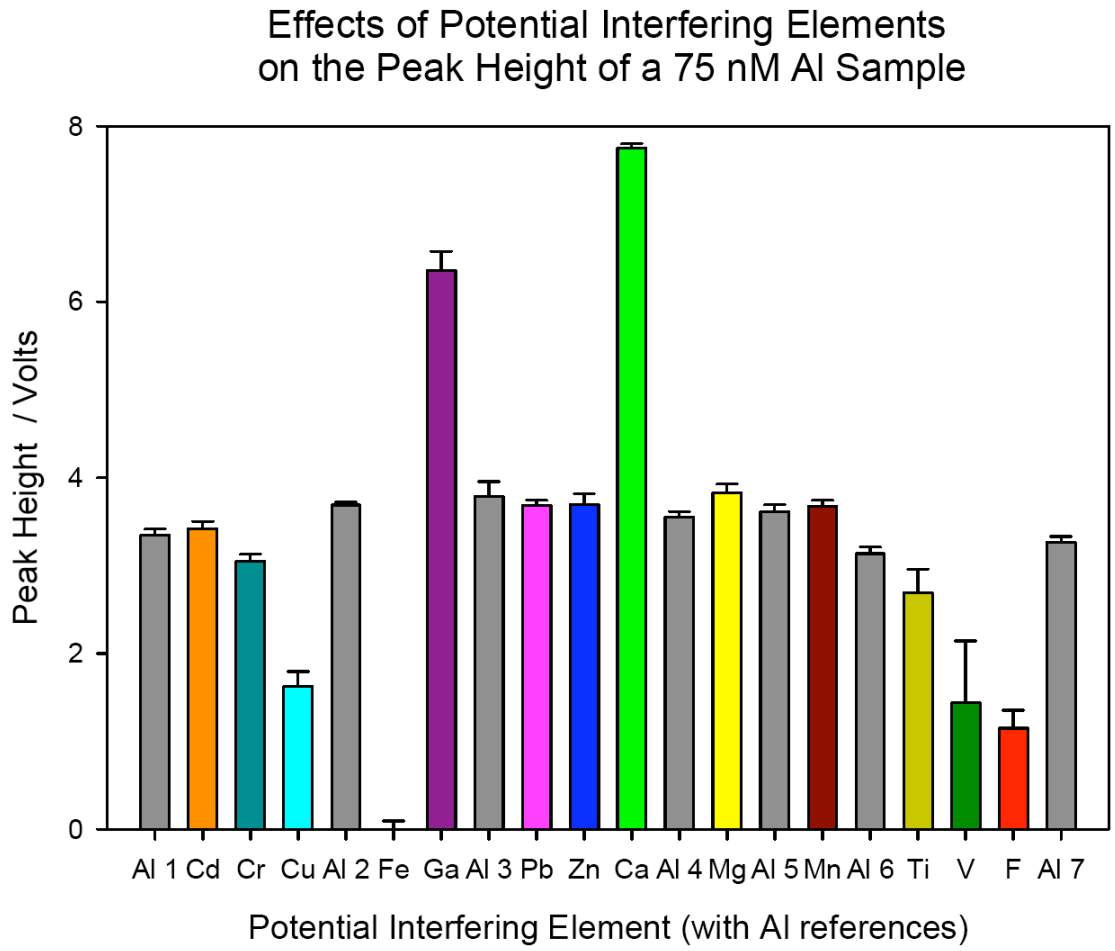

Figure 31 - Effects of adding high concentrations of potentially interfering ions on the peak height of a sample containing 75 nmol kg^{-1} of Al prepared in an acidified Milli-Q matrix. All interferents were present in a concentration of 10 μmol kg^{-1} with the exception of Mg^{2+}, Ca^{2+}, and F^{-}, which were present at concentrations of 100 mmol kg^{-1}, 40 mmol kg^{-1}, and 2 mmol kg^{-1} respectively.

From Figure 31 it can be seen that negative interference was observed for samples containing 10 μM of Cr^{3+}, Cu^{2+}, Fe^{3+}, Ti^{4+}, V^{5+}, which is in agreement of the observations of Shigematsu et al. (1967). Similarly, a 2 mmol kg^{-1} addition of fluoride to the sample resulted in over 50% suppression of the analytical signal which is in accordance with the findings of Howard et al. (1986). Furthermore, enhancement of the analytical signal was observed for Ga^{3+} and Ca^{2+}. It is

interesting to note that, while the positive interference from Ga^{3+} could be expected, previous studies have not reported Ca^{2+} to interfere with the fluorescent detection of the Al-lumogallion complex. In fact, Howard et al. (1986) recommended the addition of large amounts of Ca^{2+} in the form of $CaCl_2$ to a sample to mask the interference from fluoride. Further discussion regarding the potential interference from Ca^{2+} is reported below along with the results from the step-wise interferent addition experiment; whereby the ions that interfered in the above investigation were added to a 75 nmol kg^{-1} Al sample at more realistic environmental concentrations.

4.3.2 Seven Point Step-wise Addition of Potential Interferents

Although several elements demonstrated interference when present at significantly elevated concentrations, these elements may not be problematic when present at more environmentally relevant concentrations. Therefore, the 8 potential interfering elements were added incrementally to vials containing a 75 nmol kg^{-1} Al sample in an acidified Milli-Q matrix at concentrations that closer resemble their typical oceanic and riverine concentrations. These samples were then analyzed to determine whether the presence of these elements interfere with the analytical signal at their typical environmental concentrations. The results from the step-wise additions of these potential interferents are shown in Figure 32 and their typical oceanic and river water concentrations are shown in Table 5.

Table 5 - Typical seawater and river concentrations of the potential interfering elements. Seawater concentrations correspond to the mean oceanic concentrations as reported by (Wilde, 2010). Unless otherwise noted, river concentrations correspond to the certified values for the SLRS-4 reference material.

Element	Seawater		River	
	Concentration	Unit	Concentration	Unit
Ga	17	pM	1 - 79[a]	pM
Ti	136	pM	0.52 - 7.1[b]	nM
Fe	1	nM	1844	nM
Cu	2	nM	28	nM
Zn	5	nM	14	nM
V	39	nM	6	nM
Cr	7	pM	6347	pM
Mn	5	nM	61	nM
Cd	1	nM	0.11	nM
Pb	170	pM	415	pM
Ca	10	mM	0.15	mM
Mg	53	mM	0.07	mM
F	68	μM	2 – 178[c]	μM

[a] (Shiller and Frilot, 1996)
[b] (Skrabal, 1995)
[c] (Neal et al., 2003)

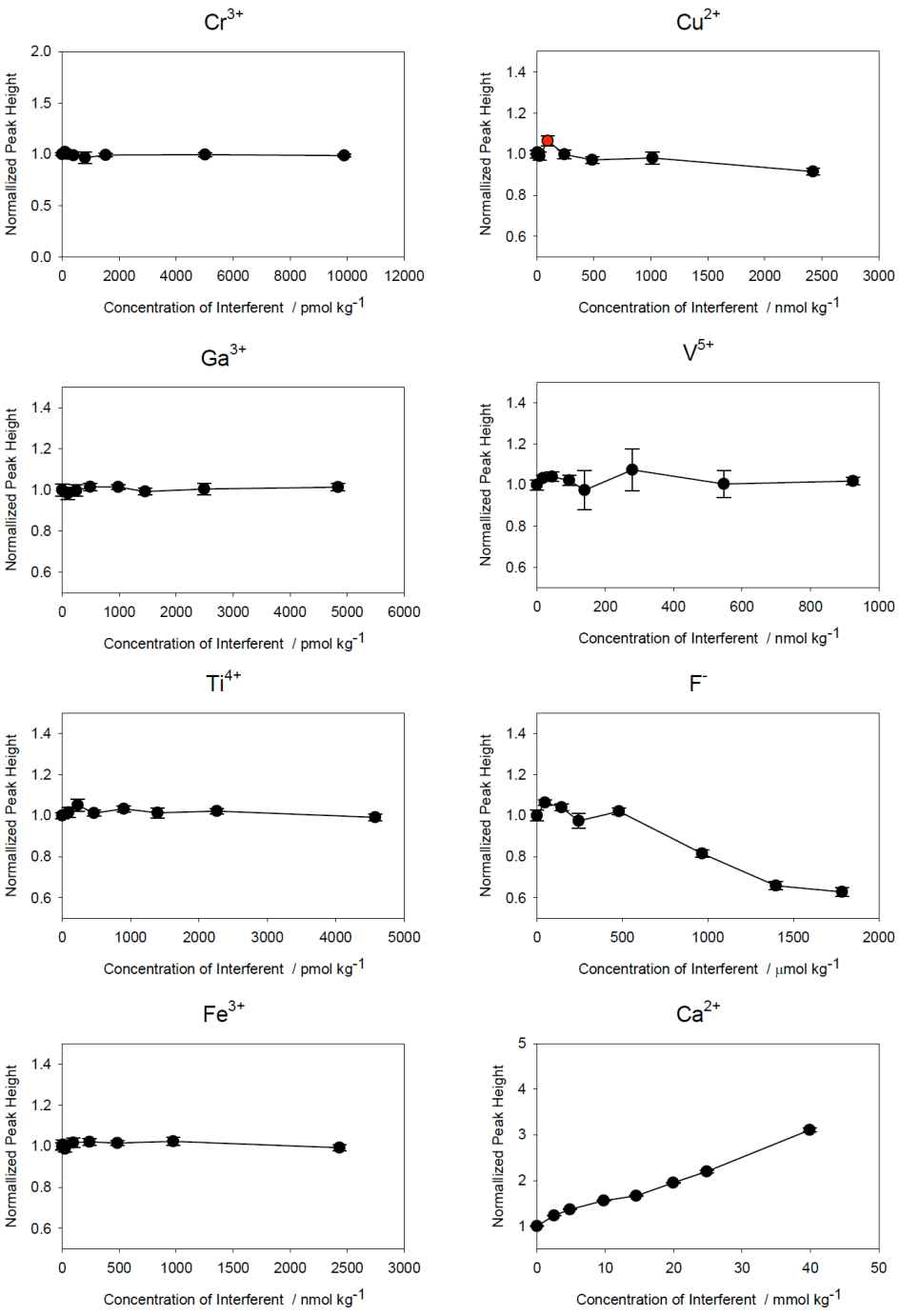

Figure 32 - 7 point incremental additions at environmentally relevant concentrations of ions that are known to interfere at elevated concentrations. Y-axis is normalized peak height that has been normalized to the peak height that was observed when no interferent was added to the 75 nmol kg^{-1} sample. Note the various concentration units used for the interferents. Points in red are believed to be contaminated.

Pico-molar Interferents: Cr^{3+}, Ga^{3+}, and Ti^{3+}

From Figure 32 it is evident that increasing the concentration of the interferents Cr^{3+}, Ga^{3+}, and Ti^{4+} had no affect on the resulting normalized peak height. As a result, it was concluded that the detection of the Al-lumogallion complex by the developed SIA method was free of interference from these ions; even at concentrations exceeding those typically observed for riverine waters. Indeed, the concentration ranges used above extend at least 2 times higher than their concentrations in the SLRS-4 certified reference material (CRM for river waters) and over 30 times higher than their mean oceanic concentrations (See Table 5). These findings are not that unexpected given these elements' low concentrations in the aquatic environment. Furthermore, it should be noted that the absence of interference from Ga^{3+} is likely due to the pH at which the reaction was maintained. Indeed, Shigematsu et al. (1967) reported that the optimal conditions for the formation of the Ga-lumogallion complex required a lower pH than its Aluminum counterpart.

Nano-molar Interferents: Fe^{3+}, Cu^{2+}, and Ti^{4+}

In contrast to previous reports of interference by the presence of Fe^{3+}, the horizontal trend in the normalized peak height indicates that Fe^{3+} does not pose a threat of interference at concentrations as high as 2.5 μmol kg^{-1}. While this concentration limit is multiple orders of magnitude higher than the mean oceanic concentration of Fe^{3+}, this upper limit is comparable to Fe^{3+} concentrations for river waters. Indeed, the SLRS-4 sample is certified to have a Fe^{3+} concentration

of 1.8 μM. Nevertheless, the plot for Fe^{3+} in Figure 32 encompasses this concentration and does not indicate any interference from ferric iron at this concentration range. Therefore, given that the intended use for the SIA method is to analyze coastal and river water samples for their Al content, it can be concluded that the method is free from interference from Fe^{3+} in these matrices.

As for interference from Cu^{2+}, it appears that interference could be expected when Cu^{2+} concentrations exceeding 1 μmol kg^{-1}. However, even at these elevated concentrations the effect on the normalized peak height was minimal, but nevertheless detectable. It is worth point out the third point (shown in red) of the Cu^{2+} plot, which displays an anomalously elevated normalized peak height relative to the neighbouring data points. It is believed that this elevated signal was due to a minor contamination from the sample vial rather than from the addition of Cu^{2+} since Cu^{2+} has been shown to attenuate rather than enhance the analytical signal (Shigematsu et al., 1967). Furthermore, subsequent samples containing higher concentrations of Cu^{2+} display no noticeable change in their normalized peak height than that of a sample containing no Cu^{2+}. In light of these observations it was determined that the SIA method would not experience interference from Cu^{2+}, provided the ions concentration in the sample remained below the 1 μmol kg^{-1} threshold. Given that copper's oceanic and river concentrations are typically in the nanomolar (nM) range; it is likely that there will be no observable interference from Cu^{2+} when performing analyses on samples of this nature.

From the Vanadium plot in Figure 32 it can be seen that the addition of V^{5+} resulted in some interesting behaviour that affected the precision of the analytical signal for some, but by no means all of the data points. In fact, this was also observed for the initial 10 μM interference test as is evident by the anomalously large error bars in Figure 31 for the peak height of Vanadium. The reasons for this behaviour is unclear but fortunately it appears to only occur at V^{5+} concentrations that exceed those found in oceanic and river waters. Furthermore, although the precision of the analytical signal suffers at elevated V^{5+} concentrations, the normalized peak height statistically remains unchanged even at concentrations approaching 1 μmol kg^{-1}. Thus, the presence of excess V^{5+} in a sample does not affect the SIA methods accuracy in determining the Al content of the sample. As a result, the presence of an environmentally relevant concentration of V^{5+} in a sample is likely not to affect the determination of Al in river and seawater samples.

Micro-molar Interferent: Fluoride

Fluoride has been previously reported to interfere with the formation of the Al-lumogallion complex resulting in the attenuation of the samples fluorescent signal (Hydes and Liss, 1976). From the fluoride plot in Figure 32, it can be seen that this is precisely what is occurring at F^- concentrations exceeding 500 μmol kg^{-1}. However, at lower fluoride concentrations the intensity of the analytical signal appears to be remain relatively constant, with the variability observed thought to be due to minor contamination of the autosampler vials. Nevertheless,

the results from the incremental addition of the fluoride interferent suggest that the SIA method should be free of F^- interference at the concentrations typically observed in the aquatic environment. Indeed, the mean oceanic concentration fluoride is only 68 μmol kg^{-1} and its river concentration is virtually always less than 200 μmol kg^{-1}. Therefore it was concluded that fluoride is not likely to interfere with the determination of Al in samples with these matrices.

Milli-molar Interferent: Calcium

As mentioned earlier, the finding that the addition of calcium to a sample resulted in a positive interference is at odds with previous studies. In the investigation performed Shigematsu et al. (1967), an addition of 100 μM of Ca^{2+} to a sample containing 1.5 μM of Al resulted in no significant increase in the determined Al concentration for the sample. Thus these findings suggest that Ca^{2+} does not result in a positive interference by reacting with lumogallion to form a complex that fluoresces near the same wavelength as the Al-lumogallion complex. In the development of their batch method for determination of Al in natural waters, Hydes and Liss (1976) did not report any interference by calcium. Furthermore, Howard et al. (1986) didn't even consider calcium as a potential interferent and actually recommended the addition of large amounts of Ca^{2+} in the form $CaCl_2$ to mask the interference from fluoride if one was evident. Lastly, when adapting this chemistry for a FIA based method for Al determination in seawater (which contains ~10 mM of Ca^{2+}) Resing and Measures (1994) didn't even consider Ca^{2+} in their interferent study. Thus, based on the actions of

previous investigators, our findings of Ca^{2+} as a positive interferent in the determination of Al via the lumogallion method may require further review.

From Figure 32 it can be seen that increasing the concentration of Ca^{2+} in the 75 nmol kg^{-1} Al sample results in a steady increase in the normalized peak height, again suggesting positive interference from the presence of Ca^{2+}. However, it should be noted that the Ca^{2+} additions performed here came from the same Ca^{2+} stock solution as that was used in the initial investigation that first suggested Ca^{2+} as a positive interferent. Therefore, it was thought that the positive interference observed may be due to an Al impurity in the $CaCl_2$ salt used to prepare the 6 M Ca^{2+} stock solution rather than from interference from calcium itself. A look at the $CaCl_2$ salt used revealed that the product was of reagent grade quality and only had a purity of ≥90% assay. Furthermore, the $CaCl_2$ salt used was on loan from an undergraduate laboratory where the history of the stock was largely unknown and thus further questioning the integrity of the $CaCl_2$ used. To determine the degree of Al impurity required to be present in the $CaCl_2$ salt to yield the observed enhancement of the analytical signal in Figures 32 and 33, a series of calculations were performed and are shown in Appendix 3. From these calculations it was determined that if only 1/10000th of a percent (by mass) of the $CaCl_2$ salt's impurity corresponded to a form of Al that would readily enter solution, a 100 μL addition of the 6 M $CaCl_2$ stock to a 25 mL sample would result in a 95 nM increase in the samples Al concentration. An increase of this magnitude would easily account for the increase in the peak height observed.

Therefore, it is probable that the presence of an Al impurity, rather than Ca^{2+} itself was responsible for the observed enhancement of the analytical signal.

To determine if Ca^{2+} was indeed an interferent, two samples were prepared; One containing 70 nmol kg^{-1} of Al and 12.5 mmol kg^{-1} of Ca^{2+} that was obtained from a 1000 ppm atomic absorption standard solution and one containing 70 nmol kg^{-1} of Al and no added Ca^{2+}. The matrix for these samples was acidified Milli-Q. These samples were then analyzed using the SIA method and examples of the resulting peaks are shown in Figure 30.

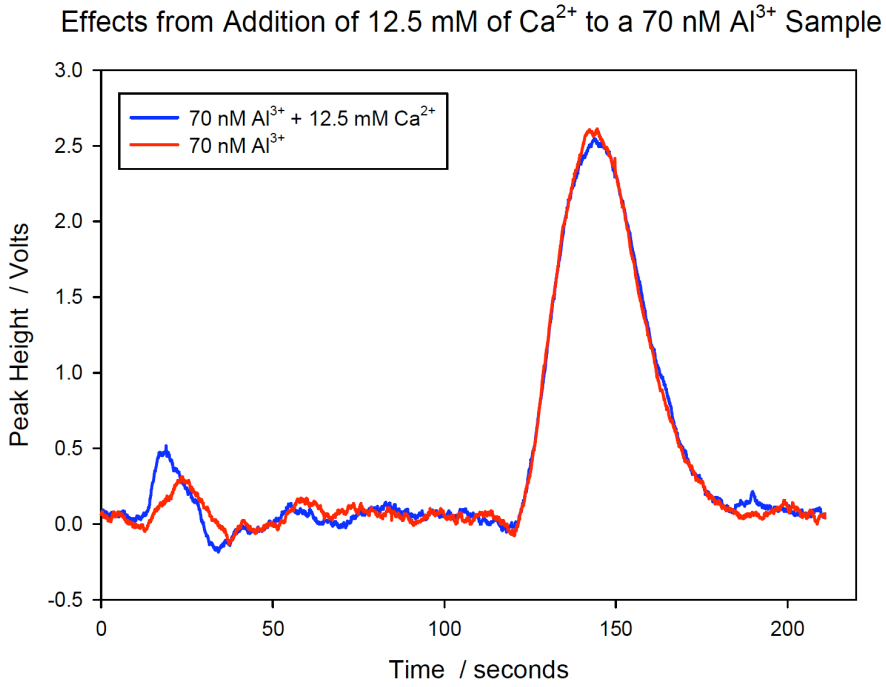

Figure 33 – Overlay plot indicating the absence of a positive interference on the analytical signal from the addition of 12.5 mmol kg^{-1} Ca^{2+} to a sample containing 70 nmol kg^{-1} Al. The similar peak heights observed for the two samples confirms that Ca^{2+} does not interfere with the determination Al, even when present at concentrations comparable to those observed in seawater. Noise in baseline is atypical and likely due to the use of an aged (days old) lumogallion buffer solution.

As can be seen from the overlapping peaks of Figure 33, the addition of over 12 mmol kg^{-1} of Ca^{2+} had no affect on the analytical signal, thereby indicating that Ca^{2+} does not interfere with the methods ability to detect the Al content in a sample containing a significant concentration of calcium. This finding is in agreement with previous investigations into the potential interferents for the Al-lumogallion method of detection and the reports of the methods high selectivity (Shigematsu et al., 1967). Further confirmation of this conclusion is presented later in the discussion of the analysis of the SLRS-4 certified reference material.

4.4 Sensitivity and Linearity of the SIA Method

From the interference investigations and the optimizations performed above, it appears the use of SIA may yield a selective method for the determination of elevated concentrations of Al in natural or coastal waters provided the desired sensitivity is achieved. As can be seen from Figure 34, increasing the concentration of Al by 20 nmol kg^{-1} resulted in a considerable increase in the intensity of the analytical response. Furthermore, a linear relationship between the Al concentration and the peak height was observed for the 25 - 180 nmol kg^{-1} concentration range as indicated in the calibration curve in Figure 35. Below a concentration of approximately 25 nmol kg^{-1}, a dip in the baseline similar to that shown in Figure 34 for 0 nmol kg^{-1} Al was observed where a peak was observed at higher concentrations. The source of the depression in

the baseline is thought to be due to a change in the refractive index of the reagent stream relative to the milli-Q baseline by the addition of the lumogallion buffer and Brij-35 surfactant to the reagent stream. Changing the refractive index of the solution passing through the detector cell will alter the direction of the light (Snell's Law) that is typically observed by the photomultiplier tube, thereby attenuating the intensity of light reaching the detector. The reduced intensity of the light that is incident on the detector would result in a depression of the reagent stream baseline being observed. The trough in the baseline corresponds to the negative intercept reported for the calibration curve in Figure 35.

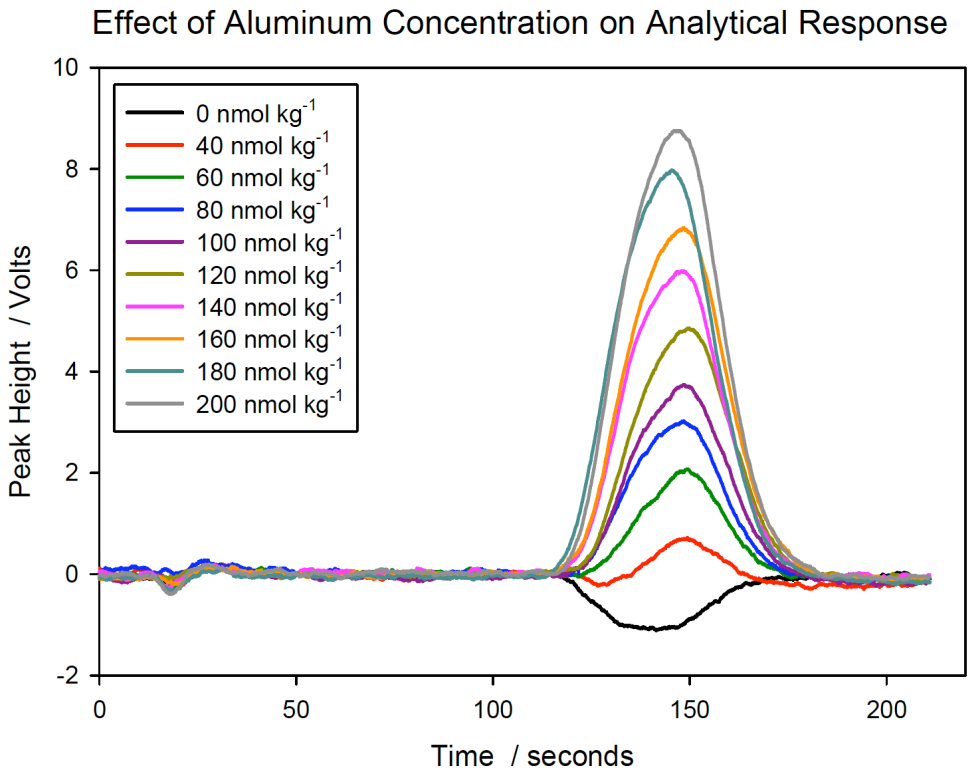

Figure 34 – Overlay plot indicating the sensitivity of the SIA method to an increase in the Al concentration. Note the depression of the baseline when no Al is present in the sample.

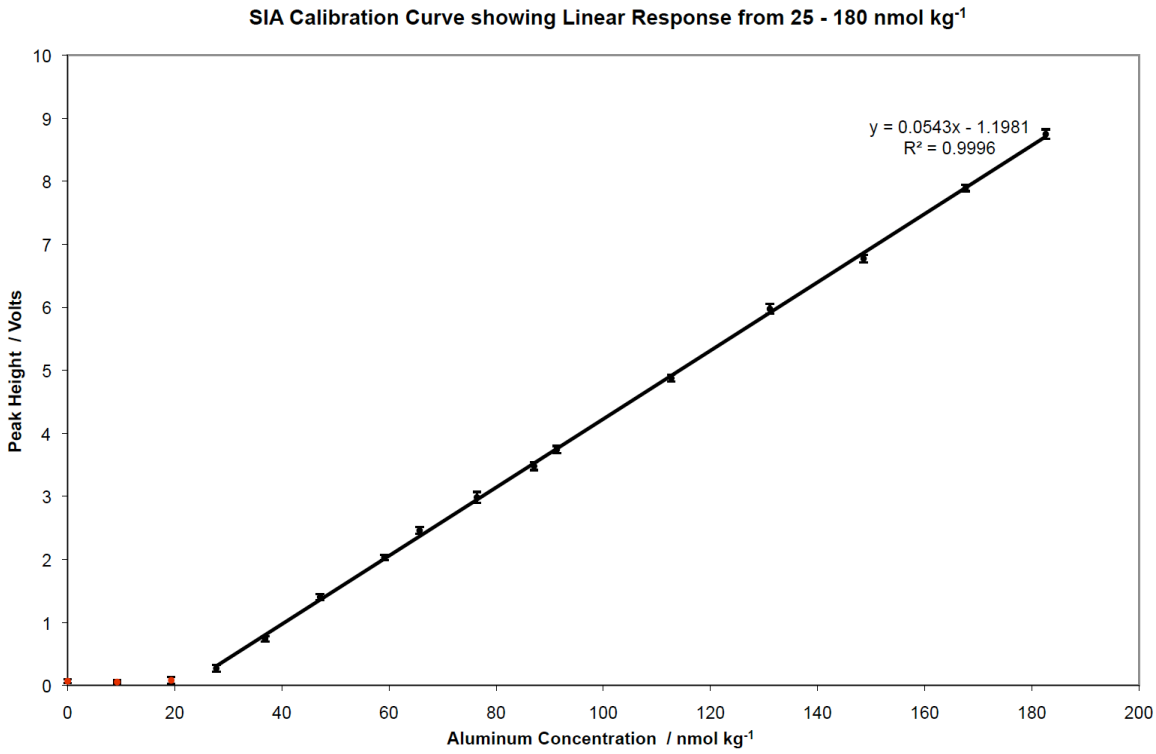

Figure 35 - Calibration of the SIA method demonstrating the method's linear response to an increase in the Al concentration. The linear range starts at ~25 nmol kg^{-1} and extends beyond 180 nmol kg^{-1}. The upper limit of the linearity was not determined. Note that for concentrations below 20 nmol kg^{-1} the maximum peak height is indiscernible from the baseline. The negative intercept observed for the fit of the linear curve corresponds to the depression in the baseline that was observed for samples with low Al concentrations as shown in Figure 34.

However, it should be noted that the near zero peak height values displayed in Figure 35 for the samples containing 20 nmol kg^{-1} or less were due to the manner in which the peak height was calculated and the large analytical window (from 100 to 180 seconds) used to determine the peak height. In particular, the peak height was calculated as the highest point within in the analytical window relative to the corrected baseline value determined at fifty seconds from the start of data acquisition. Thus for a low Al standard that

resulted in a trough rather than a peak, it's calculated peak height was essentially zero and corresponded to the highest point of the baseline within the analytical window.

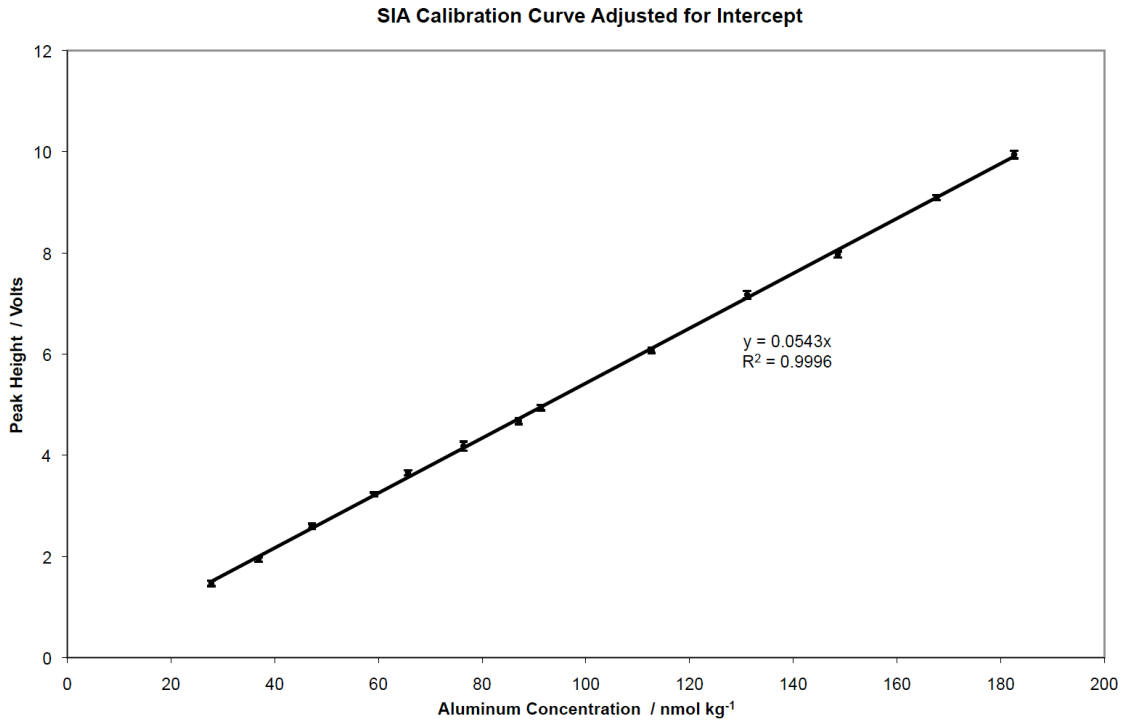

Figure 36 - Calibration curve of SIA method corrected for negative intercept.

To account for the negative non-zero baseline, the absolute value of the intercept was added to the average peak heights for all the points lying on the curve in Figure 35, and were then plotted against their Al content to yield the intercept adjusted curve in Figure 36. This was performed since it is desirable to have a calibration curve pass through the origin of the vertical and horizontal axes. It should be noted that in order to determine the Al concentration in an unknown sample, the same process of adding the intercept to the samples average peak height was performed. This adjusted peak height was then divided

by the slope of the calibration curve to yield the sample's calculated Al content in units of nmol kg^{-1}.

4.4.1 Limits of Detection and Quantification

Typically the limit of detection (LOD) for a method is calculated as three times the standard deviation of the analytical signal corresponding to a blank sample and the resulting value being calculated as a concentration. Similarly, the limit of quantification (LOQ) is defined as ten times the standard deviation of a blank sample. However, the presence of a non-zero intercept like that observed for the SIA method calibration requires a correction factor. Thus, to obtain more realistic values for the limits of detection and quantification for the SIA method, the standard deviations for the 0 nmol kg^{-1} and 19 nmol kg^{-1} standards from Figure 35 were used. Table 6 displays the LOD and LOQ calculated by conventional means as well as those corrected for the intercept and some operationally defined limits.

Table 6 - Determination of Limits of Detection and Quantification and reported Precision for the SIA method.

Statistical Parameter	SIA	
	0 nmol kg^{-1}	19 nmol kg^{-1}
Conventional LOD and LOQ		
LOD 3σ / nmol kg^{-1}	2	3
LOQ 10σ / nmol kg^{-1}	6	10
AI Concentration Correction for non-zero Intercept / nmol kg^{-1}	22	
LOD and LOQ Corrected for Intercept		
LOD (3σ + Intercept) / nmol kg^{-1}	24	25
LOQ (10σ + Intercept) / nmol kg^{-1}	28	32
Operationally Defined LOD and LOQ		
LOD / nmol kg^{-1}	24	
LOQ / nmol kg^{-1}	30	
Precision (%RSD) at 75 nmol kg^{-1}	2%	

In comparing the traditionally determined LODs and LOQs displayed in Table 6 to the calibration curve in Figure 35, it is evident that these calculated limits are unrealistic as the SIA method is clearly not capable of detecting, much less quantifying at these low concentrations. Even the 10 nmol kg^{-1} LOQ calculated from the standard deviation of the 19 nmol kg^{-1} standard is a seemingly low concentration for a practical LOD or LOQ for the SIA method. As a result, the concentration corresponding to the absolute value of the intercept was determined to be 22 nmol kg^{-1} and this value was added to the conventionally determined LOD and LOQ to yield limits that were corrected for the negative intercept. These corrected values, ranging from 24 to 32 nmol kg^{-1}, appear to be much more reasonable limits and seem to agree with the lower part of the curve in Figure 35. Thus, in order to have single values for each of the limits, the

corrected values determined from the 0 nmol kg^{-1} and 19 nmol kg^{-1} standards were average to yield the operationally defined limits presented in Table 6. Therefore the LOD and LOQ for the SIA method were concluded to be 24 nmol kg^{-1} and 30 nmol kg^{-1} respectively. By contrast, the LOD and LOQ for the FIA method described in Chapter 2 were 0.1 nmol kg^{-1} and 0.33 nmol kg^{-1} respectively. Similarly, Brown and Bruland (2008) reported a detection limit of 0.1 nM for their flow-based method. As a result, it is evident that the FIA based methods that incorporate a pre-concentration step yield a detection limit that is about 240 times lower than the proposed SIA method. However, directly comparing limits obtained for the SIA and FIA methods leaves the SIA at an unfair disadvantage since no pre-concentration of the sample is performed in the SIA method. A more valid comparison of the detection limits would be to compare the detection limit of the SIA to that obtained for the FIA methods when the pre-concentration column has been replaced with a sample loop. Unfortunately, the latter's detection limits have not been reported in the literature. Nevertheless, Brown and Bruland (2008) have reported to negate the use of a pre-concentration column only for samples with Al concentrations exceeding 80 nM; only at these elevated concentrations is a sample loop used in place of the pre-concentration column. Similarly, for the analyses performed in Chapter 3, any sample having an Al concentration greater than 50 nmol kg^{-1} was analyzed with the use of a loop rather than a column, thereby removing any pre-concentration factor. Comparing these operational values to the LOQ reported for the SIA method suggests that in the absence of pre-concentration the methods display

similar limits of detection and quantification. It is interesting to note that although the batch method developed by Hydes and Liss (1976) did not have a pre-concentration step, it was reported to have a detection limit of only 1.9 nM, over a factor of 10 lower than that obtained for the SIA method. It is believed that the reason for the lower detection limit observed for the batch method was due to the extended period in which the analyte was allowed to equilibrate with the lumogallion ligand. This prolonged development period would permit a more quantitative formation of the Al-lumogallion complex, thereby providing a stronger analytical signal and a corresponding lower limit of detection.

4.5 Analysis of Coastal and River Samples and FIA Comparison

In order to determine the validity and accuracy of the Al measurements obtained using the SIA method, a subset of samples that were previously analyzed using the more established FIA method and of appropriate Al concentration were selected for analysis by SIA. Also, to account for any temporal variability in the Al concentration, the samples were re-analyzed via the FIA method. Lastly, to ensure the accuracy of the measurements obtained from both of the methods, a diluted sample of the SLRS-4 certified reference material and a check standard containing approximately 94 nmol kg^{-1} of Al in acidified Milli-Q were prepared and analyzed using the two analytical methods. The results from these analyses are presented in Tables 7 and 8 respectively.

Table 7 - Results from Analysis of Selected Coastal and River samples and comparison to values obtained from using FIA

Sample	FIA		SIA		Absolute Difference	SIA Percent Difference
	[Al] nmol kg^{-1}	Error nmol kg^{-1}	[Al] nmol kg^{-1}	Error nmol kg^{-1}	[Al] nmol kg^{-1}	%
KC 1000						
800 m	37.9	0.2	35	1	2.9	+9%
900 m	62	1	69	1	8	+13%
KC 500						
145 m	27.6	0.3	27	1	-0.6	-2%
225 m	31.6	0.1	31	1	-0.6	-3%
300 m	118.0	0.3	121	3	3	+3%
450 m	103.2	0.2	108	2	4.8	+5%
KC 200						
10	26.0	0.1	28	1	2	+9%
25	16.3	0.1	N/A	N/A	N/A	N/A
50	268	1	268	2	0	0%
75	183	1	186	2	3	+2%
125	33.0	0.4	30	1	-3	-8%
175	51.0	0.2	55	1	4	+8%
River Samples						
Western River	71.5	0.3	78	2	6.5	+10%
Hood River	84.5	0.4	89	2	4.5	+5%

From Table 7 it can be seen that overall the Al concentrations determined from the two methods agree quite well, yielding percent differences of 10% or less for all but one of the samples analyzed. It is worth noting that the higher percent differences in Table 7 were generally observed for samples with Al concentrations towards the lower end of the linear range of Figure 35; however, this is at partly due to the manner in which the percent differences were calculated. The percent differences reported in Table 7 were calculated as the absolute value of the difference between the Al concentrations determined by the

two methods divided by the Al concentration determined from the more established FIA method and presented as a percentage. Thus, for two samples on either end of the concentration range with the same absolute difference between their determined Al concentrations, the sample with the lower Al concentration will have a smaller denominator and therefore yield a higher percent difference.

In comparing the reported errors in Table 7 for the two methods, it appears that the FIA method of analysis consistently yielded a higher level of precision in the determination of the Al concentration in the samples. Thus given that the methods provide similar values for a sample's Al content, it seems the FIA method would be a better choice due to the increased precision it provides. However, it is believed that the enhanced precision observed for the FIA method is largely due to the different sensitivity of the fluorometers used in the FIA and SIA analyses. As reported previously, the SIA manifold used a Gilson Model 121 filter fluorometer that irradiated the flow cell with a 50 W halogen lamp. By contrast, detection of Al-lumogallion in the FIA method was performed using a Shimadzu RF-535 fluorometer that used a 150 W Xe lamp for its excitation light source. Using a lamp with 3 times the wattage for the excitation source as well the use of a monochromator rather than a filter for the selection of the excitation wavelength will undoubtedly result in a dramatic increase in the intensity of the light used to irradiate the sample relative to the filter fluorometer used in the SIA method. This increase will in turn amplify the fluorescence intensity because the

number of Al-lumogallion molecules that have been excited and subsequently relaxed, potentially emitting a photon that is red-shifted relative to the excitation photon will have increased. Thus, increasing the excitation intensity will yield a stronger, and likely more consistent analytical signal, thereby providing a higher level of precision. Also, while both of the detectors utilized a photomultiplier tube (PMT) for detection of the fluorescence signal, their relative stability and sensitivity likely differ, potentially resulting in one detector yielding more precise results. It is worth noting that an attempt was made to acquire the fluorescence signal from the SIA using the more sensitive Shimadzu RF-535 detector but considerable drift in the instrument's baseline was observed when flow to the detector was halted for several minutes, making the detector unsuitable for SIA. Nevertheless, despite the lower precision observed for the SIA method relative for FIA, the SIA was capable of providing a precision (%RSD) of 2% for replicate analyses of a 75 nmol kg^{-1} sample (see Table 4), which is more than acceptable for most applications.

As a final point regarding Table 7, it should be pointed out that the Al concentrations determined by the SIA for the KC500 145 m and KC200 10 m samples are below the LOQ that was previously operationally defined. However, in comparing the SIA determined concentration to that obtained by FIA, it Is evident that the SIA was capable of accurately determining the sample concentrations. This finding suggests that perhaps the operationally defined LOD and LOQ for the SIA method may need to be revised.

4.5.1 Analysis of SLRS-4 Certified Reference Material (CRM) and Check Standard

As a final step in the validation of the SIA method, analysis of two samples with certified or known Al concentrations were analyzed by SIA and FIA to ensure the methods provided accurate, reliable results. The first sample analyzed was the SLRS-4 river reference material for trace metal that was prepared by the National Research Council of Canada. However, since this sample contains over 2 μmol kg^{-1} of Al, the sample was diluted prior to analysis by taking a 1 mL aliquot of the SLRS-4 and diluting the sample to 25 mL in Milli-Q that was acidified to pH 1.7. This dilution resulted in the SLRS-4 sample having a concentration of 75 ± 6 nmol kg^{-1} at the 95% confidence level. The second sample was a Check Standard that was prepared by spiking a known volume of Milli-Q at pH 1.7 with an aliquot of the Al standard stock solution to yield a final concentration of 94 nmol kg^{-1}. The 2 nmol kg^{-1} error associated with the check standard is an estimate of the 95% confidence interval for the sample based on the errors in the volumetric and gravimetric measurements performed in the preparation of the sample.

Table 8 - Results from the analysis of the SLRS-4 Certified Reference Material and the 94 nmol kg^{-1} Check Standard

Data	SLRS-4		Check Standard	
	[Al] nmol kg^{-1}	Error nmol kg^{-1}	[Al] nmol kg^{-1}	Error nmol kg^{-1}
Known Concentration	75	6[a]	94	2[b]
Concentration Determined by FIA	70.5	0.2	93.9	0.4
Percent Error for FIA	-6%		-1%	
Concentration Determined by SIA	79 78	2 2	96	1
Percent Error for SIA	4% - 6%		2%	

From Table 8 it can be seen that both the SIA and FIA methods were able to detect the correct Al concentration in the SLRS-4 sample within it's 95% confidence interval. In fact, the SIA method correctly determined the Al content of the SLRS-4 sample on two separate analyses of the sample. To compare the mean Al concentration determined to the mean of the known concentration, the percent errors were calculated and suggested that the SIA method overestimated the concentration by 4 - 6%. However, it should be stressed that the Al concentration of the SLRS-4 sample as determined by the SIA method lies well within the certified range for the sample. Similarly, although the Al concentration determined by the FIA method was lower than the known value, the concentration is still under the umbrella of the 95% confidence interval reported for the SLRS-4 sample. From these results, it can be concluded that both the SIA and FIA methods provided accurate determinations of the Al concentration in the SLRS-4 certified reference material.

With the confirmation of the SIA method's ability to accurately determine the Al concentration of the diluted SLRS-4 sample, it can also be concluded that the presence of Ca^{2+} in the sample matrix does not result in a positive interference. This reasoning follows from the fact that the standards used to determine the Al concentration in the diluted SLRS-4 sample were prepared in low-Al seawater with a Ca^{2+} concentration of about 10 mM. By contrast, the SLRS-4 is a river water reference material with a certified Ca^{2+} concentration of only 0.15 mM before the $1/25^{th}$ dilution. Therefore, the Ca^{2+} concentration in the diluted SLRS-4 sample was approximately 6 μM; that is, over a factor of 1000 less than the Ca^{2+} concentration present in the standards used to the determine the Al content in the SLRS-4 sample. If Ca^{2+} did indeed result in a positive interference, it's presence at milli-Molar concentrations in the seawater matrix used to prepare the Al standards would have considerably enhanced the analytical signal of the standards. Furthermore, the comparatively low Ca^{2+} concentration in the diluted SLRS-4 sample would have resulted in the SIA method to significantly underestimate the Al concentration in the sample as the sample's analytical signal would not have been affected to the same extent as the Al standards. However, this was not observed and the SIA method was able to accurately determine the Al content in the SLRS-4 sample.

In a similar fashion to the analysis of the SLRS-4 sample, both the SIA and FIA methods were able to correctly determine the concentration of Al in the Check Standard. The SIA determined the Al concentration of the Check Standard

to be 96 ± 1 nmol kg^{-1}, while the FIA reported a concentration of 93.9 ± 0.4 nmol kg^{-1}; thus both determined concentrations fall within the approximated 95% confidence interval stated for the Check Standard. Even in light of the perhaps seemingly generous confidence interval for the Check Standard, it is evident by the low percent errors reported that the SIA and FIA methods are capable of accurately determining the Al concentration in an aqueous matrix.

Recently Al-Kindy et al. (2007) have published a sequential injection method for the fluormetric determination of Al in drinking water. The method involves chelating Al with 8-hydroxy-7-(4-sulfo-1-naphthylazo)-5-quinoline sulfonic acid (HSNQ) and monitoring the fluorescence at 492 nm with an excitation wavelength of 357 nm. Al-Kindy et al. (2007) report a linear response from 100-800 ppb (3–29 μM) and a limit of detection, calculated as three times the standard deviation of a blank solution (3σ), to be 4 ppb (148 nM). Comparing the SIA method that was developed in this work to that reported by Al-Kindy et al (2007), it is evident that our SIA method provides a lower limit of detection (24 nmol kg^{-1} vs. 148 nM) and is operational at the nano-molar scale. The reported precision (%RSD) for the two methods are comparable (1.4% and 2% for Al-Kindy et al. and this work respectively) which indicate that the methods are capable of high precision when performing analyses in their respective concentration ranges. Although the analytical window reported by Al-Kindy et al. (2007) is considerably larger than that reported for our SIA method, this is likely due to our method operating at a lower concentration scale. Furthermore, the

extent of the linear range for our SIA method was not determined in this work and may well exceed 200 nmol kg^{-1}. Both methods are reported to be relatively free of interference from other elements, however both methods report an attenuation of the analytical signal when elevated concentrations of Fe are present in the sample. In terms of efficiency, the method reported by Al-Kindy et al. (2007) is superior in that it only requires 75 seconds to perform a single analysis on a sample. By contrast, the time required to complete a single run using our SIA method is approximately 5 minutes.

4.6 Concluding Remarks

The main goal of this work was to develop a low volume sequential injection method for the accurate and precise determination of Al in aqueous media at nano-molar concentrations. Ideally the method would provide a rapid analysis on a sample while minimizing the amount of sample and reagent used. The method would also allow for a high level of automation and not require any sample manipulation from the analyst.

The development of the SIA method described in this work involved rigorous optimization of the chemical ratios and instrumental parameters to identify the ideal conditions for the formation and fluorometric detection of the Al-lumogallion complex. Furthermore, the selectivity of the lumogallion ligand for the analyte was examined in an extensive investigation into the potential for

interference by other elements. From the initial interference investigation, 8 elements (Cr^{3+}, Ga^{3+}, Ti^{4+}, Fe^{3+}, Cu^{2+}, V^{5+}, F^-, and Ca^{2+}) of the 13 tested were found to interfere with the analytical signal when present at concentrations far exceeding those typically observed in oceanic and river waters. However, in a subsequent interference test carried out at lower interferent concentrations, only Ca^{2+} appeared to result in a positive interference at environmentally relevant concentrations. This finding contradicted the results of previous interference tests performed by other investigators and upon further inquiry into the matter it was concluded that the positive interference observed in the first two tests was likely due to an Al impurity in the $CaCl_2$ used to prepare the Ca^{2+} solution. From this evaluation of potential interferents it became evident that the lumogallion ligand was highly selective for the Al analyte.

In analyzing standards of increasing concentration, the optimized SIA method, which was capable of making a measurement every 5 minutes, was found to be sensitive and to respond linearly with increasing concentration from 25 to at least 180 nmol kg^{-1}. The limits of detection and quantification were concluded to have operationally defined values of 24 nmol kg^{-1} and 30 nmol kg^{-1} respectively; however, it appears the method may be capable of quantifying below this limit. The precision of the method was found to be 2% (%RSD) for a sample with an Al concentration of 75 nmol kg^{-1}. As for the accuracy of the SIA method, analysis of samples that were previously analyzed via FIA yielded comparable values and the method was successful in the determination of the Al

content in a diluted sample of a SLRS-4 CRM on two separate occasions. Furthermore, analysis of the 94 ± 2 nmol kg^{-1} Check Standard resulted in a determined Al concentration of 96 ± 1 nmol kg^{-1}. Based on the analysis of the SLRS-4 CRM and the prepared Check Standard, it was concluded that the SIA method was capable of rapidly performing highly accurate and precise measurements of the Al content in samples with an aqueous matrix.

4.7 Future Work

Future development that could extend off this work would be to adapt the SIA method for the determination of Al at open-ocean concentrations. This would require the development of a rapid and efficient online pre-concentration step for incorporation into the current SIA method. This could potentially be performed using the same pre-concentration resin used in for the FIA method presented previously. However, doing so would require the sample's pH to be adjusted, either on or off-line, prior to the pre-concentration step as the resin is incapable of retaining Al at low pH. Preliminary investigations into the above proposed modifications have been unsuccessful and have resulted in lengthy analysis times of approximately 1 measurement every 20 minutes. Nevertheless, more complex SIA manifolds involving multiple pumps can be envisioned whereby while one sample is being sent to the detector, another sample is being buffered online and pre-concentrated onto a column, thus reducing the analysis time.

The SIA method could also be used as is and applied to the determination of Al content in a variety of aqueous samples and in a variety of fields. Areas where this method could be useful other than in the analysis of coastal and fresh water samples include health care and beverage industries. In particular, monitoring the Al content in dialysis fluids is an important measurement frequently preformed in the health industry as the Al in the source waters used to prepare dialysis fluids has been shown to accumulate in patients with renal failure, causing adverse side effects (Bohrer et al., 1998; Silva et al., 2005). As a result, regulations have been developed to limit the Al concentration in source waters used to prepare dialysis solutions (Silva et al., 2005). As for the beverage industry, elevated concentrations of Al in beverages, particularly of the alcoholic variety, have been shown to give an unfavourable flavour (Vela et al., 1998).

Bibliography

Aagaard, K., Coachman, L.K. and Carmack, E., 1981. On the halocline of the Arctic Ocean. Deep Sea Research Part A. Oceanographic Research Papers, 28(6): 529-545.

Al-Kindy, S.M.Z., Al-Ghamari, S.S. and Suliman, F.E.O., 2007. A sequential injection method for the fluorimetric determination of aluminum in drinking water using 8-hydroxy-7-(4-sulfo-1-naphthylazo)-5-quinoline sulfonic acid. Spectrochimica Acta Part A: Molecular and Biomolecular Spectroscopy, 68(5): 1174-1179.

Armbrust, E.V., 2009. The life of diatoms in the world's oceans. Nature, 459(7244): 185-192.

Bohrer, D., Gioda, A., Binotto, R. and CÌcero do Nascimento, P., 1998. On-line separation and spectrophotometric determination of low levels of aluminum in high-salt content samples: application to analysis of hemodialysis fluids. Analytica Chimica Acta, 362(2-3): 163-169.

Broeker, W.S. and Peng, T.H., 1982. Tracers in the Sea, Eldigio Press, New York.

Brown, E.T. and Measures, C.I. (Editors), 1996. The Impact of African Dust Across the Mediterranean. Estimating dust input to the Atlantic Ocean using surface water Al concentrations. Kluwer, Dordrecht, 389 pp.

Brown, M., Bruland, K. and Smith, G.J., 2010. Dissolved aluminum in the North Atlantic and North Pacific SAFe and GEOTRACES Intercalibration Results, Eos Trans. AGU.

Brown, M.T., 2009. Email Correspondence regarding use of Global FIA Columns for Al FIA method.

Brown, M.T. and Bruland, K.W., 2008. An improved flow injection analysis method for the determination of dissolved aluminum in seawater. Limnology and Oceanography: Methods, 6(1): 87-95.

Carmack, E.C. and MacDonald, R.W., 2002. Oceanography of the Canadian Shelf of the Beaufort Sea: a setting for marine life. Arctic, 55(2): S29(17).

Darby, D.A., Naidu, A.S., Mowatt, T.C. and Jones, G. (Editors), 1989. The Arctic Seas. Sediment composition and sedimentary processes in the Arctic Ocean. Vann Nostrand-Reinhold, New York, 888 pp.

Dierssen, H., Balzer, W. and Landing, W.M., 2001. Simplified synthesis of an 8-hydroxyquinoline chelating resin and a study of trace metal profiles from Jellyfish Lake, Palau. Marine Chemistry, 73(3-4): 173-192.

Eicken, H. et al., 2005. Sediment transport by sea ice in the Chukchi and Beaufort Seas: Increasing importance due to changing ice conditions? Deep Sea Research Part II: Topical Studies in Oceanography, 52(24-26): 3281-3302.

Gehlen, M. et al., 2002. Unraveling the atomic structure of biogenic silica: evidence of the structural association of Al and Si in diatom frustules. Geochimica et Cosmochimica Acta, 66(9): 1601-1609.

Hans Wedepohl, K., 1995. The composition of the continental crust. Geochimica et Cosmochimica Acta, 59(7): 1217-1232.

Howard, A.G., Coxhead, A.J., Potter, I.A. and Watt, A.P., 1986. Determination of dissolved aluminium by the micelle-enhanced fluorescence of its lumogallion complex. Analyst, 111: 1379 - 1382.

Hydes, D.J., 1979. Aluminum in Seawater: Control by Inorganic Processes. Science, 205(4412): 1260-1262.

Hydes, D.J., 1983. Distribution of aluminium in waters of the North East Atlantic 25∞N to 35∞N. Geochimica et Cosmochimica Acta, 47(5): 967-973.

Hydes, D.J., de Lange, G.J. and de Baar, H.J.W., 1988. Dissolved aluminium in the Mediterranean. Geochimica et Cosmochimica Acta, 52(8): 2107-2114.

Hydes, D.J. and Liss, P.S., 1976. Fluorometric method for the determination of low concentration of dissolved aluminium in natural waters. Analyst, 101: 922-931.

Hydes, D.J. and Liss, P.S., 1977. The behaviour of dissolved aluminium in estuarine and coastal waters. Estuarine and Coastal Marine Science, 5(6): 755-769.

Johnson, K.S. et al., 2007. Developing standards for dissolved iron in seawater. Eos, 88(11): 131-132.

Kempema, E.W., Reimnits, E. and Barnes, P.W., 1989. Sea ice sediment entrainment and rafting in the Arctic. J. Sed. Pet., 59: 308-317.

Kramer, J., Laan, P., Sarthou, G., Timmermans, K.R. and de Baar, H.J.W., 2004. Distribution of dissolved aluminium in the high atmospheric input region of the subtropical waters of the North Atlantic Ocean. Marine Chemistry, 88(3-4): 85-101.

Landing, W.M., Haraldsson, C. and Paxeus, N., 1986. Vinyl polymer agglomerate based transition metal cation-chelating ion-exchange resin containing the 8-hydroxyquinoline functional group. Analytical Chemistry, 58(14): 3031-3035.

MacCarthy, P., Klusman, R.W., Cowling, S.W. and Rice, J.A., 1993. Water analysis. Analytical Chemistry, 65(12): 244R-292R.

Mackin, J.E. and Aller, R.C., 1984. Processes affecting the behavior of dissolved aluminum in estuarine waters. Marine Chemistry, 14(3): 213-232.

Martin, J.H. and Fitzwater, S.E., 1988. Iron deficiency limits phytoplankton growth in the north-east Pacific subarctic. Nature, 331(6154): 341-343.

McLaughlin, F.A., Carmack, E.C., Macdonald, R.W. and Bishop, J.K.B., 1996. Physical and geochemical properties across the Atlantic/Pacific water mass front in the southern Canadian Basin. J. Geophys. Res., 101.

Measures, C.I., 1999. The role of entrained sediments in sea ice in the distribution of aluminium and iron in the surface waters of the Arctic Ocean. Marine Chemistry, 68(1-2): 59-70.

Measures, C.I. and Edmond, J.M., 1989. Shipboard determination of aluminum in seawater at the nanomolar level by electron capture detection gas chromatography. Analytical Chemistry, 61(6): 544-547.

Measures, C.I. and Edmond, J.M., 1992. The distribution of Aluminum in the Greenland Sea and its relationship to ventilation processes. J. Geophys. Res., 97.

Melling, H., 1993. The formation of a haline shelf front in wintertime in an ice-covered arctic sea. Continental Shelf Research, 13(10): 1123-1147.

Melling, H., 2009. Personal Communication - Characteristics of Brine-Enriched Shelf Waters

Melling, H. and Lewis, E.L., 1982. Shelf drainage flows in the Beaufort Sea and their effect on the Arctic Ocean pycnocline. Deep Sea Research Part A. Oceanographic Research Papers, 29(8): 967-985.

Middag, R., de Baar, H.J.W., Laan, P. and Bakker, K., 2009. Dissolved aluminium and the silicon cycle in the Arctic Ocean. Marine Chemistry, In Press, Accepted Manuscript.

Moore, J.K., Doney, S.C., Glover, D.M. and Fung, I.Y., 2001. Iron cycling and nutrient-limitation patterns in surface waters of the World Ocean. Deep Sea Research Part II: Topical Studies in Oceanography, 49(1-3): 463-507.

Moore, R.M., 1981. Oceanographic distributions of zinc, cadmium, copper and aluminium in waters of the central arctic. Geochimica et Cosmochimica Acta, 45(12): 2475-2482.

Moore, R.M., Melling, H. and Thompson, K.R., 1992. A Description of Water Types on the Mackenzie Shelf of the Beaufort Sea During Winter. J. Geophys. Res., 97.

Moore, R.M. and Millward, G.E., 1984. Dissolved-particulate interactions of aluminium in ocean waters. Geochimica et Cosmochimica Acta, 48(2): 235-241.

Moran, S.B. and Moore, R.M., 1991. The potential source of dissolved aluminum from resuspended sediments to the North Atlantic Deep Water. Geochimica et Cosmochimica Acta, 55(10): 2745-2751.

Moran, S.B., Moore, R.M. and Westerlund, S., 1992. Dissolved aluminum in the Weddell Sea. Deep Sea Research Part A. Oceanographic Research Papers, 39(3-4): 537-547.

Neal, C., Neal, M., Davies, H. and Smith, J., 2003. Fluoride in UK rivers. The Science of The Total Environment, 314-316: 209-231.

NSIDC, 2007. Arctic Sea Ice Shatters all Previous Record Lows The National Snow and Ice Data Center, Boulder.

Obata, H., Nozaki, Y., Alibo, D.S. and Yamamoto, Y., 2004. Dissolved Al, In, and Ce in the eastern Indian Ocean and the Southeast Asian Seas in comparison with the radionuclides 210Pb and 210Po. Geochimica et Cosmochimica Acta, 68(5): 1035-1048.

Orians, K.J., 2010. Personal Communication - Preliminary Results on the Barium Distribution along the Kugmallit Canyon Transect.

Orians, K.J. and Bruland, K.W., 1985. Dissolved aluminium in the central North Pacific. Nature, 316(6027): 427-429.

Orians, K.J. and Bruland, K.W., 1986. The biogeochemistry of aluminum in the Pacific Ocean. Earth and Planetary Science Letters, 78(4): 397-410.
Resing, J.A. and Measures, C.I., 1994. Fluorometric Determination of Al in Seawater by Flow Injection Analysis with In-Line Preconcentration. Analytical Chemistry, 66(22): 4105-4111.
Rusakov, V.Y. et al., 2004. Distribution and mineral composition of particulate matter in the Franz Victoria Trough (Northern Barents Sea). Oceanology, 44(2): 247-256.
Shigematsu, T., Nishikawa, Y., Hiraki, K. and Kiyotoshi, M., 1967. Fluorophotometric Determination of Aluminum and Gallium with Lumogallion. Bunseki Kagaku, 16: 692-697.
Shiller, A.M. and Frilot, D.M., 1996. The geochemistry of gallium relative to aluminum in Californian streams. Geochimica et Cosmochimica Acta, 60(8): 1323-1328.
Silva, E.L.d., Ganzarolli, E.M. and de Queir√≥z, R.o.R.U., 2005. Determination of Aluminum Traces in Hemodialysis and Tap Water Using Standard Method's Procedure Modified and Flow Injection Ionic Exchange Preconcentration. Analytical Letters, 38(13): 2089 - 2101.
Skrabal, S.A., 1995. Distributions of dissolved titanium in Chesapeake Bay and the Amazon River Estuary. Geochimica et Cosmochimica Acta, 59(12): 2449-2458.
Stoffyn, M., 1979. Biological Control of Dissolved Aluminum in Seawater: Experimental Evidence. Science, 203(4381): 651-653.
Stoffyn, M. and Mackenzie, F.T., 1982. Fate of dissolved aluminum in the oceans. Marine Chemistry, 11(2): 105-127.
Taylor, S.R., 1964. Abundance of chemical elements in the continental crust: a new table. Geochimica et Cosmochimica Acta, 28(8): 1273-1285.
Tria, J., Butler, E.C.V., Haddad, P.R. and Bowie, A.R., 2007. Determination of aluminium in natural water samples. Analytica Chimica Acta, 588(2): 153-165.
Vela, M.M., Toma, R.B., Reiboldt, W. and Pierri, A., 1998. Detection of aluminum residue in fresh and stored canned beer. Food Chemistry, 63(2): 235-239.
Vink, S. and Measures, C.I., 2001. The role of dust deposition in determining surface water distributions of Al and Fe in the South West Atlantic. Deep Sea Research Part II: Topical Studies in Oceanography, 48(13): 2787-2809.
Wilde, P., 2010. Periodic Table for Seawater, Berkeley.
Williams, W.J., Melling, H., Carmack, E.C. and Ingram, R.G., 2008. Kugmallit Valley as a conduit for cross-shelf exchange on the Mackenzie Shelf in the Beaufort Sea. J. Geophys. Res., 113.

Appendix

Appendix 1 – Optimized Sequence for SIA Method

	Device	Parameters	Function
Optimized SIA Sequence			
name sample	single channel data	Al Sample	name sample
Lumogallion Zone			
Lumogallion Mix		4	
Lumogallion	18 Port Valve	10	go to port
MilliGAT Pump aspirate	MilliGAT Pump	35,20,1	aspirate
wait 2 seconds	system	2	wait
Sample	18 Port Valve	5	go to port
MilliGAT Pump aspirate	MilliGAT Pump	200,25,1	aspirate
wait 2 seconds	system	2	wait
Lumogallion	18 Port Valve	10	go to port
wait 2 seconds	system	2	wait
MilliGAT Pump aspirate	MilliGAT Pump	35,20,1	aspirate
Gilson Detection No Column			
Detector	18 Port Valve	6	go to port
MilliGAT Pump slew	MilliGAT Pump	30	slew
To Detector	Brij Valve	5	go to port
Gilson 121 start acquire	Gilson 121	0.1	start acquire
Acquire	system	210	wait
Gilson 121 stop acquire	Gilson 121	N/A	stop acquire
subtract baseline	single channel data	50	subtract baseline
set data window	single channel data	100,180	set data window
calc peak height	single channel data	N/A	calc peak height
calc peak area	single channel data	N/A	calc peak area
save data to file	single channel data	N/A	save data to file
MilliGAT Pump stop	MilliGAT Pump	N/A	stop
To Bulk	Brij Valve	6	go to port

Appendix 2 – Calculation of Brij-35 : Reagent Zone Ratio for SIA

In order to allow a direct comparison of the Brij-35 : Reagent Zone ratio that was determined to be optimal for the SIA method to the ratios reported in Table 4 for the various FIA methods, the volume of the reagent zone was arbitrarily fixed to a value of 1000 μL.

Reagent Zone (RZ) Volume = 1000 μL

Now given that the ideal flow rate for the reagent stream was previously determined to be 30 μL s^{-1}, we can determine the length of time required to flow the 1000 μL Reagent Zone.

Time required to flow RZ = RZ Volume / RZ Flow Rate
Time required to flow RZ = 1000 μL / 30 μL s^{-1} = 33.3 seconds
Time required to flow RZ = 33.3 seconds

Finally, the volume of Brij-35 that was dispensed into the Reagent Zone over this time interval can be determined since the optimal flow rate of the surfactant was determined to be 5.3 μL s^{-1}

Volume of Brij-35 added to RZ = Time required to flow RZ × Brij-35 Flow Rate
Volume of Brij-35 added to RZ = 33.3 seconds × 5.3 μL s^{-1} = 176.7 μL
Volume of Brij-35 added to RZ = 176.7 μL

Therefore the Brij-35 : Reagent Zone ratio is :

176.7 μL : 1000 μL

Appendix 3 – Calculation of Potential Al Impurity in $CaCl_2$

To determine if the positive interference observed from the addition of Ca^{2+} to the sample may be due to an Al impurity in the salt, a calculation was performed to determine the degree of Al impurity that would be required to cause the observed enhancement of the analytical signal. The Table below is a summary of the raw values used to perform the calculation. The spike and sample volumes reported are ideal but approximate the actual volumes used in the interference investigation.

Table of Raw Values used for Calculation

Data	Value
Mass of $CaCl_2$ used (g)	80.80
Volume of $CaCl_2$ stock (L)	0.125
Molecular Weight of $CaCl_2$ (g mol^{-1})	110.98
Purity of $CaCl_2$ (assumed minimum value)	90%
Concentration of Ca^{2+} in Stock Corrected for Purity (M)	5.24
Atomic Mass of Al (g mol^{-1})	26.981
Volume of Ca^{2+} Stock used to Spike Sample (mL)	0.100
Final Volume of Sample (mL)	25.00

To determine the mass of Al in the $CaCl_2$ salt used to prepare the standard for a given percentage of Al impurity, the calculation is as follows:

Mass of Al = Mass of $CaCl_2$ used for stock x Percent Al impurity in $CaCl_2$ Salt

Mass of Al = 80.80 g x 1/10000th % Al = 8.08 x 10^{-5} g

Mass of Al = 8.08 x 10^{-5} g

Calculating the concentration of Al in the sample for the above percentage Al impurity:

$[Al]_{stock}$ = (Mass of Al / Molecular Wt of Al) / Volume of $CaCl_2$ Stock

$[Al]_{stock}$ = (8.08 x 10^{-5} g / 26.981 g mol^{-1}) / 0.125 L = 2.40 x 10^{-5} M

$[Al]_{stock}$ = 24.0 μM

Now to calculate the concentration of Al added to the sample due to the impurity in the $CaCl_2$ salt:

$[Al]_{sample}$ = ($[Al]_{stock}$ x Volume of Spike) / Final Volume of Sample

$[Al]_{sample}$ = (24.0 μM x 0.100 mL) / 25.00 mL = 0.0958 μM

$[Al]_{sample}$ = 95.8 nM

The table below is a summary of the results for the above calculation for various theoretical levels of Al impurity in the $CaCl_2$ salt. As can be seen from the above calculation, for an Al impurity of only 1/10000th of a percent, addition of only 100 μL of the stock would have resulted in a 95.8 nM increase in the samples Al concentration.

Percent Al Impurity in $CaCl_2$ Salt	Values corresponding to theoretical % Al impurity		
	Mass of Al in Ca^{2+} Stock Solution (g)	[Al] in Ca^{2+} Stock Solution (μM)	[Al] in Sample after 100 uL addition of Ca^{2+} Stock Solution (nM)
1/100000 %	8.08 x 10^{-6}	2.4	9.6
1/10000 %	8.08 x 10^{-5}	24	95.8
1/5000 %	4.04 x 10^{-4}	119.8	479.2
1/1000 %	8.08 x 10^{-4}	239.6	958.3

Appendix 4 - Dissolved Al for KC Transect and Coronation Gulf

KC2700		
Pressure (dbars)	Al (nmol kg^{-1})	Error (nmol kg^{-1})
11	1.88	0.04
26	2.69	0.05
52	1.02	0.07
99	0.60	0.03
177	1.11	0.06
305	2.57	0.19
455	3.10	0.08
559	4.41	0.25
659	3.74	0.05
812	5.56	0.09
1014	5.88	0.10

KC2000		
Pressure (dbars)	Al (nmol kg^{-1})	Error (nmol kg^{-1})
11	3.79	0.12
24	2.45	0.06
51	0.87	0.13
136	1.12	0.06
151	1.34	0.11
253	3.72	0.10
303	3.39	0.08
456	4.86	0.12
556	4.82	0.06
658	7.05	0.11
810	5.41	0.10
1013	6.77	0.12

KC1500		
Pressure (dbars)	Al (nmol kg^{-1})	Error (nmol kg^{-1})
10	2.57	0.21
25	2.21	0.11
51	0.15	0.08
146	1.09	0.09
227	1.54	0.13
254	2.04	0.09
303	3.02	0.02
455	4.36	0.05
556	4.71	0.10
658	5.03	0.14
809	5.41	0.15
1014	5.58	0.04

Values in RED are known or suspected to be contaminated.

KC1000		
Pressure (dbars)	Al (nmol kg^{-1})	Error (nmol kg^{-1})
10	1.12	0.08
25	3.12	0.05
67	0.47	0.05
127	3.20	0.10
152	0.61	0.16
203	1.26	0.06
354	3.18	0.08
456	5.25	0.13
557	4.55	0.09
658	5.44	0.04
810	5.59	0.10
909	7.22	0.15

KC500		
Pressure (dbars)	Al (nmol kg^{-1})	Error (nmol kg^{-1})
9	5.84	0.05
52	9.35	0.10
146	1.10	0.05
228	2.41	0.03
305	3.98	0.07
453	9.53	0.09

KC200		
Pressure (dbars)	Al (nmol kg^{-1})	Error (nmol kg^{-1})
10	2.38	0.05
26	1.22	0.03
51	0.38	0.04
76	0.72	0.04
127	0.88	0.04
178	3.05	0.08

CG Stn 24		
Depth (m)	Al (nmol kg^{-1})	Error (nmol kg^{-1})
15	1.59	0.06
25	0.89	0.05
40	0.78	0.12
75	1.56	0.11
100	7.81	0.07
150	2.79	0.07
200	2.00	0.05

CG Stn 30		
Depth (m)	Al (nmol kg^{-1})	Error (nmol kg^{-1})
15	2.41	0.12
25	1.27	0.15
35	0.91	0.12
75	0.73	0.06
100	1.03	0.08
125	1.46	0.05
150	1.24	0.03
175	1.95	0.14

Appendix 5 – Total Al for KC Transect

KC2700		
Pressure (dbars)	Al (nmol kg^{-1})	Error (nmol kg^{-1})
11	5.02	0.06
26	11.31	0.05
52	6.27	0.06
99	1.66	0.08
177	3.04	0.03
305	4.29	0.05
455	6.65	0.11
559	3.66	0.05
659	6.30	0.05
812	8.51	0.06
1014	9.26	0.05

KC2000		
Pressure (dbars)	Al (nmol kg^{-1})	Error (nmol kg^{-1})
11	11.16	0.04
24	14.09	0.17
51	2.33	0.04
136	9.63	0.04
151	10.19	0.05
253	6.71	0.04
303	12.35	0.03
456	12.63	0.05
556	13.60	0.02
658	12.15	0.02
810	13.30	0.20
1013	12.62	0.12

KC1500		
Pressure (dbars)	Al (nmol kg^{-1})	Error (nmol kg^{-1})
10	9.55	0.14
25	15.10	0.17
51	2.63	0.01
146	6.95	0.12
227	6.27	0.16
254	6.74	0.20
303	9.26	0.09
455	10.47	0.14
556	9.80	0.06
658	10.65	0.12
809	14.74	0.05
1014	13.32	0.08

KC1000		
Pressure (dbars)	Al (nmol kg^{-1})	Error (nmol kg^{-1})
10	7.38	0.03
25	16.53	0.02
67	1.77	0.03
127	2.45	0.02
152	6.49	0.03
203	6.79	0.09
354	16.71	0.05
456	16.41	0.07
557	17.71	0.10
658	26.09	0.18
810	37.93	0.17
909	62	1

KC500		
Pressure (dbars)	Al (nmol kg^{-1})	Error (nmol kg^{-1})
9	9.8	0.0
52	34.2	0.7
146	27.6	0.3
228	31.6	0.1
305	118.0	0.3
453	103.2	0.2

KC200		
Pressure (dbars)	Al (nmol kg^{-1})	Error (nmol kg^{-1})
10	26.0	0.1
26	16.3	0.1
51	268	1
76	183	1
127	33.0	0.4
178	51.0	0.2